Mechanistic Studies of the Pyrolysis of Methylated Furans

by

Jong Hyun Kim

B.S., Korea University, 2000

M.S., Korea University, 2003

A thesis submitted to the

Faculty of the Graduate School of the

University of Colorado in partial fulfillment

of the requirement for the degree of

Doctor of Philosophy

Department of Chemistry and Biochemistry

2013

This thesis entitled:
Mechanistic Studies of the Pyrolysis of Methylated Furans
written by Jong Hyun Kim
has been approved for the Department of Chemistry and Biochemistry

G. Barney Ellison

Mark R. Nimlos

Date_____

The final copy of this thesis has been examined by the signatories, and we find that both the content and the form meet acceptable presentation standards of scholarly work in the above mentioned discipline.

Kim, Jong Hyun (Ph.D. Physical Chemistry)

Mechanistic Studies of the Pyrolysis of Methylated Furans

Thesis directed by Professor G. Barney Ellison

Furans are important biomass monomers. They are also under consideration as possible biofuels for internal combustion engines. This thesis considers the pyrolysis of methylated furans. In particular, the thermal decomposition of 2-methylfuran, 3-methylfuran, and 2,5-dimethylfuran has been studied in a high temperature (1000 K — 1600 K) microtubular flow reactor. The approximate residence time in the heated SiC reactor is 100 — 200 μsec. The nascent pyrolysis products are identified by 118.2 nm (10.487 eV) photoionization mass spectroscopy and are complemented by matrix infrared absorption spectroscopy. The three furans that are the subject of this thesis are shown to undergo pyrolysis in a manner that is completely analogous to the parent compound, furan.

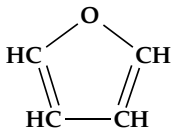

furan

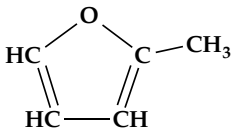

2-methylfuran
2MF

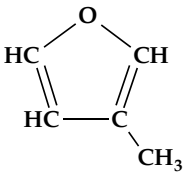

3-methylfuran
3MF

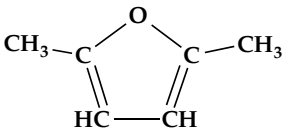

2, 5-dimethylfuran
DMF

The result of this thesis is the validation of a general mechanism for unimolecular, thermal decomposition of any alkylated furans. The initial steps in the pyrolysis are the formation of a set of carbenes. These carbenes undergo further fragmentation to a set of simple alkynes, ketenes, and CO.

Dedicated to the Saviour, Jesus Christ

You are my Lord

Acknowledgements

It's been 7 years since I came in CU Boulder on Aug. 10, 2006. When I touched down in Boulder, CO., I didn't know what would happen to me. Many things happened and many people I met, in which I could grow up and could be trained.

First, I thank to my advisor, Prof. G. Barney Ellison. He is a great teacher. He always tried to teach me Chemistry and English with superhuman patience. He was like a great reservoir of Chemistry. I could learn lots of things from him. He also showed me the balance between work and family. As a father, he understood my situation and taught me "family is the highest priority." I learned from Barney more than what I expected to get. "Really thank you, Barney."

I would like to thank my old lab mates. Tim D'Andrea (T-bone) was the best colleague in studying surface chemistry. Whenever I asked him, he answered it with generosity. He said "Jong, you have a question and I have an answer." He was right. He taught me everything about our OH radical generating machine. Besides, he was a good teacher for a long-board, a guitar, a softball game and a golf game. Thank you for guitar effectors. Luis Cuadra (Cobra) – Rodriguez is a man of men. He was always gentle and gave me zillions of advices. We sang a song, played golf and softball, and skied together. I have beaucoup good memories with him. Finally, he went San Francisco, CA., that's what he wanted. Be happy, Luis. AJ, you're the special friend of mine. You listened all my word and gave me precious advices. I think you have a warm heart to help others. I can't forget the "big dog" happening and the Christmas with Maggie, those are very fun and good memories. I also remember that your wedding was the first American style wedding to my family, it was a good time for us. Adam is a good friend of mine. Unlike others, he always taught me a formal English speaking and grammar, which

improved my English very much. Every May, he held a party, Cinco de Mustache, it was fun and a chance to meet a lot of physic's guys and rock climbing people. We also played softball together, he always cheered up the only Asian player. Thank for mead, it was delicioso. Brad, we just spent a short time, you were always kind and treated me with an open mind. I still kept the "Disrespect" jersey that you donated me. As you said to me "Good luck", I finally got a good luck to finish my Ph.D. degree. Thank you for the dining table. Beth, you're a good colleague while building up the PIMS. You helped me with good information of optics and electronic devices. Because you understood Asian culture, we could talk much. It was a good memory with you. Krzysztof, you talked too much. (Just, kidding, man.) I felt your considerate mind during your staying. You always tried to make a cordial atmosphere in our group. I can't forget the traditional Eastern Europe style dinner and the big table Christmas dinner. And I think it's not true that Polish is the easiest language in the world. And Kim, you're the transition friend between old and present. After leaving all old pals, you're still be an English teacher to me, even though I am a little bit worried about Minnesota accent. (Just joking.) I enjoyed working with you over the years, I hope that you get a good luck on your research.

Here are more recent group members: Tom, I thank you for your help and advice for matrix isolation system and Berkeley shirt, I love it. You also gave me information of Barker reservoir in Nederland, CO., with which I could eat the baked fish for dinner several times. Good luck to your studying. Jessie, I know what you did last winter, you were a hard worker. Just keep going, you can reach your goal. I also thank you for your kindness. Grant, you're so smart and diligent, and I believe that you can successfully complete all your work in graduate school, good luck.

Prof. John W. Daily, he always encouraged me with his dashing voice, like "hey, Jong." Even when I got a big trouble in generating 118 nm laser beam, he cheered me up and said that everything would be alright. Like his words, the problem was solved. I also thank to Dr. Xu Zhang. She showed me her enthusiasm for an experiment, which is necessary to the experimental scientists. She never gave up, just trying and trying. While working with Xu, I learned what the "doing someone's best" means. I can't miss Dr. Mark R. Nimlos. He's very nice guy. Whenever I talked to him, I felt his humbleness. He also gave me a lot of advices while building up the PIMS. And as the 2nd reader of my thesis, he did spare no effort. Thank you, Mark. Dr. David Robichaud, I owed him a lot. He provided tons of advices for the PIMS. Without the optics simulation program in Excel, the LabView software for the PIMS, the Gage card, and lots of information from him, I could not finish my work. Many times, he stopped by CU and helped me. I also thank to Dr. Don David and his colleagues in the machine shop and the electronic shop. They helped me with all machining work and electronics. Without their help, I could not imagine building up the PIMS.

I thank to Super ion group members: Prof. Lineberger, Prof. Bierbaum, Prof. Weber, Prof. Depuy, and all their group members. We could discuss various topics on the every Tuesday morning, it broadened my scientific point of view.

When I decided to enter Ph.D program, I got a big help from Prof. Yong-Sang Choi, Prof. Jong-Ho Choi, Prof. Jeunghee Park, and Prof. Kang-Jin Kim. With their help, I could get a chance to study in US and finish my Ph.D. degree.

I cannot forget my family and friends in S. Korea. They prayed for me day and night and always cheered me up. Thank you for your tears and prayers.

Lastly, My beloved wife and two sons, (Sung Min, Peter Boyoung, and Andrew Keeyoung), I really want to say “I love You”. Because we were together, we could do this.

Thank you, all of you.

Table of Contents

List of Tables

List of Figures

Chapter I Introduction

1.1 Background

Biomass is a plant or plant-derived material, which has been used as a fuel since the beginning of mankind. Along the progress of civilization, human society needed energy-intensive resources, and found and developed coal and oil in 19th century. Especially, oil has higher energy density than any resources used earlier and has been well investigated from collection to combustion. Because of the ease in storing and transporting, oil is used as major energy source in the world. But, with declining oil deposits, related to increased demand, and environmental effects, it is urged to find sustainable and economical energy resource. Even though, many kinds of alternative energy resources are studied and developed, currently, biomass is the only renewable resource for liquid transportation fuel, also carbon neutral resource.[1] In U.S., most vehicles run on the road with fuel mixture containing up to 10 % ethanol.[2] Motor vehicle companies produce cars geared to run on the higher blending of ethanol. Because of the connection between climate change and energy, carbon based fuels from biomass have the advantage of being carbon neutral.

The 1st generation biofuel is ethanol. Ten states in U.S., have alcohol blending compulsory, and ethanol blends are available in other states. Ethanol is mainly produced by fermentation of corn. U.S. produces 32 % of the world's corn supply,[3] part of it is used to produce alcohol.

1.2 Introduction to Biomass

Biomass consists of three main components: cellulose, hemicellulose, and lignin.

Cellulose

Cellulose is a linear polysaccharide and the most abundant organic compound on the planet and is responsible for about 40 – 60 wt.% of lignocellulosic biomass. The structure of cellulose is a strand of repeating cellobiose (disaccharide), connected by β(1→4)-glycosidic linkage of glucose, with an average molecular weight[4] of about 100,000. The hydroxyl groups on the glucose make hydrogen bonding on the intra- and inter-strand of chain, which makes cellulose firm. This strength is important in cell walls. Fig. 1.1 shows two cellulose strands connected by hydrogen bonding (dashed lines).

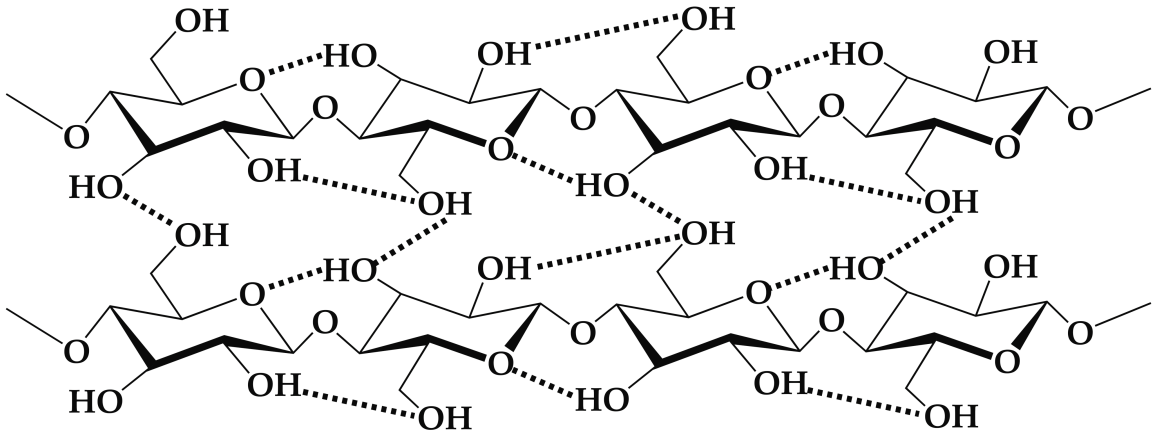

Figure 1.1 A strand of cellulose with the hydrogen bonding (dashed lines).

Hemicellulose

Hemicellulose is a branched polysaccharide and is abundant organic compound accounting for about 20 – 40 wt.% of lignocellulosic biomass. Hemicellulose is also commonly associated with cellulose in plant cell wall. While cellulose consists of dimeric sugar and is firm due to hydrogen bonds, hemicellulose is a branched polymer of xylose and is not rigid. An average molecular weight[4] is about < 30,000. Unlike cellulose, hemicellulose is a complex branched polymer.

Lignin

Lignin is a complex phenolic polymer structure and comprises about 10 – 25 wt.% of lignocellulosic biomass.[4] According to the structural studies of lignin[5-8], this polymer is made of three kinds of hydroxyphenyl-propanols: *p*-coumaryl alcohol, coniferyl alcohol, and sinapyl alcohol (Fig. 1.2). Each moleucule has a different number of methoxy group attached to phenyl ring. Fig. 1.3 shows a representative chemical structure of lignin.

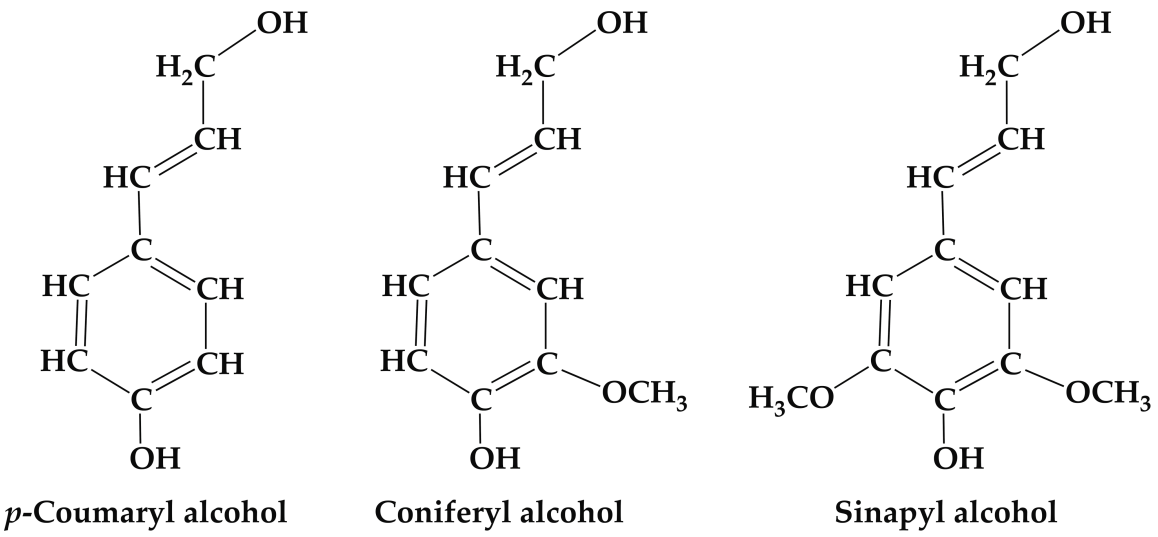

Figure 1.2 The building blocks of lignin.

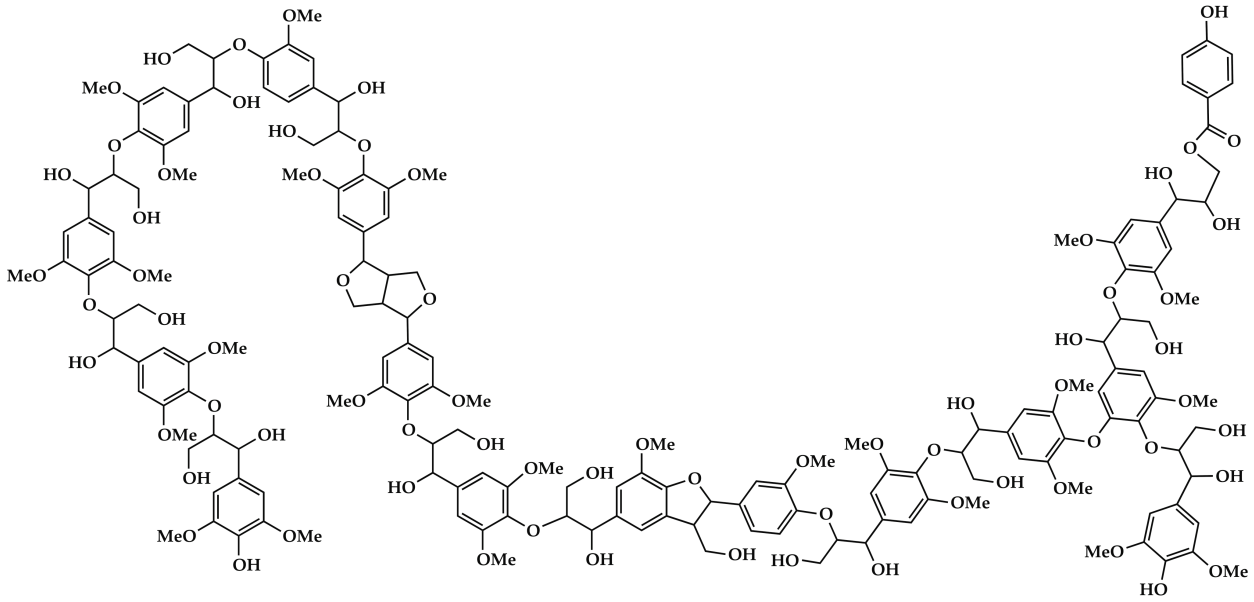

Figure 1.3 The chemical structure of lignin.[8]

Besides efforts to extract fuels directly from cellulose and lignin, chemical methods have been developed to convert cellulose to fuels. Recently, chemical engineers have converted lignocellulosic biomass into 2-methylfuran (2MF) and 2,5-dimethylfuran (DMF). In particular, DMF shows high energy density (29.6 kJ cm^{-3}), similar to gasoline (≅ 32 kJ cm^{-3}), and is better than ethanol (21.2 kJ cm^{-3}) by 40 %. Due to these advantage conditions, 2MF and DMF are considered as prominent candidates for 2nd generation biofuels, various researches for furan's combustion and pyrolysis are progressed.

We use the microtubular reactor studying pyrolysis of furans, in which residence time is approximately 100 – 200 msec and the surface temperature goes up to 1600 K.

1.3 Scope

This thesis is an experimental study of the pyrolysis of 2MF, 3MF, and DMF. We are also to identify the initial set of products formed as these furans are thermally

cracked. This thesis elaborates how furans are pyrolyzed, what the products of thermally decomposed furans are, and how to detect the pyrolysis products, and explains experimental method used for research.

Chapter II describes the tubular reactor for pyrolysis of methylated furans and two techniques to detect products: Ar matrix isolation FT-IR absorption spectroscopy and photoionization mass spectroscopy.

Chapter III describes pyrolysis of 2MF and 3MF and Chapter IV deals with pyrolysis of DMF.

Reference for Chapter I

(1) Huber, G. W.; Iborra, S.; Corma, A. *Chemical Reviews* **2006**, *106*, 4044.

(2) *American energy: The renewable path to energy security*, Worldwatch Institute Center for American Progress, 2006.

(3) *EPA, Major Crops Grown in the United States,* http://www.epa.gov/agriculture/ag101/cropmajor.html.

(4) McKendry, P. *Bioresource Technology* **2002**, *83*, 37.

(5) Sannigrahi, P.; Ragauskas, A. J.; Tuskan, G. A. *Biofuels, Bioproducts and Biorefining* **2010**, *4*, 209.

(6) Bose, S. K.; Francis, R. C.; Govender, M.; Bush, T.; Spark, A. *Bioresource Technology* **2009**, *100*, 1628.

(7) Reale, S.; Di Tullio, A.; Spreti, N.; De Angelis, F. *Mass Spectrometry Reviews* **2004**, *23*, 87.

(8) Vanholme, R.; Demedts, B.; Morreel, K.; Ralph, J.; Boerjan, W. *Plant Physiology* **2010**, *153*, 895.

Chapter II Experimental

2.1 Introduction

The purpose of the research is to establish the pyrolysis mechanisms of the substituted furans: 2-methylfuran (2MF), 3-methylfuran (3MF) and 2, 5-dimethylfuran (DMF). The goal of the experiments is to subject a dilute sample (roughly 0.1 % or less) of furans in a buffer gas (either He or Ar) to pyrolysis in a heated flow tube. The microtubular reactor exhausts to vacuum chamber held at a pressure of 10^{-5} Torr; consequently the contents of the flow tube are heated to a high temperature (1000 K — 1700 K) for a few μsec. However once the samples exit the reactor, all collisions cease and all chemistry is quenched. The products are to be identified by photoionization mass spectroscopy and infrared spectroscopy. The goal of these experiments is to detect all of the nascent products from pyrolysis.

We are using a microtubular reactor patterned after the pioneering experiments of Peter Chen.[1-7] These reactors are fabricated from SiC and complete[8] the pyrolysis within 100 – 200 μsec. The resultant molecular beam is analyzed by VUV photoionization mass spectroscopy (PIMS) as well as by matrix-isolation infrared absorption spectroscopy (IR). These techniques complement each other in several ways. A) Both are universal (all molecules can be ionized and all polyatomic molecules have an IR spectrum). B) Both are very sensitive (PIMS has small background signals while matrix IR collects dilute molecular samples over a few hours). C) Both are multiplexed (PIMS uses a time-of-flight device to monitor the entire mass spectrum for each laser shot and the IR spectrometer is a Fourier-Transform device and scans the entire vibrational spectrum from 4000 cm^{-1} — 400 cm^{-1}).

2.2 Microtubular Reactor

The microtubular reactor is used for pyrolysis of furans and producing thermally decomposed products. As mentioned earlier, it is based in the original designs of Chen.[1-7] Our current design for the pulsed reactor has been recently described by Vasiliou *et al*.[9] and the workings of a CW reactor are outlined by Urness *et al*.[10] A sketch of the pulsed reactor is shown in Fig. 2.1.

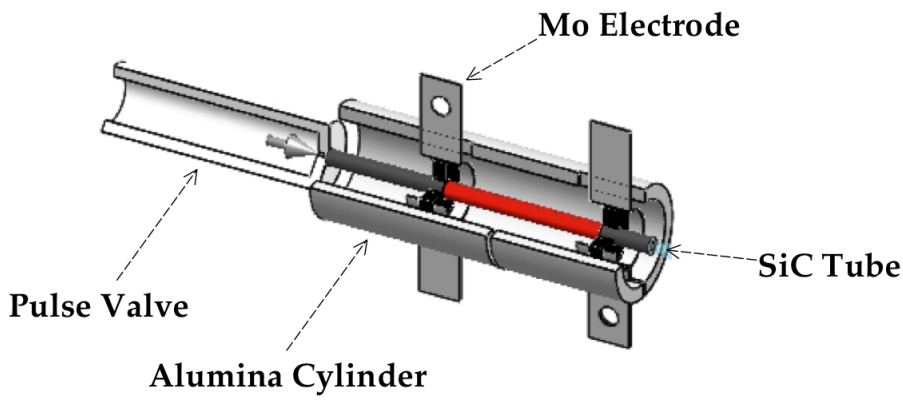

Figure 2.1 The picture of reactor assembly: the silicon carbide microtubular reactor, carbon discs, molybdenum electrodes, and alumina heat shield. The pulsed valve and poppet are shown to the left. The heated region of the reactor is shown in red.

The microtubular reactor is 3 cm long, 2 mm outer diameter, 1 mm inner diameter, and made of silicon carbide. This microtubular reactor is inserted into two carbon discs, which are clamped in the molybdenum clips. Two copper wires make a connection between the molybdenum clips and the variable transformer and the electrical circuit is completed. With a thin coating of graphite on the outer surface of the SiC tube, it can be resistively heated up to 1700 K with about 10 A. Temperature is measured by a type C thermocouple which is installed on the middle between two carbon discs and is controlled in ± 10 K during the experiment, but temperature

measurement[11] is very sensitive to the contact of the thermocouple and the SiC tube and a typical uncertainty is ± 100 K.

A type C thermocouple is prepared with two kinds of wires, tungsten/rhenium alloys (Omega.com), 26 % W and 5 % W, which are spot-welded on a piece of tantalum foil (4 mm × 4 mm). A type C thermocouple is wrapped on a SiC and tightened by a tantalum wire, and is connected to the main control box and measures the temperature of SiC surface.

This assembly of the SiC tube is enclosed by a cylindrical alumina tube which shields radiative heat release and protects the other components. The combined SiC nozzle and alumina heat shield is mounted onto a stainless steel circular plate with 0.25 mm orifice. The SiC tube is centered on the 0.25 mm orifice, through which gas mixture flows. A solenoid pulse valve (parker Hannifin Series 9 Pulse Valve) installed on the other side of a stainless steel circular plate controls a poppet's back and forth motion to close and open the 0.25 mm orifice (20 Hz, 200 μsec valve open time) and creates an adiabatic expansion, cooling the gas. The gas in the heated SiC flow reactor has a short residence time,[8] roughly 100 – 200 μsec, and produces a high yield of radicals,[12] approximately 10^{13} radicals/pulse.

A gas sample is prepared with 1 – 2 Torr of a gas sample or a liquid sample (with a high vapor pressure) with 1520 Torr of Helium for PIMS and 800 Torr of Argon for matrix FT-IR Spectrometry. For less volitle liquid samples, a sample heated probe is used to volatilize the sample. The sample probe consists of a quartz tube, a resistive heater, a type K thermocouple connected to the main control box, in which a quartz tube loading a sample is resistively heated. With a type K thermocouple, the temperature is monitored and is stabilized by feedback control. Cooled water

circulation is applied to guard the components behind a stainless circular plate from the conductive heat for PIMS while a stainless circular plate provides a surrounding cooling water jacket for matrix FT-IR spectrometer.

2.3 Photoionization Time-of-Flight Mass Spectrometer

PIMS is comprised of three vacuum chambers: a source chamber, an ionization chamber, and a time-of-flight chamber. Each chamber has its own vacuum system and gate valves separate the chambers. The molecular beam is photoionized by a pulsed 118.2 nm (10.487 eV) laser beam in the ionization chamber. The resulting cations are analyzed by a Wiley/McLaren time-of-flight mass spectrometer[13] and detected via a reflectron. An overview of this apparatus is shown in Fig. 2.2.

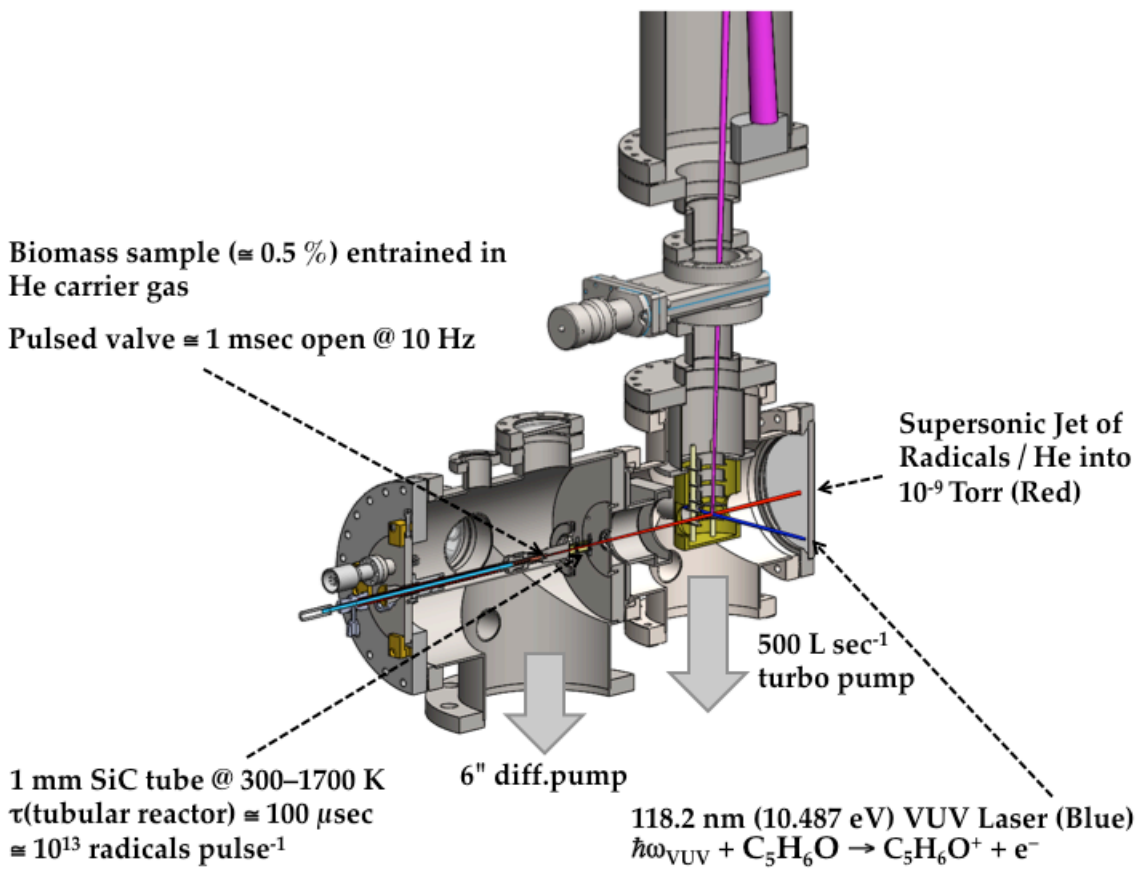

Figure 2.2 Picture of photoionization time of flight mass spectrometer.

A gas mixture of 0.06 % furan diluted in 1520 Torr He, is prepared in a manifold and is expanded supersonically into vacuum through the general pulse valve (Fig. 2.1). A portion of the molecular beam is collimated by passing through a skimmer, forming a molecular beam. The skimmer is 3 mm to 10 mm away from the exit of a SiC nozzle and is 1 mm diameter. The vacuum is maintined by a 6 inch diffusion pump (Varian, model: VHS-6) backed by a mechanical pump; the pumping speed of the diffusion pump is 2400 L s^{-1} for air. The pressure of the source chamber is 7×10^{-7} Torr with no gas load and 2×10^{-6} Torr with a molecular beam. The pressure in the vacuum chamber is measured by an ion gauge. To prevent back-streaming of the diffusion pump oil (Santovac 5), liquid nitrogen trap (10 L capacity) is used. A flow controller monitors the cooling water circulation to protect the system against water outage.

The incoming, collimated molecular beam from the source chamber is photoionized by 118.2 nm (10.487 eV) laser. A tubromolecular pump (Pfeiffer, TMU 521) is installed on the bottom of the chamber. The turbomolecular pump speed is 500 L sec^{-1} and is backed by a mechanical pump. The pressure in the chamber is 2×10^{-9} Torr with no gas load and rises to 8×10^{-7} Torr with the molecular beam. The distance between the vertex of the skimmer and the ionization spot is 17 cm long.

The time-of-flight chamber is connected to the ionization chamber upward and the reflectron is at the other end of the time-of-flight chamber. Two microchannel plate (MCP) detectors are installed on upward and downward, but only the downward MCP detector (2 inch diameter) is used for a better resolution. In the time-of-flight chamber, the ions from the ionization chamber fly toward the reflectron in the field free region and rebound downward to the MCP detector, on which ions are measured. The flight length is 140 cm between the accelerator and the refletron, 86 cm from the reflectron to

the MCP detector. A turbomolecular pump (Agilent, model: V81-M ISO 63) keeps the vacuum at 3×10^{-9} Torr without a gas load and 8×10^{-7} Torr during the experiment. The pumping speed is 80 L sec^{-1} (for N_2).

2.3.1 Photoionization with Vacuum Ultraviolet (118.2 nm, 10.487 eV) Laser

118.2 nm Vacuum Ultraviolet (VUV, 10.487 eV) is generated in xenon tripling cell using the 9th harmonic generated from a Nd:YAG laser (Spectra Physics, Quanta-Ray Pro-230-10Hz). The fundamental (1064 nm) is doubled in the first KD*P crystal and the second harmonic (532 nm) is mixed with a residual fundamental in the second KD*P crystal to generate the third harmonic (354.7 nm).

The 354.7 nm beam is focused on the center of xenon tripling cell (30 cm long, 1.375 inch inner diameter) using a fused silica lens (plano-convex lens, 1 inch diameter, 30 cm focal length, Thorlabs), which is 15 cm away from a quartz window of xenon tripling cell. On the focal spot, tripling of the 10 Hz 354.7 nm photons generates a photon of 118.2 nm, with an 8 nsec pulse width and 40 mJ $pulse^{-1}$. Both beams (118.2 nm and 354.7 nm) are focused by MgF_2 lens (bi-convex lens, 1 inch diameter, 63 mm focal length, CVI Melles Griot (part #: BICX-25.4-50.6-MF)). Due to the different refractive indices between 118.2 nm and 354.7 nm beams, the 118.2 nm photons are focused on the molecular beam and the focus of 354.7 nm is beyond chamber where it enters a beam dump (Kentek corp., Trap-It Beam Dump, product #: ABD-2NP) installed on the collinear window.

An outline of the Xe tripling cell is shown in Fig. 2.3.

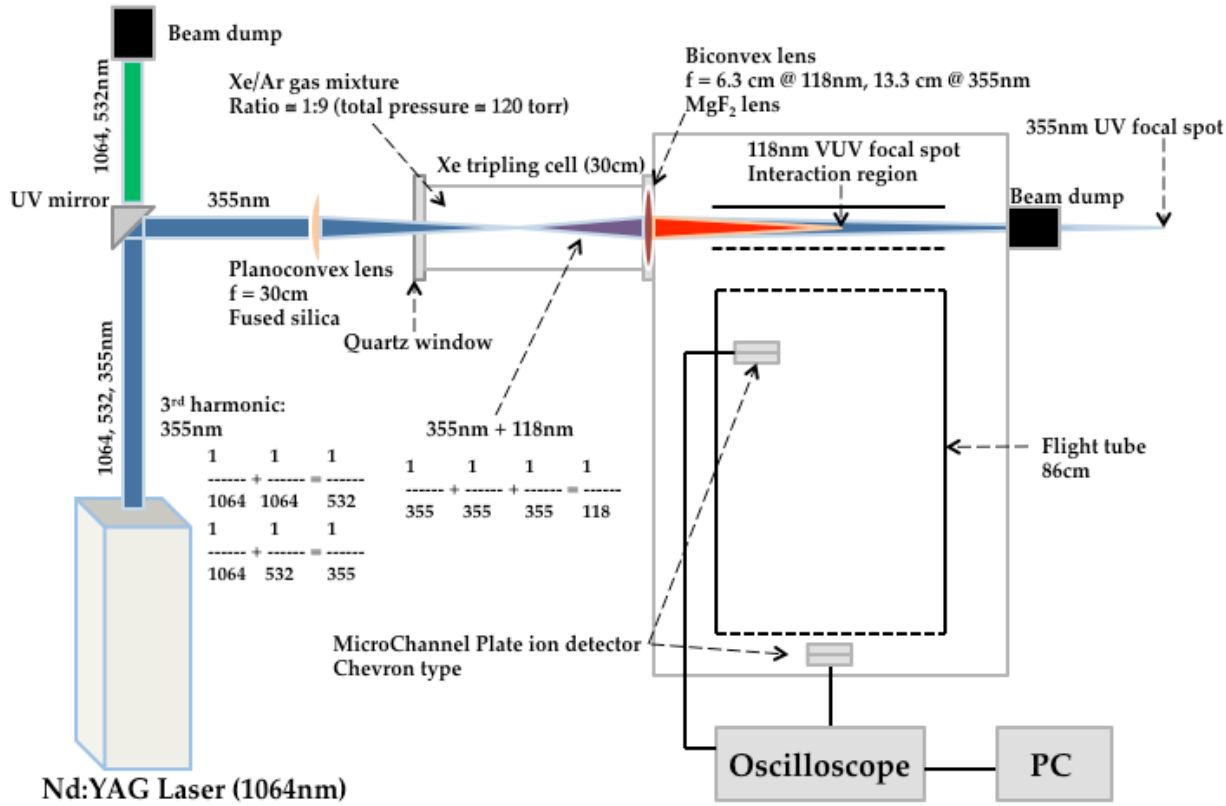

Figure 2.3 Vacuum UV generation from Nd-YAG laser *via* xenon tripling cell.

The performance of the Xe tripling cell in Fig. 2.3 is shown in Fig. 2.4. Xenon tripling cell is filled with 12 torr of xenon gas (99.999%, Ultra High Purity, aka UHP) and 108 torr of argon gas (99.999%), the ratio of Xe : Ar = 1 : 9. Because 118.2 nm beam is readily absorbed by air, the turbomolecular pump maintains a high vacuum (7×10^{-6} Torr) in xenon tripling cell before filling with Xe/Ar gas mixture. The optimal pressure in the Xe tripling cell is found to be 120 Torr by maximizing the ion signal from acetone, $[CH_3COCH_3]^+$.

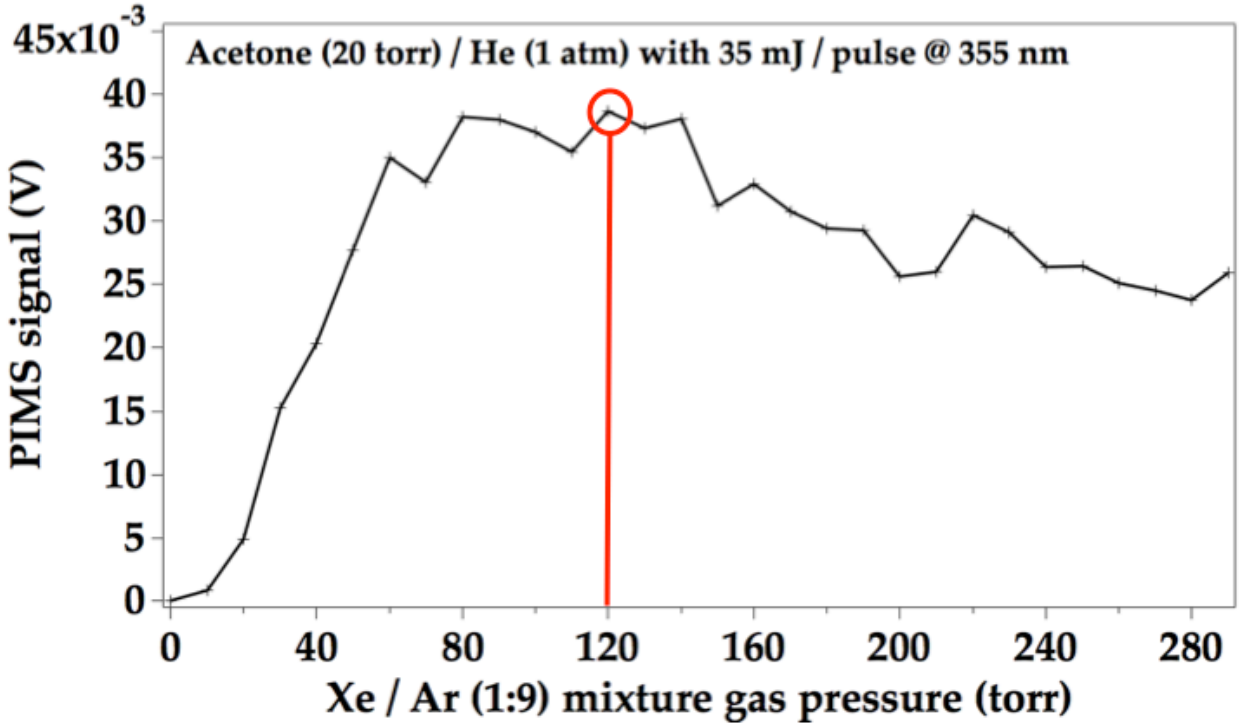

Figure 2.4 PIMS signal change depending on the Xe : Ar (1:9) total pressure. While increasing mixture gas pressure, PIMS signal shows a steep slope and maximizes at 120 torr of total pressure. After that, PIMS signal gradually decreases.

2.3.2. Reflectron

The advantage of Wiley and McLaren's two-step acceleration mass spectrometer is space focusing.[13] Two ions formed at different positions will be focused at a point at the same time where a detector is located. This is true, if each ion has the same initial kinetic energy, but each ion has its own traverse velocity to the molecular beam stream, even some ions might have an opposite directional initial kinetic energy. To solve this problem, a two-step reflectron is installed at the end of the field free region (See Fig. 2.5).

When two ions arrive at the reflectron, due to the different initial kinetic energy, two ions penetrate into and decelerate respectively.

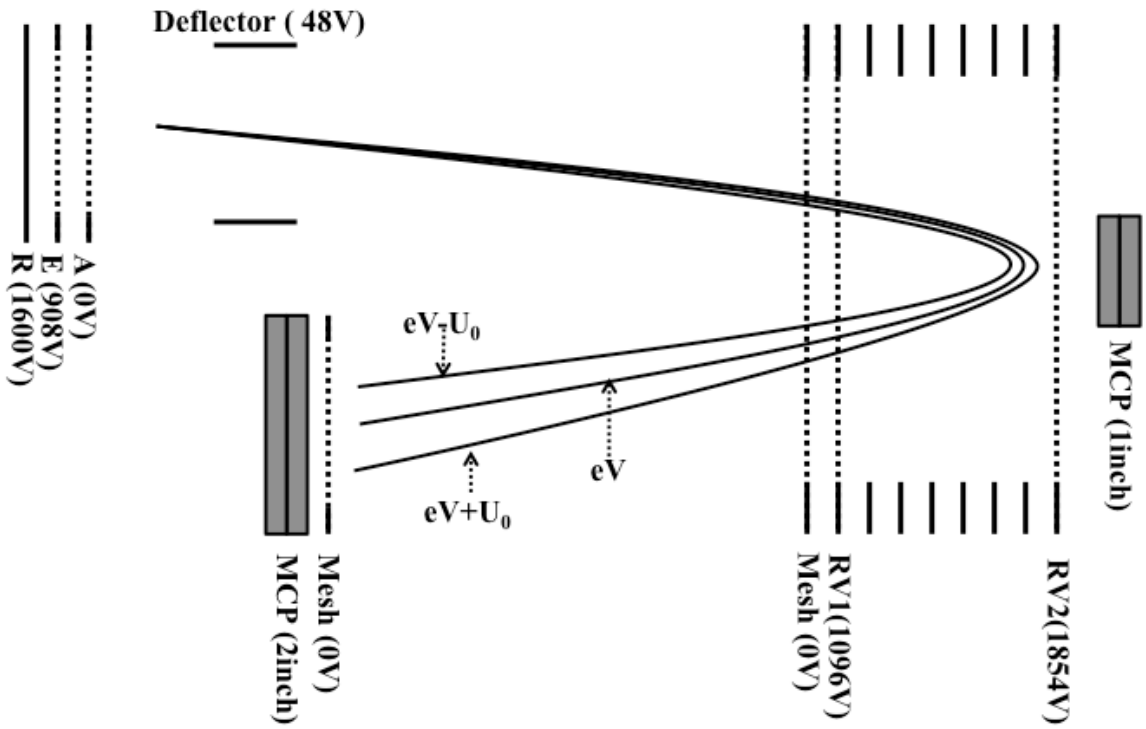

Figure 2.5 Dual stage electrostatic mirror (Refletron). The ions with $+U_0$ more penetrate into the electric field, while the ion with $-U_0$ less penetrate.

More energetic ion penetrates more deeply while the less energetic ions makes a shallow entrance. These two ions are re-accelerated from the second region so the rest of process is the exactly same as Wiley and McLaren's two-step acceleration.

2.3.3 Microchannel Plate (MCP) Detector

The Microchannel plate (MCP) detector, an array of electron multipliers, is used for gathering ions and converting an ion signal into a current. A chevron type MCP detector is installed in the PIMS, in which two microchannel plates are stacked at 180º relative to each other. The ions transmitted by the reflectron fly through a field-free

region and arrive on a mesh biased at 0 V. Because two MCPs are biased by -1000 V respectively, the ions passing through a mesh accelerate into the first MCP and trigger an electron cascade on a channel wall, after which induced electrons trigger an electron cascade in the second MCP again. An electron signal is amplified by over 10^7 times through the electron avalanche in a chevron type MCP detector and hit a grounded metal anode on the back. Consequently, MCP detector turns an ion signal into a current signal. (Fig. 2.6)

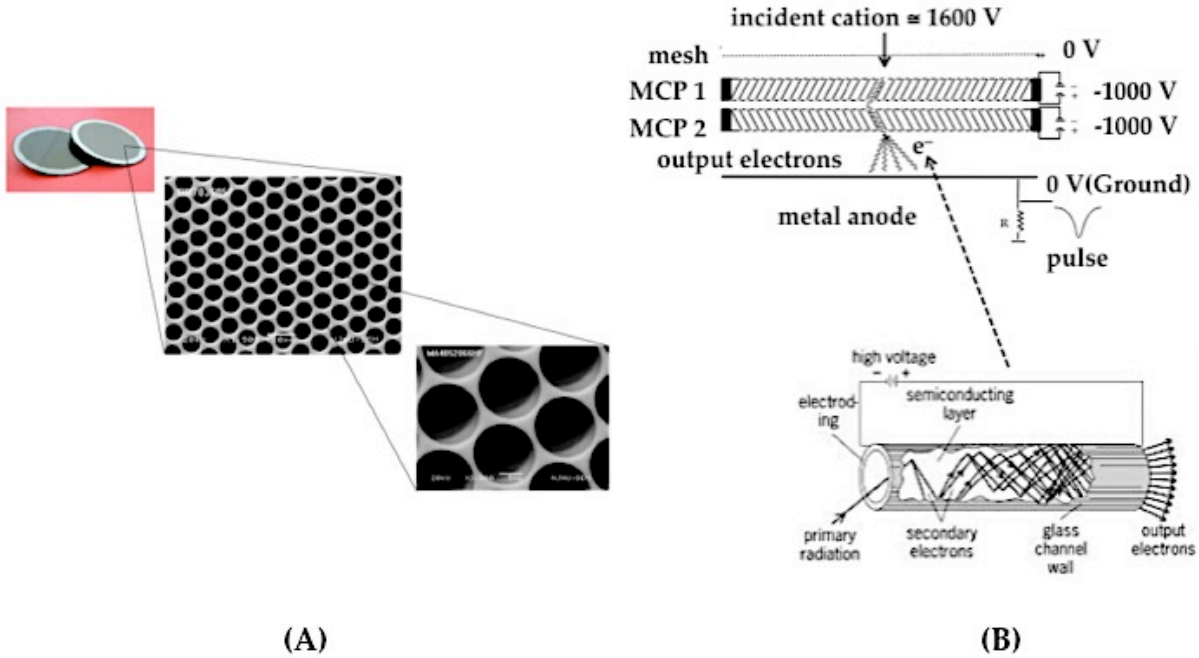

Figure 2.6 A magnified picture of a microchannel plate's surface: (A) Enlarged microchannel plate's surface: each pore represents single channel electron multiplier. (B) Chevron type microchannel plates' description: incident cation triggers an electron avalanche, which makes a current.[14]

2.3.4 Data Acquisition

Data acquisition is performed using a 12 bit digitizer PCI card (GAGE CS 12400) and a Labview program, in which a current signal from MCP detector at a repetition rate of 10 Hz is transformed into a voltage signal and time-of-flight is converted to mass-to-charge. Each spectrum is averaged over 400 — 2000 scans to get a better signal-to-noise ratio.

2.4 Matrix Isolation Fourier Transform Infrared Spectrometer

In the pyrolysis of complex fuels, many reactive species (such as organic radicals and metastables) are produced. Because of the instability of these intermediates, it is difficult to identify them using conventional techniques.[15] In matrix isolation system, products are embedded in an inert solid at the very low temperature (roughly 20 K) and secondary chemical reactions are averted. Because of the dilute gas mixture, typically 0.1 %, the reactive species, such as radicals, are surrounded by inert argon atoms. The argon matrix is transparent to infrared absorption in which only isolated molecules absorb infrared. This makes it possible to study IR absorption spectroscopy of the products and the argon matrix vibrational frequencies are very close to gas phase data.[16] These characteristics make matrix isolation technique a powerful diagnostic tool for transient molecules.

At the exit of a heated SiC flow reactor, thermally decomposed molecules entrained in argon carrier gas supersonically expand into the vacuum. The expansion traverses 2 – 3 cm and impinges upon a cooled CsI window (about 20 – 30 K) that is connected to the cold finger of a cryostat. Because of very low temp of CsI window, most of molecular beams are deposited on the cold CsI window. Typical deposition

rates are about 4 monolayer sec^{-1} (4 ML sec^{-1}) at 10^{-5} torr. Since the VdW radius of Ar is 1.88 Å (1.88×10^{-8} cm), there are $[1.88 \times 10^{-8}]^{-1}$ or 5.3×10^{7} Ar atoms in 1 cm so 1 ML is 2.8×10^{15} Ar atoms cm^{-2}. Consequently in 1 hour, (60 x 60 x 4) ML will be deposited. This corresponds to ($1.4 \times 10^{4} \times 2.8 \times 10^{15}$) or 4×10^{19} Ar atoms cm^{-2} (6.7×10^{-5} moles cm^{-2}). The thickness of the matrix will be about ($1.4 \times 10^{4} \times 1.88 \times 10^{-8}$) cm or 2.7×10^{-6} m or 2.7 micron. After accumulating samples for about 1 hour, the infrared spectrum of the sample is acquired using a commercial FT-IR spectrometer (Nicolet 6700 Advanced) with MCT A and/or B detectors.

Reference for Chapter II

(1) Chen, P.; Colson, S. D.; Chupka, W. A.; Berson, J. A. *Journal of Physical Chemistry* **1986**, *90*, 2319-2321.

(2) Chen, P.; Pallix, J. B.; Chupka, W. A.; Colson, S. D. *Journal of Chemical Physics* **1987**, *86*, 516-521.

(3) Kohn, D. W.; Clauberg, H.; Chen, P. *Review of Scientific Instruments* **1992**, *63*, 4003-4005.

(4) Blush, J. A.; Clauberg, H.; Kohn, D. W.; Minsek, D. W.; Zhang, X.; Chen, P. *Accounts Chem. Res.* **1992**, *25*, 385-392.

(5) Chen, P. In *Unimolecular and Bimolecular Ion-Molecule Reaction Dynamics*; Ng, C. Y., Baer, T., Powis, I., Eds.; John Wiley: Cambridge, UK, 1994, p 371-397.

(6) Rohrs, H. W.; Wickham-Jones, C. T.; Berry, D.; Ellison, G. B.; Argrow, B. M. *Rev. Sci. Instrum.* **1995**, *66*, 2430.

(7) Zhang, X.; Friderichsen, A. V.; Nandi, S.; Ellison, G. B.; David, D. E.; McKinnon, J. T.; Lindeman, T. G.; Dayton, D. C.; Nimlos, M. R. *Review of Scientific Instruments* **2003**, *74*, 3077-3086.

(8) Guan, Q.; Daily, J. W. **2013**, *to be published*.

(9) Vasiliou, A.; Piech, K. M.; Reed, B.; Zhang, X.; Nimlos, M. R.; Ahmed, M.; Golan, A.; Kostko, O.; Osborn, D. L.; Urness, K. N.; David , D. E.; Daily, J. W.; Stanton, J. F.; Ellison, G. B. *Journal of Chemical Physics* **2012**, *137*, 164308.

(10) Urness, K. N.; Golan, A.; Daily, J. W.; Nimlos, M. R.; Stanton, J. F.; Ahmed, M.; Ellison, G. B. *J. Chem. Phys.* **2013**, *in press*.

(11) There are at least five potential sources of error for measuring the temperature of the SiC tube. (a) The inherent accuracy of the thermocouple is listed by Omega Engineering as the greater of 4.5 ºC or 1.0% from 0 — 2320 ºC. (b) Imperfect thermal contact between the thermocouple and the SiC tube. This is difficult to quantify but it is probably not the dominant factor since most of the heat transfer is expected to be by radiation, at least at higher temperatures. (c) Cooling along the thermocouple wire away from the thermocouple junction/SiC contact point. This is probably the most important loss factor and is likely on the order of 10s ºC. (d) Extra radiative losses from the surface area added by the thermocouple. (e) The thermocouple cold junction is at the vacuum feedthrough instead of at the meter (where it would be properly compensated). The latter consideration probably contributes less than a few ºC to the error. The best way to determine the error is by experiment, either with a sample with known kinetics or by inserting a thermocouple inside the SiC tube during normal operation.

(12) The leak rate of Ar is measured through a pulsed reactor to be 1 Torr min^{-1} as it passes through a SiC reactor at 300 K that is pulsed at 20 Hz and opens for 1

msec. The Ar gas is leaking from a reservior of 1.2 L at 1 atm pressure. Since PV = nRT, we can use: $dn/dt = (dP/dt)(V/RT) = (1\ \text{Torr min}^{-1})\ (1.2\ \text{L})\ (62.4\ \text{Torr L mol}^{-1}\ \text{K}^{-1} * 300\ \text{K})^{-1}$ which yields $dn/dt = 6.4 \times 10^{-5}$ mol min^{-1} or 1×10^{-7} mol sec^{-1}. The pulsed valve fires at 20 Hz and delivers 3×10^{16} Ar atoms pulse^{-1}. Typical gas mixtures are 1 Torr CH_3CHO in 1 atm Ar or 0.1 %; consequently the reactor delivers about 4×10^{13} organics pulse^{-1}.

(13) Wiley, W. C.; McLaren, I. H. *Review of Scientific Instruments* **1955**, *26*, 1150-1157.

(14) Wiza, J. L. *Nuclear Instruments & Methods* **1979**, *162*, 587-601.

(15) Jacox, M. E. *Chemical Society Reviews* **2002**, *31*, 108-115.

(16) Jacox, M. E. *Journal of Molecular Spectroscopy* **1985**, *113*, 286-301.

Chapter III Pyrolysis of 2-methylfuran and 3-methylfuran

3.1 Introduction

Both 2-methylfuran (2MF) and 2,5-dimethylfuran (DMF) have been proposed as a 2nd generation biofuels. Compared to the ethanol in current use, 2MF has several practical advantages.[1,2] In recent years, the transformation from lignocellulosic biomass to biofuels by a few chemical steps provides a direct, practical pathway to the production of 2MF and DMF. A major advantage of these improved methods is that they do not use edible resources but to utilize non-food biomass.[3]

While 2MF is being considered as a biofuel, there are a few data of combustion or pyrolysis of this oxygenated aromatic. In 1985, Grela *et al.*[4] pyrolyzed 2MF at low pressures (1 mTorr) in a heatable molecular flow reactor over the temperature range 1050 – 1270 K and analyzed the products with on-line EI-mass spectrometer. They concluded that the unimolecular reaction of 2MF was initiated by ring opening, making a biradical which rearranged to the final products *via* plausible intromolecular H-atom transfer. They observed ions of m/z 54 (C_4H_6), 39 (C_3H_3), and 28 (CO), in which 39 (C_3H_3) was attributed to the fragment of the m/z 54 (C_4H_6). The major product was carbon monoxide. Analysis of the kinetics of decomposition yielded a rate constant, log ($k_{1,2MF}$, s^{-1}) = 15.3 – 74.2/θ, (θ = 4.575 × 10^{-3}T kcal/mol). Methylating the furan ring resulted in higher decomposition rates.[4] Sometime later, Lifshitz *et al.*[5] performed a single pulse shock tube experiment of the mixture gas (700 Torr) of 0.5% 2MF with argon gas at temperatures of 1100 – 1400 K. The products were identified *via* gas chromatographic analysis with packed columns. It was concluded that the initial unimolecular decomposition step was characterized by two channels: 1,2 shift of

hydrogen atom from 5 carbon to 4 carbon and methyl group migration from 2 carbon to 3 carbon.

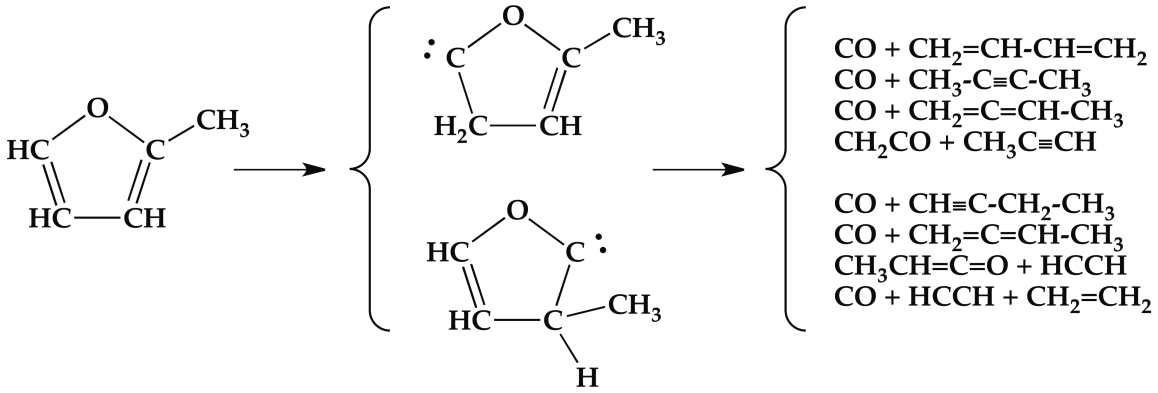

Figure 3.1 Pathway proposed[5] for the unimolecular decomposition of 2MF.

The first channel produced CO and the isomers of C_4H_6, or CH_2CO, and two isomers of C_3H_4 while the second channel generated CO and the isomers of C_4H_6, or CO, C_2H_2 and C_2H_4. The C_4H_6 isomers were identified as 1,3-butadiene, 1-butyne, 1,2-butadiene, and 2-butyne. Similar to Grela *et al.*, the kinetics data showed that alkylation of the ring increased the rate constant.[5] In 2009, Simmie and Curran carried out *ab initio* electronic structure calculations of enthalpy of formation and bond dissociation energies of alkylfurans. It was found[6] that the dissociation energies of the ring hydrogens were very high. This would be expected from the large C-H bond energy measured[7] for the parent compound, furan; DH_{298}(furyl-H) = 120 ± 2 kcal mol^{-1}. In contrast, the CH bonds of the methyl groups are much weaker because the resultant radicals are benzylic. This implies that methylation of the furan ring will lead to increased reactivity which is supported by the experimental shock tube findings of Grela *et al.*[4] and Lifshitz *et al.*[5]

More practical experiments have been carried out to characterize the performance 2MF in an engine. Thewes *et al.*[8] and Wu *et al.*[9] did the combustion experiment of 2MF compared to conventional research octane number (RON) 95 fuel, ethanol, and DMF using a direct-injection spark-ignition engine. They concluded that 2MF has shorter combustion delay, especially in cold condition, 61% reduction of hydrocarbon emission but more nitrogen oxides issue, better knocking suppression than conventional fuel, and produces 30 % less aldehyde than gasoline and bio-ethanol.[2,8]

In these earlier studies, reaction times varied in the range of msec — sec and gas chromatography (GC/FID) was used for product identification. It was difficult to detect radicals and/or short-lived metastables. In contrast to these studies, the use of a heated microtubular reactor with its spectroscopic detection techniques makes it possible to identify all the products resulting from pyrolysis of 2MF. Earlier studies[10] of the pyrolysis of the parent compound, furan, were carried out in such a heated microflow tube. Two channels for unimolecular decomposition of furan were identified which went through a α-carbene or a β-carbene intermediate; see Scheme I. The decomposition products were found to be CH_2=C=O and HCCH (*via* the α-carbene) and CH_3CCH, CO, $HCCCH_2$ and H atoms resulting from the β carbene.

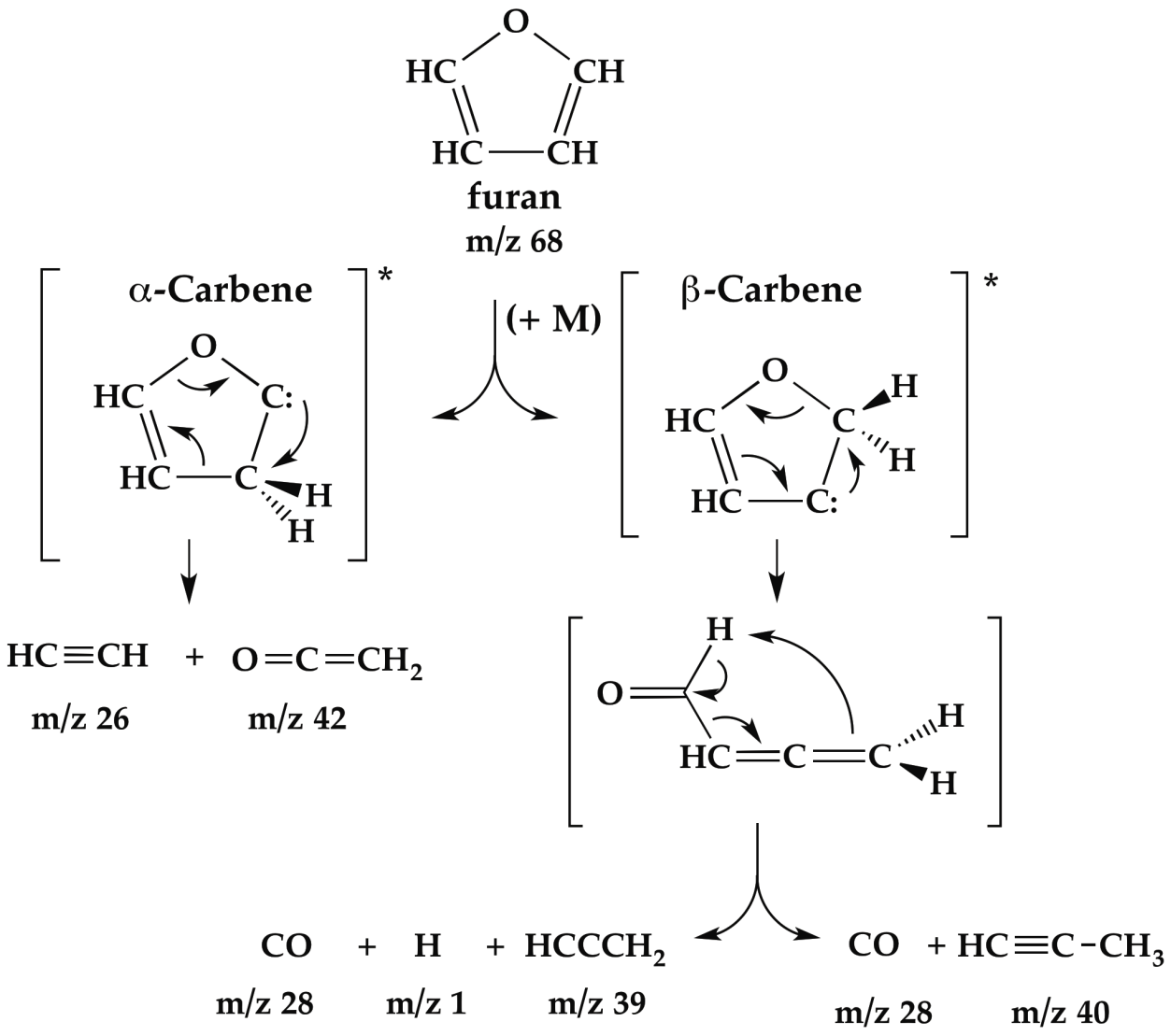

Figure 3.2 Pyrolysis Mechanism[10,11] for Furan.

This mechanism has recently been verified and the branching ratios were measured.[11]

Based on these earlier studies of the pyrolysis of furan,[10,11] a mechanism for thermally decomposing 2-methylfuran is proposed in Figure 3.3.

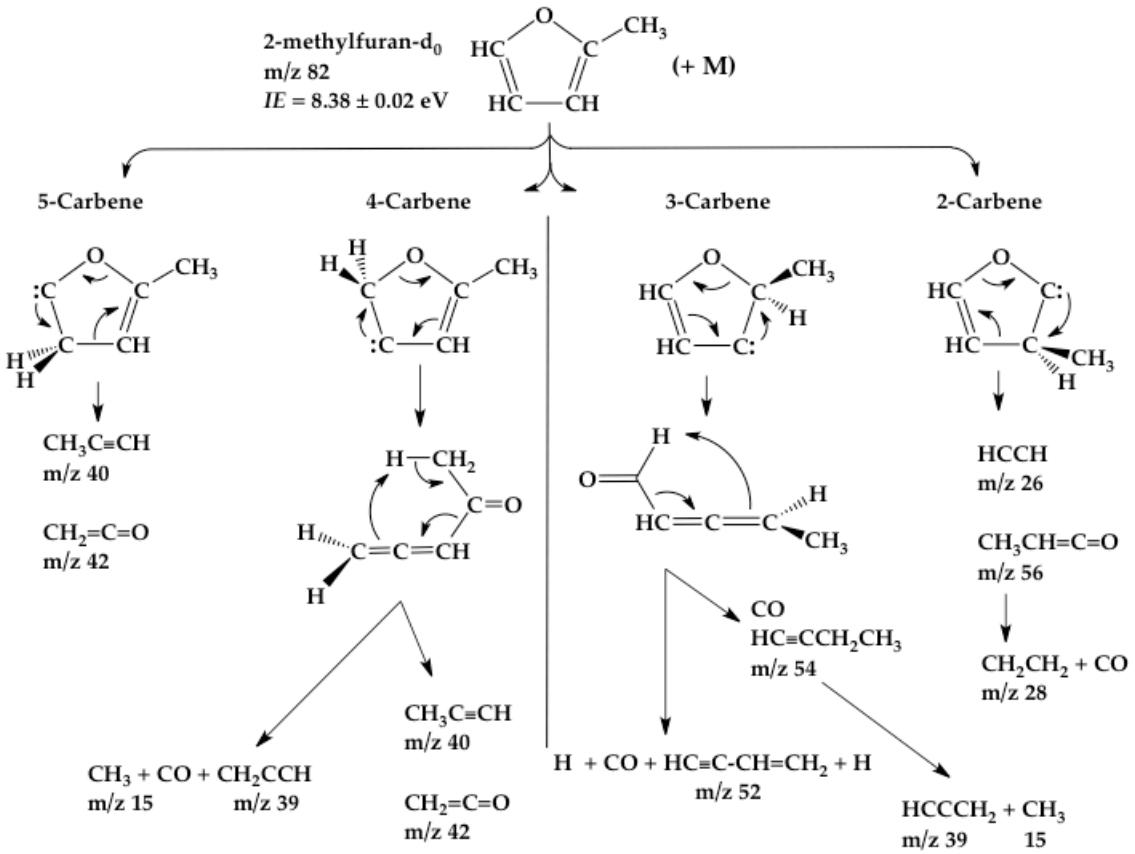

Figure 3.3 Predicted mechanism of thermally decomposed 2-methylfuran.

Unlike furan, the asymmetry of 2MF suggests four carbene intermediates. Rearrangement of the methyl group from C(2) to C(3) generates the 2-carbene which yields HC≡CH and $CH_3CH{=}C{=}O$. Methylketene is not stable in the heated microreactor and $CH_3CH{=}C{=}O$ is anticipated to fragment to $CH_2{=}CH_2$ and CO: $CH_3CH{=}C{=}O$ (+ M) → CO + [CH_3CH] → CO + CH_2CH_2. Migration of H from C(3) to C(2) produces the 3-carbene. This carbene rearranges to an allenyl aldehyde which can fragment in two ways. Isomerization of the allenyl aldehyde yields CO and $HC{\equiv}CCH_2CH_3$. Alternatively the allenyl aldehyde could fragment as: $HCO{-}CH{=}C{=}CHCH_3$ → [H + CO + $HC{\equiv}C{-}CH{-}CH_3$] → H + CO + $HC{\equiv}C{-}CH{=}CH_2$ + H. It would be expected that the

product $HC{\equiv}C\text{-}CH_2CH_3$ would decompose to propargyl radical, $HCCCH_2$, and methyl radical.

The 4-carbene would be expected to isomerize to the ketone, $CH_2{=}C{=}CH\text{-}CO\text{-}CH_3$ which can subsequently fragment in two different ways. Rearrangement to $CH_3C{\equiv}CH$ plus $CH_2{=}C{=}O$ is possible or fragmentation to the radical set (CH_3 + CO + $HCCCH_2$) is possible. Finally, 2MF could isomerize to the 5-carbene which will fragment to $CH_3C{\equiv}CH$ and $CH_2{=}C{=}O$.

To test this mechanism, samples of 2MF were pyrolyzed in a heated microtubular reactor.

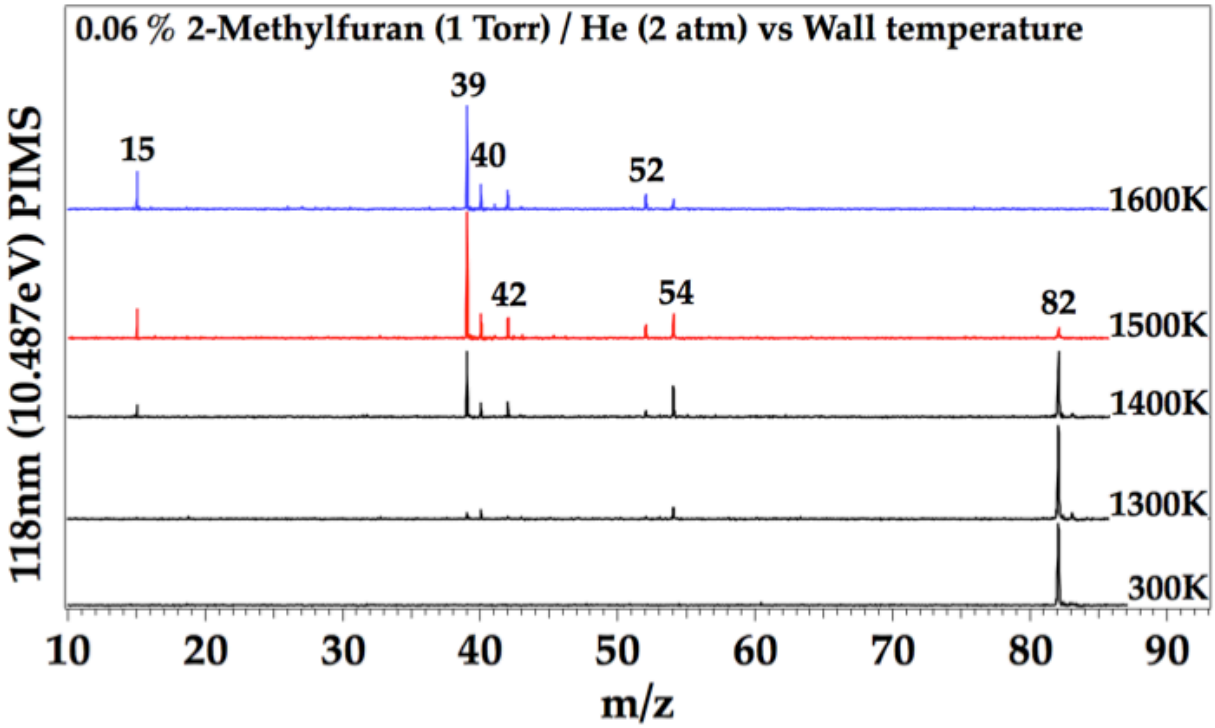

Figure 3.4 PIMS spectra of pyrolysis of 2MF at various temperatures.

3.2 Results and Discussion

PIMS spectra of thermally decomposed 2MF are shown in Figure 3.4. At 300 K, m/z 82 is 2MF parent ion and its isotope is m/z 83. The isotope ratio (83/82) is measured to be 5.4%. The ionization energy of 2MF has been reported[12] to be 8.38 ± 0.02 eV. Although 2MF is ionized by the 118.2 nm VUV (10.487 eV) PIMS, no fragmentation of 2MF is observed.

When the SiC nozzle is heated up to 1300 K (SiC nozzle wall temperature), tiny signals are observed at m/z 39, 40, and 54, which are likely to be from ionization of CH_2CCH, $CH_3C{\equiv}CH$, and $HC{\equiv}CCH_2CH_3$. Ionization energies for propargyl radical,[13] propyne,[14] and 1-butyne[15] are reported as: 8.674 ± 0.001 eV, 10.36744 ± 0.00025 eV, and 10.20 ± 0.02 eV, respectively. Because 10.487 eV VUV is used, these three species can be ionized. While SiC nozzle wall temperature increased to 1600 K, m/z 39, 40, and 54 peaks intensify and new products, m/z 15, 42, and 52, appeared. These species result from ionization of CH_3, $CH_2{=}C{=}O$, and $HC{\equiv}C\text{-}CH{=}CH_2$. Ionization energies for methyl radical,[16] ketene,[17] and vinylacetylene[15] are reported as: 9.8380 ± 0.0004 eV, 9.6191 ± 0.0004 eV, and 9.58 ± 0.02 eV.

Fig. 3.3 suggested that 1-butyne would decompose to CH_3 and CH_2CCH. In order to confirm this reaction, the PIMS spectrum of the pyrolysis of 1-butyne was studied, Fig. 3.5.

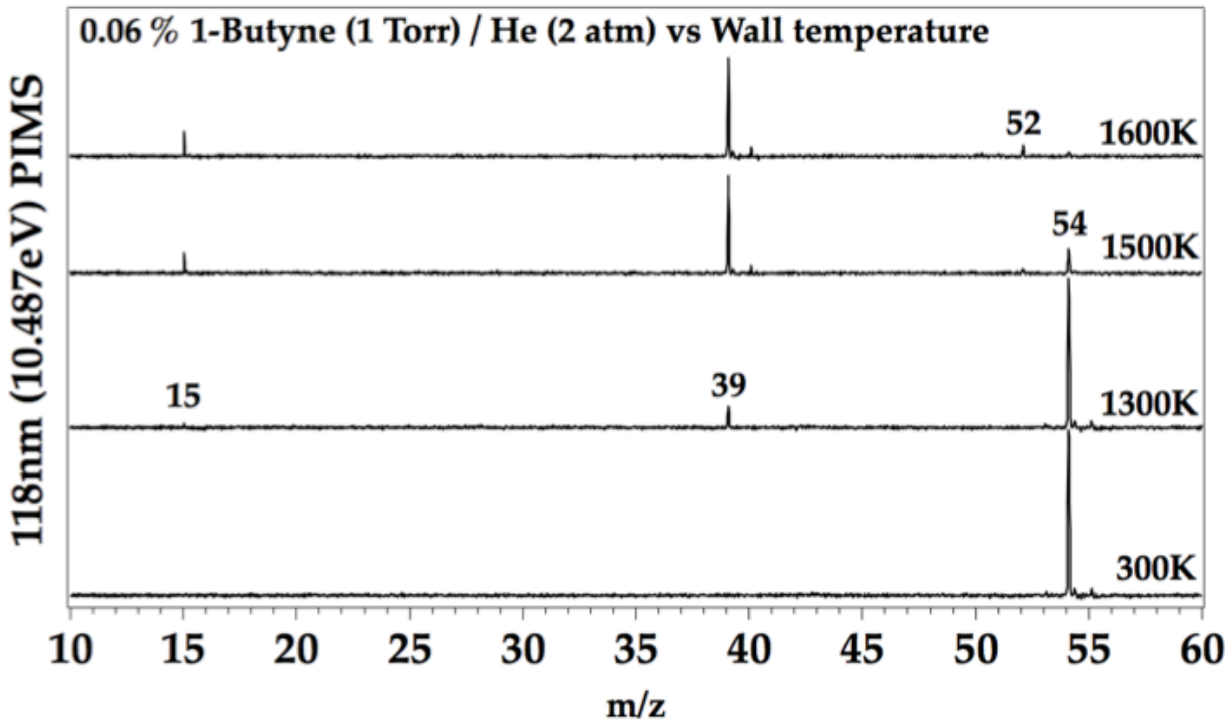

Figure 3.5 PIMS spectra for pyrolysis products of HC≡C-CH_2CH_3.

At 300 K only the HC≡CCH_2CH_3 parent peak, m/z 54, and the isotope peak, m/z 55, are observed. The isotope ratio (55/54) is 4.3%. Heating the reactor to 1300 K leads to the production of ions at m/z 15 and m/z 39 which originate from CH_3 and HCCCH_2. Further heating to 1600 K leads to the destruction of the parent m/z 54. At 1600 K, a small signal at m/z 52 is detected and is assigned to HC≡C-CH=CH_2. The pyrolysis of 1-butyne (m/z 54) in Fig. 3.5 confirms that HCC-CH_2CH_3 is a product in the thermal cracking of 2MF. These spectra validate the 3-carbene pathway in Fig. 3.3.

It is difficult to differentiate between the 4-carbene and 5-carbene products in Fig. 3.3. Both are predicted to generate CH_3CCH (m/z 40) and CH_2=C=O (m/z 42). One possible avenue to demonstrate the presence of both the 4-carbene and 5-carbene channels would be to deuterate 2MF. Figure 3.6 presents the predicted pyrolysis mechanism of 2MF-d_3.

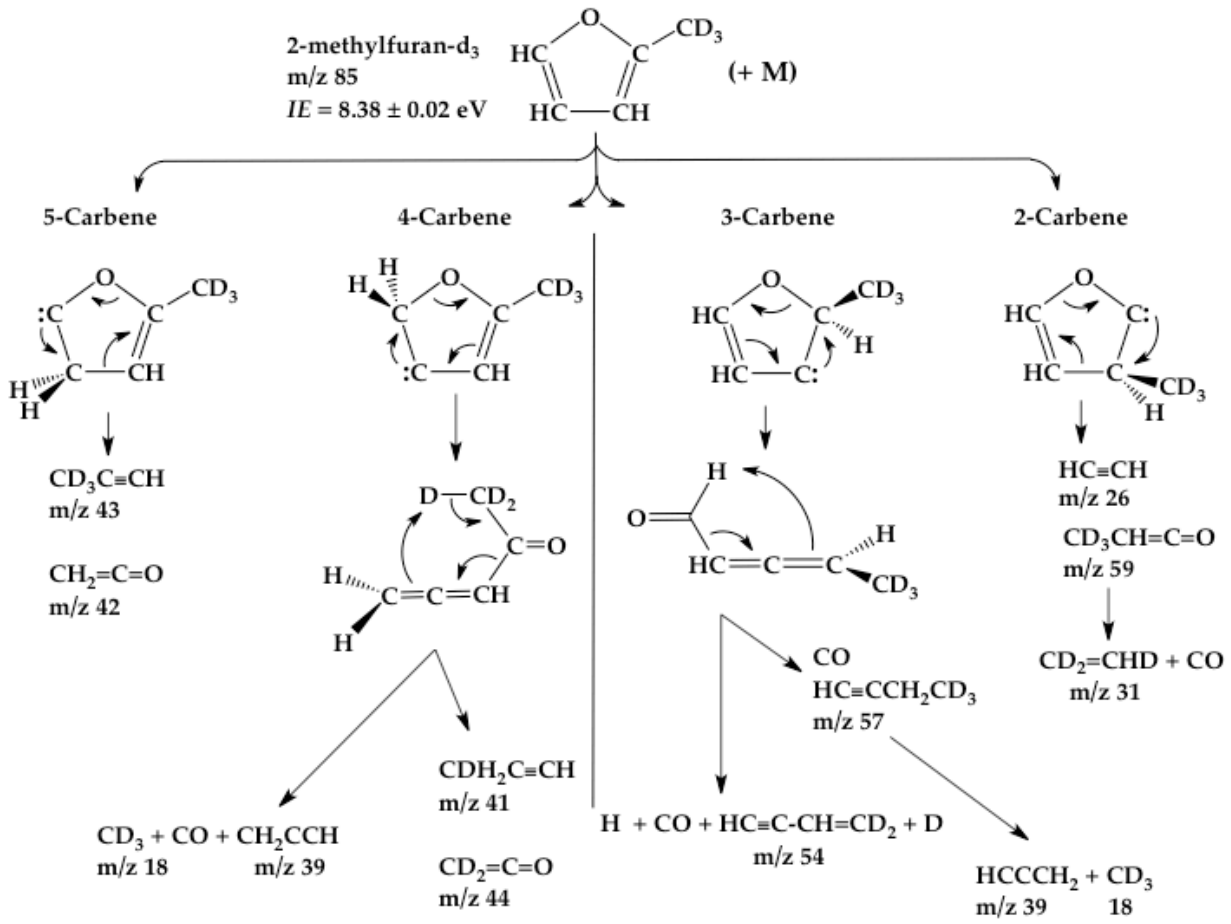

Figure 3.6 Predicted pyrolysis mechanism of 2MF-d_3 based on the Scheme in Fig. 3.2.

The –CD_3 group induces the formation of a precise set of deuterated products: CD_3CH=C=O (m/z 59), CD_2=CHD (m/z 31) for the 2-carbene channel; HC≡C-CH_2CD_3 (m/z 57), HC≡C-CH=CD_2 (m/z 54), CD_3 (m/z 18) for the 3-carbene channel;

$HC{\equiv}CCDH_2$ (m/z 41), $CD_2{=}C{=}O$ (m/z 44), CD_3 (m/z 18) for the 4-carbene channel; and $HC{\equiv}CCD_3$ (m/z 43) in 5-carbene. The pyrolysis of a pure sample of 2-methylfuran-d_3 would be a useful test for the mechanism in Fig. 3.6.

A sample of 2MF-d_3 was synthesized by Dr. Jeffrey Gazaille and Prof. Tarek Sammakia. The 2MF-d_3 sample was contaminated by lingering portions of the solvents, tetrahydrofuran (THF) and diethyl ether. NMR spectroscopy revealed that the mixture ratio of [2MF-d_3 : THF : diethyl ether] was [1 : 0.4 : 0.58]. To deal with this mixture, separate PIMS spectra were measured for THF and $CH_3CH_2OCH_2CH_3$. Then pyrolysis of the (2MF-d_3, THF, diethyl ether) mixture was examined by PIMS. The results are shown in Fig. 3.7.

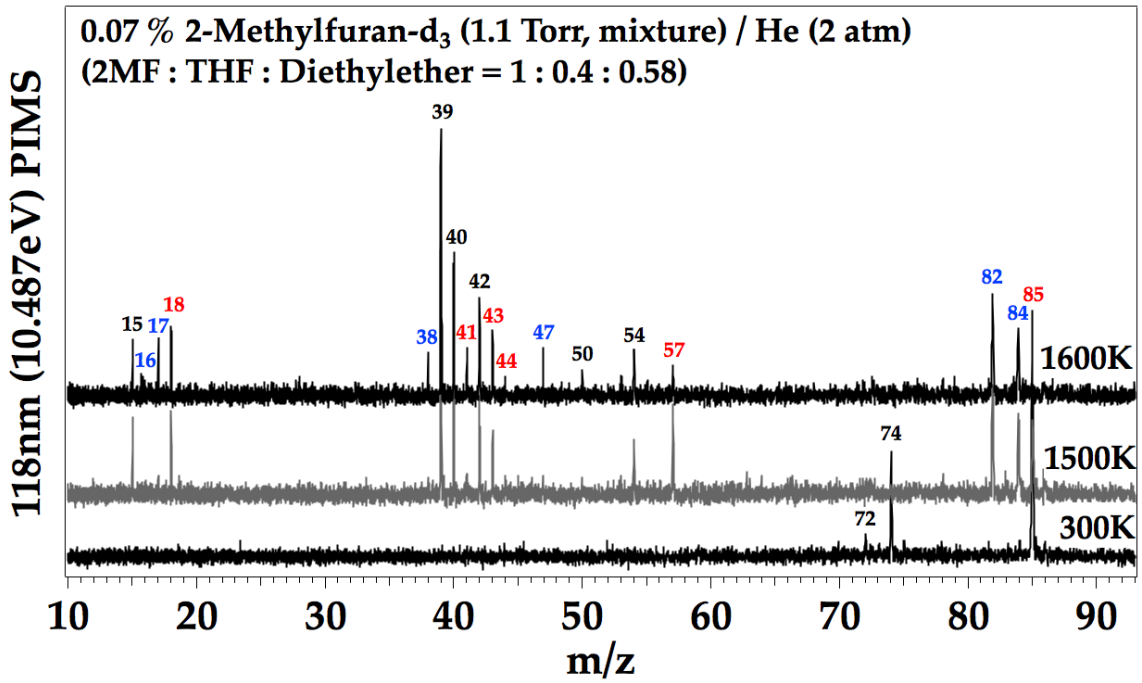

Figure 3.7 PIMS spectra of pyrolysis of 2MF-d_3 at reactor temperatures of 300 K, 1500 K, and 1600 K.

In Fig. 3.7 the ion peaks in black were present in the PIMS spectra of pyrolysis of THF and/or $CH_3CH_2OCH_2CH_3$. The blue and red colored numbers are assigned as the product ions from 2MF-d_3. At 300 K, only the parent ions are detected; THF (m/z 72), $CH_3CH_2OCH_2CH_3$ (m/z 74), and 2MF-d_3 (m/z 85). Increasing the SiC wall temperature to 1500 K induces the formation of ions at m/z 15, 18, 39, 40, 42, 43, 54, 57, 82, and 84. Further heating of the SiC reactor to 1600 K leads to the destruction of the parent 2MF-d_3 (m/z 85) and the production of new features at m/z 16, 17, 38, 41, 44, 47, and 50. Among these ion signals, the blue and red colored ones are to be considered. The ion peaks encoded in red are m/z 18, 41, 43, 44, and 57. These ions originate with CD_3, CDH_2-C≡CH, CD_3C≡CH, CD_2=C=O, and HC≡C-CH_2CD_3, respectively. Because

$CD_3C{\equiv}CH$ is predicted by the 5-carbene, the presence of this channel is confirmed by the detection of m/z 43. In the same manner, CDH_2-C≡CH and CD_2=C=O verify the 4-carbene channel while $HC{\equiv}CCH_2CD_3$ is a signature for the 3-carbene channel. Because 3-carbene channel was confirmed with m/z 52 and 54 earlier, this is doubly proved. The blue-encoded ions at m/z 16 and 17 look originate from CDH_2 and CD_2H. These radicals are likely the result of rapid H atom/CD_3 exchanges:

$$\mathbf{CD_3 + H \rightleftharpoons CD_3H^* \rightleftharpoons CD_2H + D}$$

Hydrogen atom exchanges with methyl radicals were observed[18] in earlier studies of the pyrolysis of CH_3CDO and CD_3CHO.

$$\mathbf{CH_3 + D \rightleftharpoons CH_3D^* \rightleftharpoons CH_2D + H}$$

The remaining ions, m/z 38, 47, 82, and 84, are not assigned and likely result from bimolecular reactions.

From the PIMS studies in Figs 3.4, 3.5, and 3.7, we confirm the presence of the 3-carbene, 4-carbene, and 5-carbene pathways. The products from the 2-carbene channel are HC≡CH and CH_3CH=C=O. Since the *IE*(HC≡CH) is 11.4006 ± 0.0002 eV, acetylene[19] cannot be detected with 10.487 eV VUV PIMS. *IE*(CH_3CH=C=O) has been reported[20] to be 8.95 eV but m/z 56 was not detected in PIMS spectra. One possibility is that methylketene is unstable in the hot reactor. Fragmentation of CH_3CH=C=O would produce CO and methylcarbene, [CH_3CH]. Instant isomerization of methylcarbene to CH_2=CH_2 would certainly ensue and ethylene could be observed in the IR spectrum. We have used matrix IR spectroscopy to hunt for the ethylene that would result from methylketene decomposition.

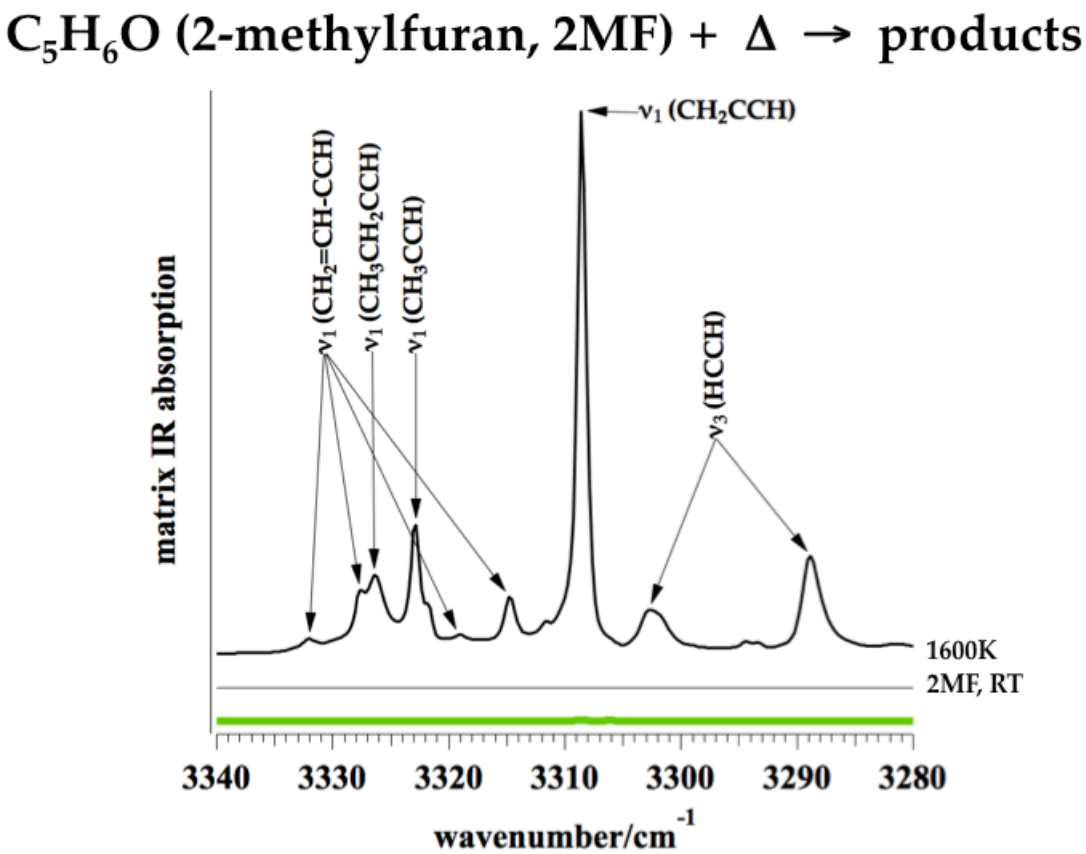

Figure 3.8 Argon matrix FT-IR spectrum of thermally decomposed 2MF at 1600 K. The green trace indicates background absorption of the buffer gas, Ar, heated to 1600 K; the narrow black spectrum is 2MF at room temperature; and the thick black spectrum results from heating 2MF to 1600 K.

In Fig. 3.8 is the argon matrix FT-IR spectra in the ≡C-H stretching region of the pyrolysis products of 2MF at 1600 K. These IR spectra confirm the products revealed in PIMS in Fig. 3.3. Vinylacetylene[21,22] is observed, ν_1(CH_2=CH-C≡CH), at 3332, 3328, 3319, and 3315 cm^{-1} (the splitting of ν_1 is likely due to different sites in the argon matrix), 1-butyne is found at[23,24] ν_1(CH_3CH_2C≡CH) of 3326 cm^{-1}, for propyne[10] the C-H stretch, ν_1(CH_3C≡CH), is at 3323 cm^{-1}, the propargyl radical[25] ν_1(CH_2CCH) is 3309 cm^{-1}, and the Darling-Dennison splitting in acetylene[10] ν_3(HC≡CH) is observed at 3303 and 3289 cm^{-1}.

A portion of the fingerprint region of the infrared spectrum of the pyrolysis products of 2MF at 1600 K is shown in Fig. 3.9. Carbon monoxide (both ^{12}CO and ^{13}CO) and ketene,[10] ethylene, and acetylene,[10] are detected in the mid-IR region; $\nu_2(CH_2{=}C{=}O)$ is observed at 2142 cm^{-1}, $\nu_7(CH_2{=}CH_2)$ and $\nu_5(HC{\equiv}CH)$ are present at 947 and 737 cm^{-1}. The pyrolysis products of $CH_2{=}CH_2$ and CO detected by IR spectra confirm the 2-carbene channel. To be sure of the exact matrix frequencies of the vibrational modes of $CH_3CH_2C{\equiv}CH$ and $CH_2{=}CH_2$, we examined the infrared spectra of authentic samples of 1-butyne and ethylene.

$$C_5H_6O \text{ (2-methylfuran, 2MF)} + \Delta \rightarrow \text{products}$$

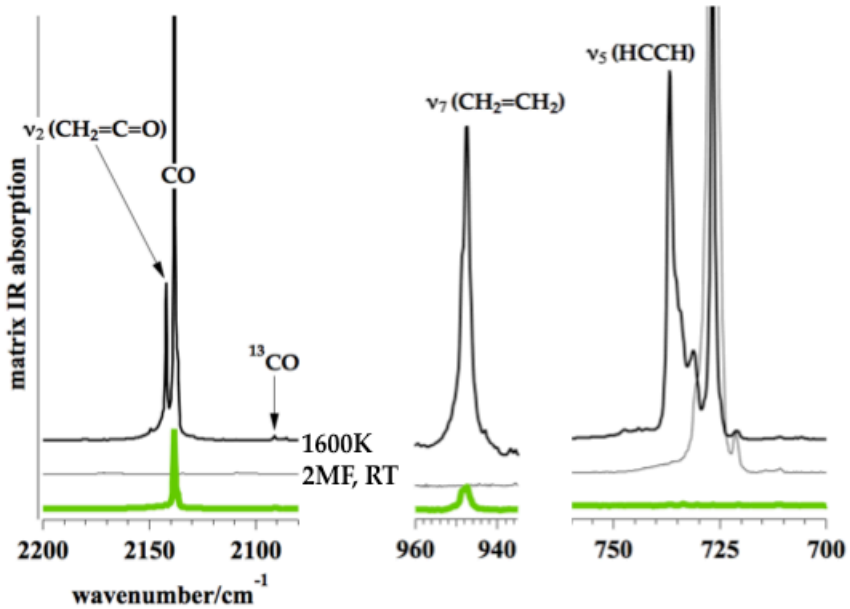

Figure 3.9 Argon matrix FT-IR spectrum of thermally decomposed 2MF at 1600 K in the mid IR range. The green trace indicates background absorption of the buffer gas, Ar, heated to 1600 K; the narrow black spectrum is 2MF at room temperature; and the thick black spectrum results from heating 2MF to 1600 K.

During the thermal decomposition of 2MF-d_3, we must be alert to the possible bimolecular reactions in the hot μtubular reactor. Lifshitz *et al.*[5] reported detection of CH_2=C=CH_2 (allene) in their shock tube experiments. A possible route for the formation of CH_2=C=CH_2 is shown in Fig. 3.10. Addition of H atoms to CH_3C≡CH could produce two isomeric vinyl radicals. Decomposition of these different radicals would produce H and CH_2=C=CH_2 or CH_3 and HC≡CH.

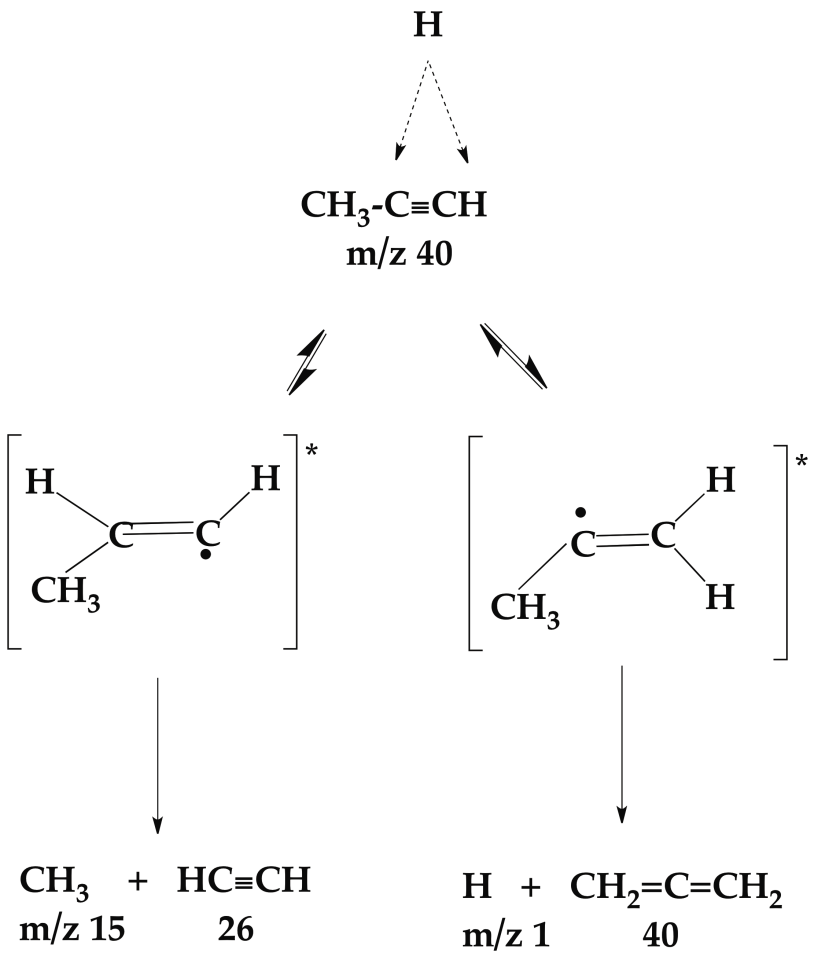

Figure 3.10 Methyl radicals or CH_2=C=CH_2 generation from (CH_3C≡CH, H atom) chemistry.

Both methylacetylene and allene are indistinguishable[14,26] in the 118.2 nm (10.487 eV) PIMS spectra in Fig. 3.4. But CH_3CCH and $CH_2{=}C{=}CH_2$ can be distinguished in the IR spectrum.

In preparation for a study of the IR spectra of 2MF pyrolysis, we show the infrared spectrum of an authentic $CH_2{=}C{=}CH_2$ sample in Fig. 3.11.

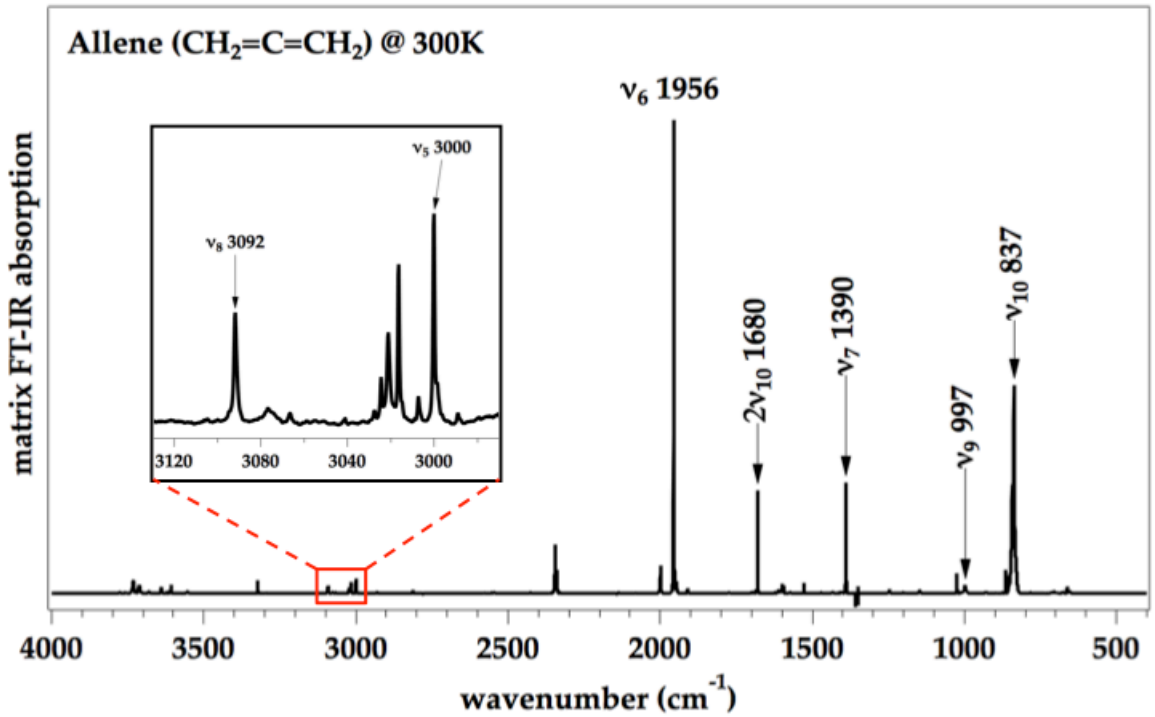

Figure 3.11 Argon matrix FT-IR spectrum of an authentic sample of $CH_2{=}C{=}CH_2$ at 300 K.

Fig. 3.12 is the IR spectrum of the products of pyrolysis of 2MF in a μtubular reactor heated to 1600 K. Comparison of IR spectrum in Fig. 3.12 with that of Fig. 3.11 reveals that most of the fundamentals of $CH_2{=}C{=}CH_2$ are present. In particular, the intense ν_6 is clearly present.

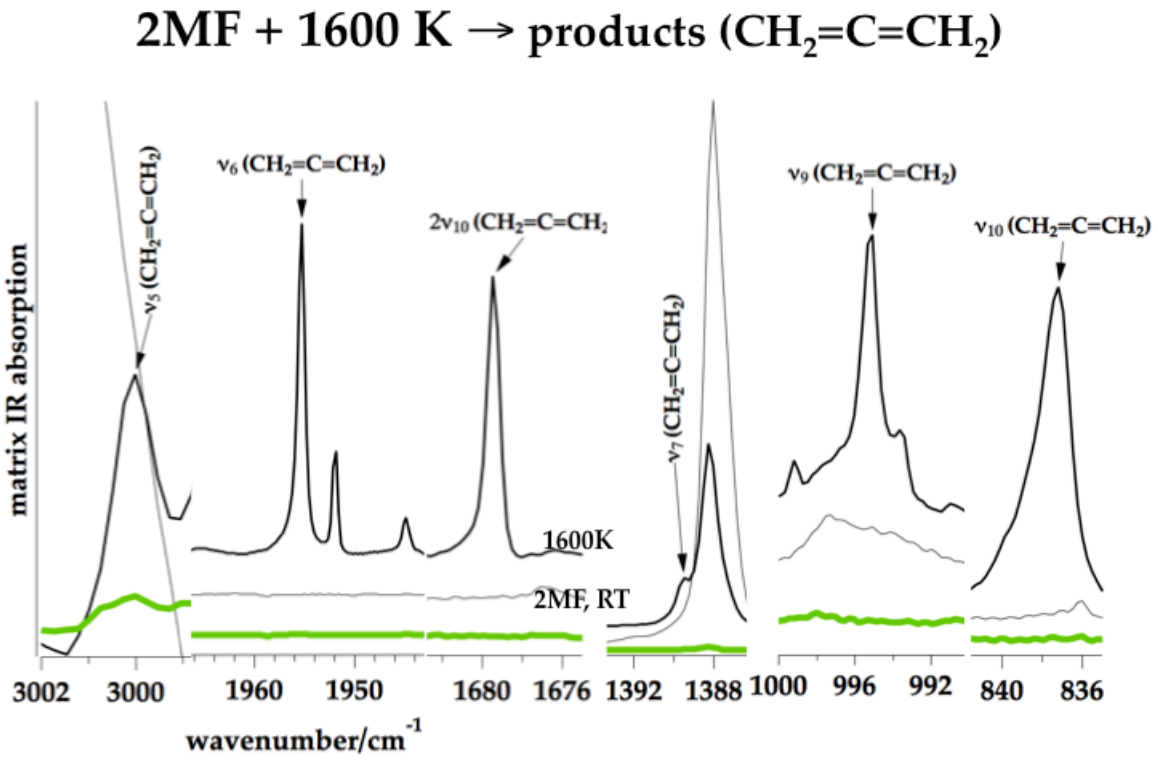

Figure 3.12 Argon matrix FT-IR spectrum of CH_2=C=CH_2 from pyrolysis of 2MF at 1600 K. The green trace indicates background absorption of the buffer gas, Ar, heated to 1600 K; the narrow black spectrum is 2MF at room temperature; and the thick black spectrum results from heating 2MF to 1600 K.

In an attempt to confirm the presence of allene, we examined the photoionization effiency curve (PIE) curve of m/z 40 following the pyrolysis of 2MF at 1600 K at LBNL's Advanced Light Source. The ionization energies for the two isomers of C_3H_4 are known. Allene is reported[26] as *IE* (CH_2=C=CH_2) = 9.6880 ± 0.0020 eV and while propyne[14] is *IE* (CH_3C≡CH) = 10.36744 ± 0.00025 eV. The PIE(m/z 40) resulting from the pyrolysis of 2MF is shown in Fig. 3.13 and there does not appear to any sign of allene. The PIE spectrum has an appearance energy around 10.3 eV and is best assigned as arising from CH_3C≡CH. It should be remembered that the IR spectrum in Fig. 3.12 and the PIE(m/z

40) in Fig. 3.13 result from different heated μtubular reactors. The IR spectra used a pulsed SiC reactor with Ar carrier gas to pyrolyze 2MF while the PIE spectrum results from a CW reactor with He buffer gas. The pulsed reactor using Ar gas is a SiC tube with a 1 mm diameter in contrast to the smaller, CW reactor with a 0.6 mm diameter. Of course another explanation could be that the ALS sample in Fig. 3.13 is simply too dilute for bimolecular (H atom, 2MF) chemistry to be important.

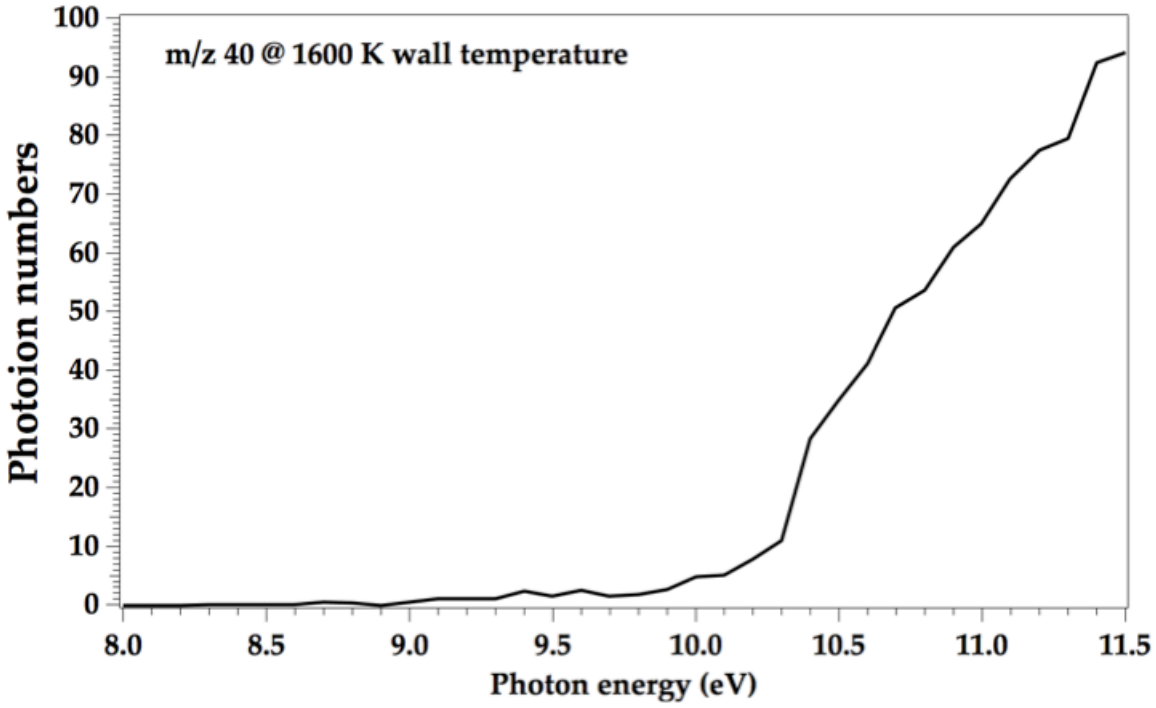

Figure 3.13 The PIE(m/z 40) curve resulting from pyrolysis of 2MF at 1600 K.

The proposed mechanism for thermal decomposition of 2MF in Fig. 3.3 seems to be verified. We have observed all products by both 118.2 nm PIMS and IR spectroscopy except $CH_3CH{=}C{=}O$. One may wonder why there is no detectable signals from

$CH_3CH{=}C{=}O$ in both PIMS and IR spectra, even though $CH_3CH{=}C{=}O$ is detectable in both diagnostic tools.

To explore this, the question of methylketene, we have investigated the pyrolysis of 3-methylfuran (3MF), an isomer of 2MF. Fig. 3.13 demonstrates that, like 2MF, 3MF could isomerize to the 2-carbene. Unlike 2MF, formation of the 2-carbene from 3MF involves an H- migration (rather than a CH_3- migration in Fig. 3.3).

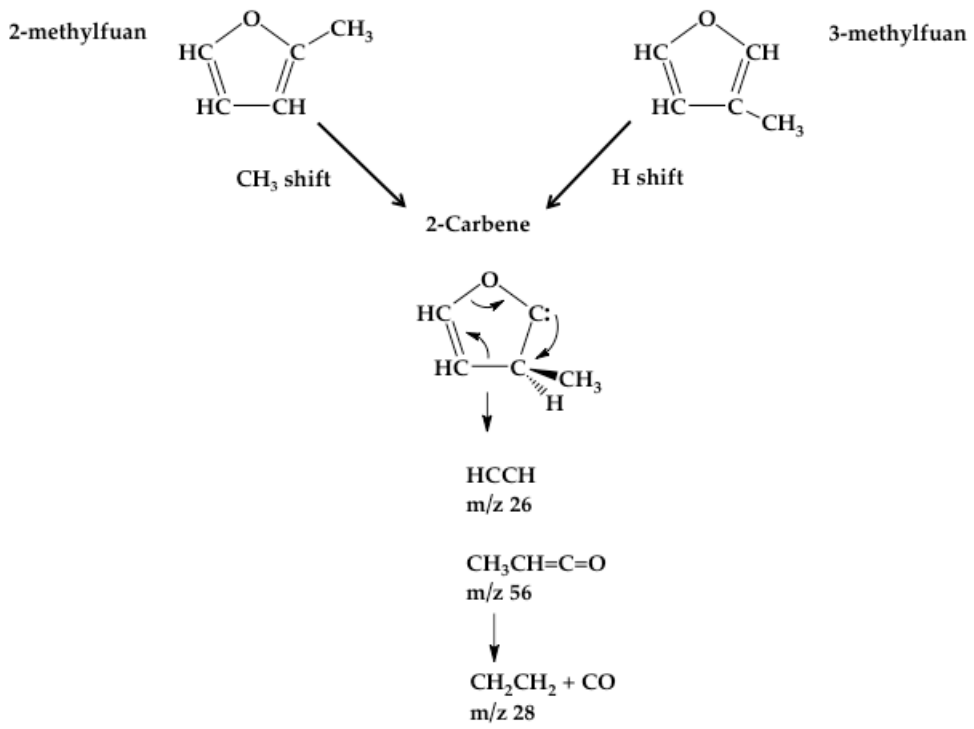

Figure 3.14 Both 2MF and 3MF can form the 2-carbene.

With this hypothesis, we subjected 3MF to pyrolysis and attempted to detect $CH_3CH{=}C{=}O$ in both the 118.2 nm PIMS and IR spectrometer. Fig. 3.15 is the complete, predicted mechanism for pyrolysis of 3MF. Many of the expected products are similar to that of 2MF (Fig. 3.3) but there are important differences.

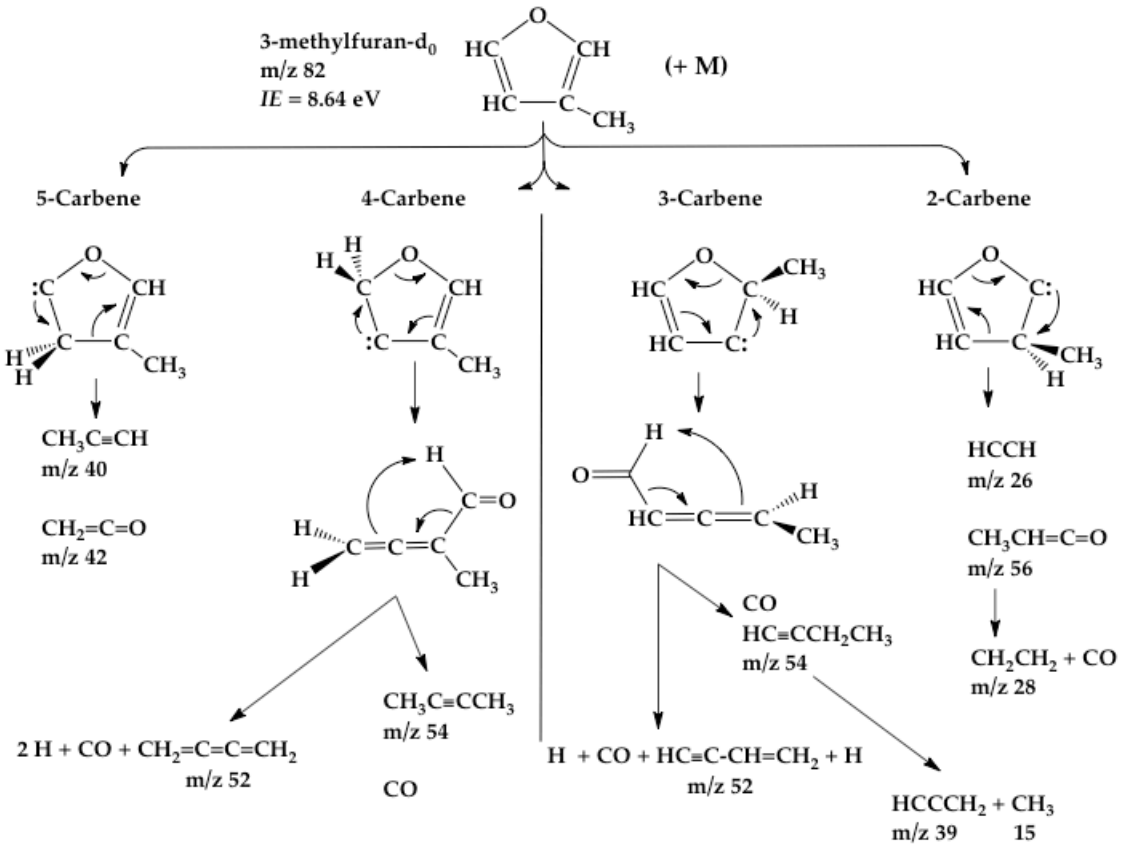

Figure 3.15 Predicted mechanism of thermally decomposed 3-methylfuran (3MF).

In Fig. 3.15, hydrogen atom migration from C(2) to C(3) leads to HC≡CH and $CH_3CH{=}C{=}O$ *via* the 2-carbene. This is identical to pyrolysis of 2MF (Fig. 3.3). Likewise CH_3 migration from C(3) to C(2) to produce the 3-carbene intermediate resulting in production of CO, $HC{\equiv}CCH_2CH_3$, H, and $HC{\equiv}C{-}CH{=}CH_2$. Again, this is identical to 2MF. Pyrolysis of 3MF to generate the 4-carbene leads to production of $CH_3C{\equiv}CCH_3$ (m/z 54) plus CO as well as to H, CO, $CH_2{=}C{=}C{=}CH_2$ (m/z 52). The 5-carbene from either 2MF or 3MF produces identical products: $CH_3C{\equiv}CH$ and $CH_2{=}C{=}O$. The scheme

in Fig. 3.15 predicts that there are two isomeric species for m/z 52 (CH_2=C=C=CH_2 and HC≡C-CH=CH_2) and for m/z 54 (CH_3-C≡C-CH_3 and HC≡C-CH_2CH_3).

Fig. 3.16 is the PIMS of the pyrolysis products from 3MF over the temperature range 300 K, 1400K, 1500 K, and 1600 K.

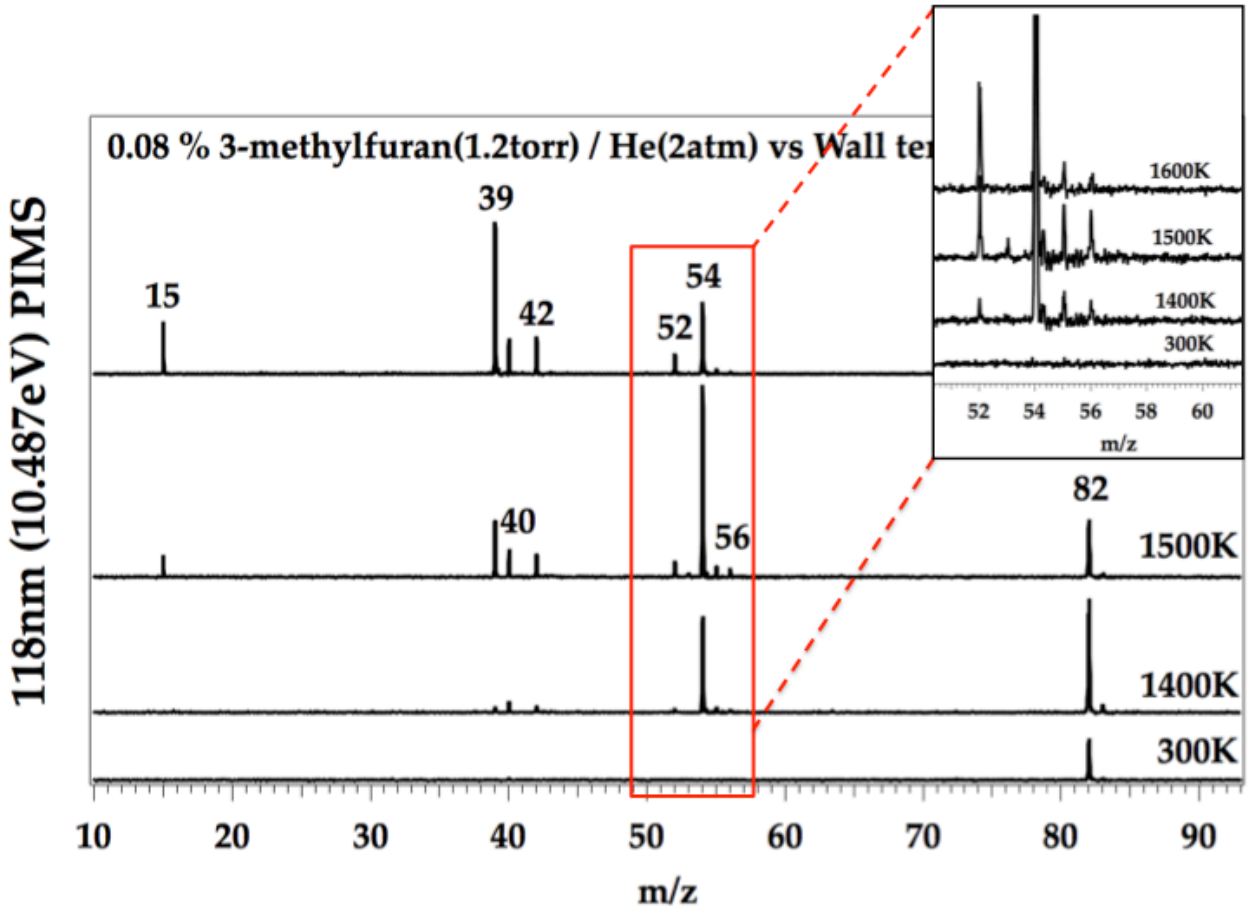

Figure 3.16 PIMS spectra of pyrolysis products of 3MF.

At 300 K, m/z 82 is 3MF parent ion and its isotope is m/z 83. The ratio of m/z (83/82) is measured to be 5.4 %. The ionization energy of 3MF was reported[27] to be 8.64 eV. Though 3MF is ionized by 10.487 eV VUV light, there is no dissociative ionization evidence. Heating the SiC nozzle to 1400 K, product ions are detected at m/z 39, 40 42, 52, 54, 55, and 56. Ions at m/z 39, 40, and 42 originate from propargyl radical,[28]

methylacetylene,[14] and ketene:[17] CH_2CCH, $CH_3C{\equiv}CH$, and $CH_2{=}C{=}O$. We believe that m/z 52 originates from both vinylacetylene[15] ($HC{\equiv}C\text{-}CH{=}CH_2$) and butatriene[15] ($CH_2{=}C{=}C{=}CH_2$) because of the infrared spectrum in Fig. 3.19. Likewise, the ions at m/z 54 result from a composite of $HC{\equiv}CCH_2CH_3^+$ and $CH_3C{\equiv}CCH_3^+$ as will be demonstrated by the IR spectrum[29]. In Fig. 3.16, the ratio of m/z (55/54) is 3.6 %, consistent with m/z 55 as the ^{13}C isotope ion peak of m/z 54. We believe the small signal at m/z 56 should be assigned to $CH_3CH{=}C{=}O$. Heating the SiC nozzle to 1600 K leads to the production of methyl radical (m/z 15) and to the destruction of m/z 54. This is consistent with pyrolysis of $HC{\equiv}CCH_2CH_3$ (m/z 54) to CH_2CCH and CH_3 (Fig. 3.5). The parent ion of 3MF, m/z 82, disappears at 1600 K. An authentic sample of methylketene was synthesized[20] and thermally cracked in Fig. 3.17. Decomposition of $CH_3CH{=}C{=}O$ (m/z 56), presumably to $CH_2{=}CH_2$ and CO, is observed in Fig. 3.17. Because of the high ionization energies of ethylene,[30] $IE(CH_2{=}CH_2) = 10.51268 \pm 0.00003$ eV and carbon monoxide,[31] $IE(CO) = 14.0136 \pm 0.0005$ eV, the 118.2 nm PIMS cannot detect these species; all that is observed in Fig. 3.17 is loss of the parent signal, m/z 56.

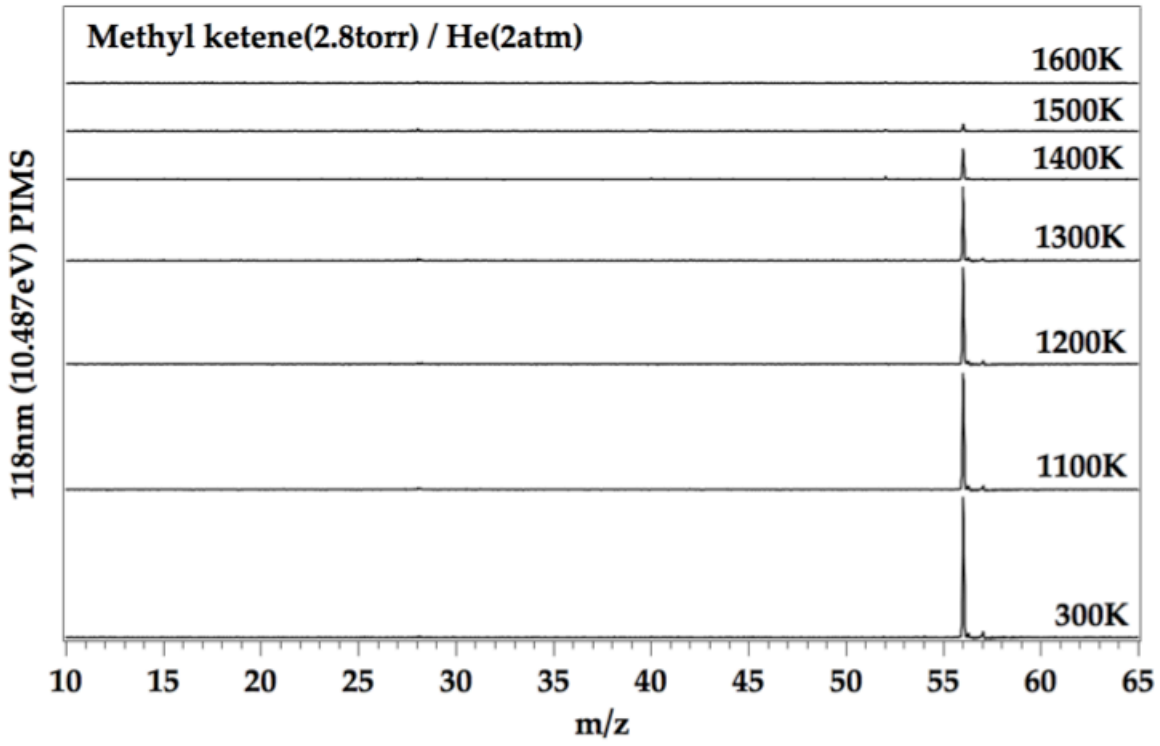

Figure 3.17 PIMS spectra of pyrolysis products from authentic $CH_3CH{=}C{=}O$ (methyl ketene).

Fig. 3.18 shows portions of the matrix IR spectrum of the products of pyrolysis of 3MF decomposed in the microtubular reactor at 1600 K.

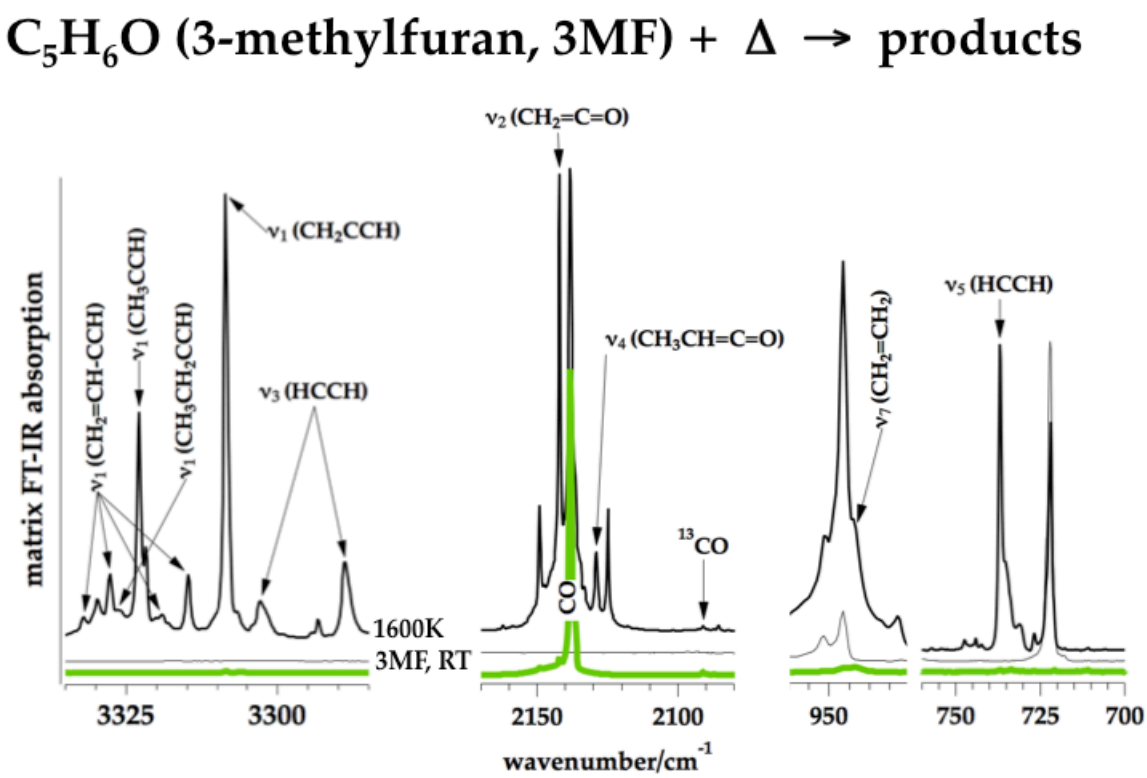

Figure 3.18 Argon matrix FT-IR spectrum of thermally decomposed 3MF at 1600 K. The green trace indicates background absorption of the buffer gas, Ar, heated to 1600 K; the narrow black spectrum is 3MF at room temperature; and the thick black spectrum results from heating 3MF to 1600 K.

Fig. 3.18 shows the complex bands of vinylacetylene,[21,22] ν_1(CH_2=CH-C≡CH), are shown at 3332, 3328, 3319, and 3315 cm^{-1}. As in pyrolysis of 2MF, ν_1(CH_2=CH-C≡CH) stretching mode appears as quartet due to site splittings in the Ar matrix. In a Ne matrix, ν_1(CH_2=CH-C≡CH) appears as a singlet after annealing.[32] Ethylacetylene,[23,24] ν_1(CH_3CH_2C≡CH), appears at 3326 cm^{-1}, propyne,[10] ν_1(CH_3C≡CH) is observed 3323 cm^{-1}, propargyl radical,[25] ν_1(CH_2CCH) is detected at 3309 cm^{-1}, and the Dennison-Darling splitting in acetylene,[10] ν_3(HC≡CH) appears at 3303 and 3289 cm^{-1}. Carbon monoxide (both ^{12}CO and ^{13}CO) and ν_2(CH_2=C=O) are detected in the mid-IR region,[10] and the

intense methylketene band, $\nu_4(CH_3CH{=}C{=}O)$, is observed at 2129 cm^{-1}. Both ethylene, $\nu_7(CH_2{=}CH_2)$ and acetylene,[10] $\nu_5(HC{\equiv}CH)$, are also present at 947 and 737 cm^{-1}.

The Ar matrix IR spectra in Fig. 3.19 definitely shows vibrational bands belonging to butatriene.

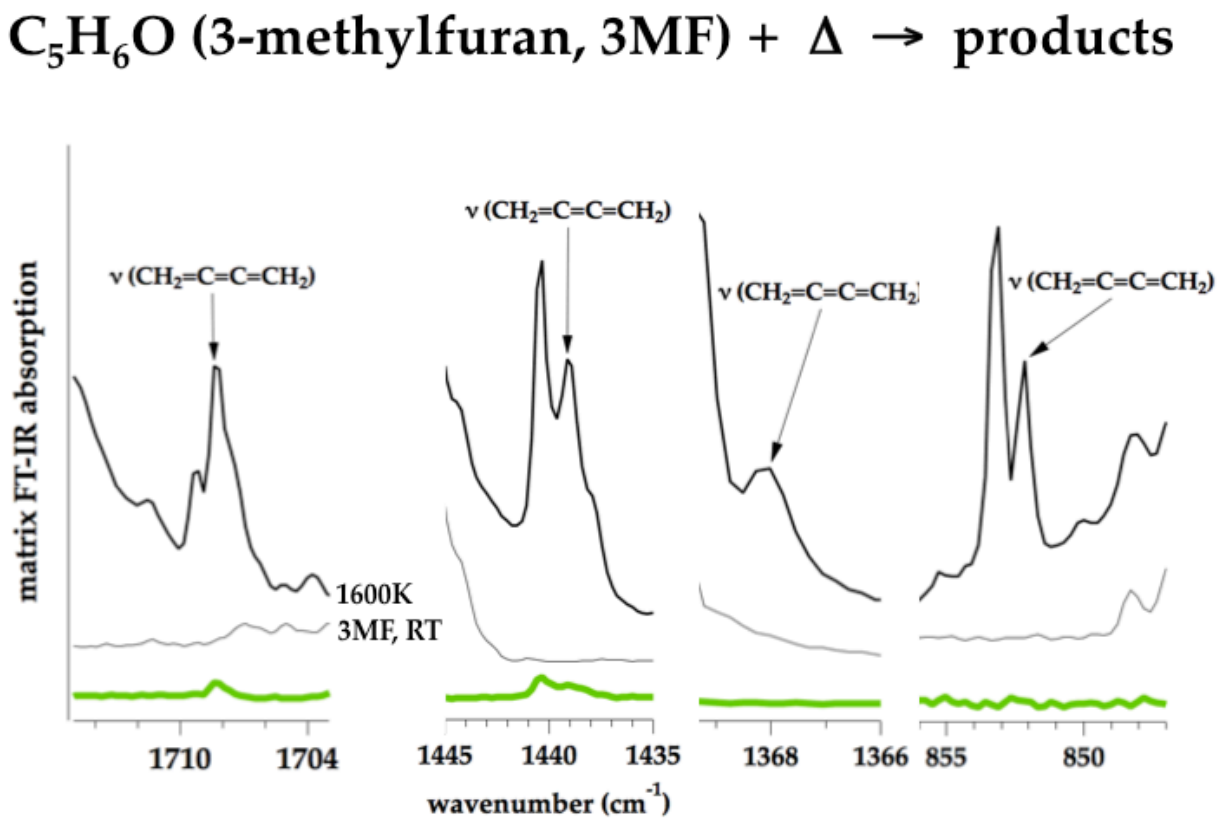

Figure 3.19 Argon matrix FT-IR spectrum of $CH_2{=}C{=}C{=}CH_2$ from thermally decomposed 3MF at 1600 K. The green trace indicates background absorption of the buffer gas, Ar, heated to 1600 K; the narrow black spectrum is 3MF at room temperature; and the thick black spectrum results from heating 3MF to 1600 K.

Authentic samples of $CH_2{=}C{=}C{=}CH_2$ were prepared by the methods of Brandsma and Verkuijsse[33] and the Ar matrix-isolated FT-IR absorption bands were

reported.[34] Use of these characteristic IR bands for butatriene[34] enables us to assign the four vibrational modes 1708, 1439, 1368, and 852 cm^{-1} in Fig. 3.19. The IR spectra in Fig. 3.19 is compatible with the predictions from the 4-carbene channel predicted in Fig. 3.15.

Besides butatriene, the IR absorption bands in the Ar matrix at 2874, 2741, 2057, 1407, 1404, 1380, and 1034 cm^{-1} are assigned[29,35] to CH_3-C≡C-CH_3 and confirms it as a product of 3MF pyrolysis. The detection in the IR of both CH_3-C≡C-CH_3 and CH_2=C=C=CH_2 confirms the 4-carbene channel in Fig. 3.15.

As in pyrolysis of 2MF, CH_2=C=CH_2 is generated by bimolecular reaction in the pyrolysis of 3MF. The ν_6(CH_2=C=CH_2), ν_8(CH_2=C=CH_2), and $2\nu_{10}$(CH_2=C=CH_2) detected at 1955, 3092 and 1680 cm^{-1}, which implies that bimolecular reactions of CH_3C≡CH and H atoms can not be avoided even at 0.1 % concentration of 3MF in the Ar carrier gas.

3.3 Conclusions

Both 2MF and 3MF have been pyrolyzed in a heated microtubular reactor to reveal the initial steps in the thermal cracking of these methylated furans. Using the mechanism for the parent species, furan, which decomposes *via* α-carbene and β-carbene,[10,11] the mechanism for thermal decomposition of 2MF is predicted in Fig. 3.3. All products from pyrolyzed 2MF, except CH_3CH=C=O, are identified by 118.2 nm-VUV PIMS, argon matrix isolation FT-IR, and tunable VUV PIMS (ALS). CH_3CH=C=O from the 2-carbene pathway is detected but ethylene and carbon monoxide are found instead. All these procedure support the proposed mechanism of pyrolysis of 2MF, Fig. 3.3.

Pyrolysis of 3MF is similar to decomposition of 2MF but the predicted pathways in Fig. 3.15 are slightly different from those in Fig. 3.3. Detection of CH_2=C=C=CH_2,

CH_3-C≡C-CH_3, and CH_3CH=C=O lends strong support to the predicted mechanism for 3MF pyrolysis in Fig. 3.15.

Use of the heated μtubular reactor has verified that both 2-methylfuran and 3-methylfuran decompose *via* a set of carbenes in exact analogy to the parent furan.[10,11] But it is a fact that, even though the dilute gas mixtures of the furans were used (≤ 0.1 %), bimolecular reactions with H atoms are still a factor in the pyrolysis of 2MF and 3MF.

Table 3.1 Gas phase and matrix IR peak position for Acetylene, CH≡CH, vibrational modes (cm^{-1}). The values given in the last two columns are for CH≡CH generated from pyrolysis of 2MF, 3MF and DMF at 1600 K.

Sym. species	Local mode	Approximate type of mode	Gas[36] Phase	Acetylene[10]	Argon matrix 2MF (1600 K)	Argon matrix 3MF (1600 K)	Argon matrix DMF (1600 K)
σ_g^+	ν_1	CH str	ia	ia	ia	ia	ia
	ν_2	CC str	ia	ia	ia	ia	ia
σ_u^+	ν_3	CH str	3295	3302	3303	3303	3303
			3282	3288	3289	3289	3289
π_g	ν_4	CH bend	ia	ia	ia	ia	ia
π_u	ν_5	CH bend	730	737	737	737	737

Table 3.2 Gas phase and matrix IR peak position for Ethylene, $CH_2{=}CH_2$, vibrational modes (cm^{-1}). The values given in the last two columns are for $CH_2{=}CH_2$ generated from pyrolysis of 2MF, 3MF and DMF at 1600 K.

Sym. species	Local mode	Approximate type of mode	Gas[36] phase	Argon matrix Ethylene (Authentic)	2MF (1600 K)	3MF (1600 K)	DMF (1600 K)
a_g	ν_1	CH_2 s-str	ia				
	ν_2	CC str	ia				
	ν_3	CH_2 scis	ia				
a_u	ν_4	CH_2 twist	ia				
b_{1g}	ν_5	CH_2 a-str	ia				
	ν_6	CH_2 rock	ia				
b_{1u}	ν_7	CH_2 wag	949	947	947		947
b_{2g}	ν_8	CH_2 wag	ia				
b_{2u}	ν_9	CH_2 a-str	3106	3112	3112		3112
				3096	3096	3096	3096
				3082	3083	3083	3083
				3070	3070	3071	3071
	ν_{10}	CH_2 rock	826	831	831	831	831
b_{3u}	ν_{11}	CH_2 s-str	2989	2995	2995		2995
				2986	2985		
				2983	2983		2983
	ν_{12}	CH_2 scis	1444	1440		1440	1440

Table 3.3 Gas phase and matrix IR peak position for Propargyl Radical, $HCCCH_2$, vibrational modes (cm^{-1}). The values given in the last two columns are for $HCCCH_2$ generated from pyrolysis of 2MF, 3MF and DMF at 1600 K.

Sym. species	Local mode	Approximate type of mode	Propargyl[25]	Argon matrix 2MF (1600 K)	Argon matrix 3MF (1600 K)	Argon matrix DMF (1600 K)
a_1	ν_1	CH_2CC-H str	3309	3309	3309	3309
	ν_2	H_2C-CCH s-str	3028	3028	3028	3028
	ν_3	$CH_2C{\equiv}CH$ - CH_2-CCH str	1935	1935	1935	1935
	ν_4	H_2C-CCH scis	1440		1440	1440
	ν_5	$CH_2C{\equiv}CH$ + CH_2-CCH str	1062	1062	1062	1062
b_1	ν_6	H2C-CCH umbrella	687	687	687	687
	ν_7	CH_2CC-H out-of-plane bend	484	484	484	484
	ν_8	CH_2-C≡CH out-of-plane bend				
b_2	ν_9	H_2C-CCH a-str				
	ν_{10}	H_2C-CCH + CH_2-C≡CH in-plane bend	1017	1017	1017	1017
	ν_{11}	CH_2CC-H in-plane bend	620	620	620	619.8 (shoulder)
	ν_{12}	CH_2-C≡CH in-plane bend				

Table 3.4 Gas phase and matrix IR peak position for Propyne, $CH_3C{\equiv}CH$, vibrational modes (cm^{-1}). The values given in the last two columns are for $CH_3C{\equiv}CH$ generated from pyrolysis of 2MF, 3MF and DMF at 1600 K.

Sym. species	Local mode	Approximate type of mode	Gas[36] phase	Propyne[10]	Argon matrix 2MF (1600 K)	Argon matrix 3MF (1600 K)	Argon matrix DMF (1600 K)
a_1	ν_1	CH str	3334	3323	3323	3323	3323
	ν_2	CH_3 s-str	2941	2935	2935	2936	2935
	ν_2	CH_3 s-str	2881	2868		2868	
	ν_3	C≡C str	2142	2137			
	ν_4	CH_3 s-deform		1383	1383	1383	1383
	ν_5	C-C str	931	928	928	928	
e	ν_6	CH_3 d-str	3008	2978	2978		
	ν_7	CH_3 d-deform	1452	1444	1444		
	ν_8	CH_3 rock	1053	1033	1033		
	ν_9	CH bend	633	630	631	631	631
				629	629	629	
	ν_{10}	CCC bend	328				

Table 3.5 Gas phase and matrix IR peak position for Allene, $CH_2=C=CH_2$, vibrational modes (cm^{-1}). The values given in the last two columns are for $CH_2=C=CH_2$, generated from pyrolysis of 2MF, 3MF and DMF at 1600 K.

Sym. species	Local mode	Approximate type of mode	Gas[36] phase	Argon matrix			
				Allen (Authetic)	2MF (1600 K)	3MF (1600 K)	DMF (1600 K)
a_1	ν_1	CH2 s-str					
a_1	ν_2	CH2 scis					
a_1	ν_3	CC str					
b_1	ν_4	CH2 twist	865				
b_2	ν_5	CH2 s-str	3007	3000	3000		3000
b_2	ν_6	CC str	1957	1956	1955	1955	1955
b_2	ν_7	CH2 scis	1398	1390	1390		1390
e	ν_8	CH2 a-str	3086	3092		3092	3091
e	ν_9	CH2 rock	999	997	995 ?	998 ?	998 ?
e	ν_{10}	CH2 wag	841	837	837		837
e	ν_{11}	CCC deform	355				
	$2\nu_{10}$			1680	1680	1680	1680

Table 3.6 Gas phase and matrix IR peak position for Ketene, CH_2=C=O, vibrational modes (cm^{-1}). The values given in the last two columns are for CH_2=C=O generated from pyrolysis of 2MF, 3MF and DMF at 1600 K.

Sym. species	Local mode	Approximate type of mode	Gas[37] phase	Ketene[10]	Argon matrix 2MF (1600 K)	Argon matrix 3MF (1600 K)	Argon matrix DMF (1600 K)
a_1	ν_1	CH_2 sym st	3071	3063	3063	3063	3063
	ν_2	C=O st	2152	2142	2142	2142	2142
	ν_3	CH_2 scissor	1388	1382	1380	1380	1380
	ν_4	C=C	1118	1114	1114	1114	1114
b_1	ν_5	CH_2 wag	588	598	592	592	591
				598	590	590	590
	ν_6	C=C=O linear bend	528	524	525	524	524
	ν_7	CH_2 asym st	3166	3158	3160		3160
	ν_8	CH_2 rock	977	973	972	972	972
	ν_9	C=C=O linear bend	438				

Table 3.7 Gas phase and matrix IR peak position for vinylacetylene, HC≡C-CH=CH_2, vibrational modes (cm^{-1}). The values given in the last two columns are for HC≡C-CH=CH_2 generated from pyrolysis of 2MF, 3MF and DMF at 1600 K.

Sym. species	Local mode	Approximate type of mode	Gas[38] Phase	Argon matrix Vinylacetylene[21,22]	2MF (1600 K)	3MF (1600 K)	DMF (1600 K)
a'	ν_1	H-CCCHCH_2 str	3330	3332	3332	3332	3332
	ν_1			3328	3328	3328	3328
	ν_1			3319	3319	3319	3319
	ν_1			3314	3315	3315	3315
	ν_2	HCCC=CH_2 a-str	3116	3120			
	ν_3	HCC(C-H)CH_2 s-str	3068	3063	3064	3064	3064
	ν_4	HCCCH=CH_2 s-str	3030	3034	3037	3037	3036
	ν_5	HC≡CCHCH_2 str	2111	2104			
	ν_6	HCCCH=CH_2 str	1599				
	ν_7	HCCCH=CH_2	1415	1414	1410	1410	1410
	ν_8	HCC(C-H)=CH_2 bend	1312				
	ν_9	HCCCH=CH_2 rock	1096	1097	1094		1094
	ν_{10}	HCC-CHCH_2 str	874	878	877		877
	ν_{11}	H-C≡CCHCH_2 bend	625	637	637		637
	ν_{12}	HCC-CH=CH_2 bend	539	543	543	543	543
a''	ν_{14}	HCC(C-H)=CH_2 bend	974	977	978	978	978
	ν_{15}	HCCCH=CH_2 wag	927	927	927	927	927
	ν_{16}	HCCCH=CH_2 twist	677	675	675	675	675
	ν_{17}	H-C≡CCHCH_2 bend	618	615	615	615	615

Table 3.8 Gas phase and matrix IR peak position for 1,2,3-butatriene, $H_2C=C=C=CH_2$, vibrational modes (cm^{-1}). The values given in the last two columns are for $H_2C=C=C=CH_2$ generated from pyrolysis of 3MF at 1600 K.

Sym. species	Local mode	Approximate type of mode	Gas[39] phase	Argon Matrix 1,2,3-butatriene[34]	Argon Matrix 3MF (1600 K)
a_g	ν_1	C-H str	ia		
	ν_2	C=C str	ia		
	ν_3	CH_2 scis	ia		
	ν_4	C=C str	ia		
a_u					
	ν_5	Torsion	ia		
b_{1u}	ν_6	C-H str	2994	2996	
	ν_7	C=C str	1608	1609	
	ν_8	CH_2 scis	1370	1367	1368
b_{2g}	ν_9	CH_3 wag	ia		
	ν_{10}	Skeletal bend	ia		
b_{2u}	ν_{11}	C-H str	3080		
	ν_{12}	CH_2 rock	1060		
	ν_{13}	Skeletal bend	215		
b_{3g}	ν_{14}	C-H str	ia		
	ν_{15}	CH_2 rock	ia		
	ν_{16}	Skeletal bend	ia		
b_{3u}	ν_{17}	CH_2 wag	854	852	852
b_{3u}	ν_{18}	Skeletal bend	?		
	?			2924	
	?			1708	1708
	?			1439	1439
	?			1228	
	?			1030	
	?			1022	
	?			977	

Table 3.9 Gas phase and matrix IR peak position for 1-butyne, $HC{\equiv}CCH_2CH_3$, vibrational modes (cm^{-1}). The values given in the last two columns are for $HC{\equiv}CCH_2CH_3$ generated from pyrolysis of 2MF, 3MF and DMF at 1600 K.

Sym. species	Local mode	Approximate type of mode	Gas[40,41] Phase	Argon matrix 1-butyne	2MF (1600 K)	3MF (1600 K)	DMF (1600 K)
a'	ν_1	≡C-H str	3332	3330		3330	
				3326	3326	3326	3326
	ν_2	CH_3 s-str	2988				
	ν_3	CH_3 s-str	2953				
	ν_4	CH_2 s-str	2939				
	ν_5	C≡C str, C-C str	2132	2130	2130		
				2129			
	ν_6	CH_2 wag, C-C str	1322				
	ν_7	C-C-C a-str	1008				
	ν_8	C-C-C s-str	827				
	ν_9	C≡C-H bend	634	634	634		
				633	633	633	633
	ν_{10}	C-C-C≡C bend	509	509	509	509	
	ν_{11}	C-C≡C bend, C-C-C bend	208				
a''	ν_{12}	CH_3 a-str	2991				
	ν_{13}	CH_2 a-str	2939				
	ν_{14}	CH_3 a-bend	1462				
	ν_{15}	CH_3 rock, CH_2 rock, CH_2 twist	1090				
	ν_{16}	CH_2 rock, CH_3 rock	782	780			779
	ν_{17}	C≡C-H bend	630	627		627	
				626	626	626	626 (shoulder)
	ν_{18}	C-C-C≡C bend	340				

Table 3.10 Gas phase and matrix IR peak position for 2-butyne, $H_3CC{\equiv}CCH_3$, vibrational modes (cm^{-1}). The values given in the last two columns are for $H_3CC{\equiv}CCH_3$ generated from pyrolysis of 3MF at 1600 K.

Sym. species	Local mode	Approximate type of mode	Gas[36] phase	Argon matrix 2-butyne[29,35]	Argon matrix 3MF (1600 K)
a'_1	ν_1	CH_3 s-str	ia		
a'_1	ν_2	C≡C str	ia		
a'_1	ν_3	CH_3 s-deform	ia		
a'_1	ν_4	C-C str	ia		
a''_1	ν_5	CH_3 torsion	ia		
a''_2	ν_6	CH_3 s-str	2938	2936	
a''_2	ν_7	CH_3 s-deform	1382	1379	1380
a''_2	ν_8	C-C str	1152	1157	
e'	ν_9	CH_3 d-str	2973	2976	
e'	ν_{10}	CH_3 d-deform	1456	1448	
e'	ν_{11}	CH_3 rock	1054	1040	
e'	ν_{12}	CCC deform			
e	ν_{13}	CH_3 d-str	ia		
e	ν_{14}	CH_3 d-deform	ia		
e	ν_{15}	CH_3 rock	ia		
e	ν_{16}	CCC deform	ia		
?	?			2873	2874
?	?			2742	2741
?	?			2057	2057
?	?			1408	1407
?	?			1406	1404
?	?			1132	
?	?			1035	1034

Table 3.11 Gas phase and matrix IR peak position for methylketene, $CH_3CH{=}C{=}O$, vibrational modes (cm^{-1}). The values given in the last two columns are for $CH_3CH{=}C{=}O$ generated from pyrolysis of 3MF and DMF at 1600 K.

Sym. species	Local mode	Approximate type of mode	CH_3CHCO[32] (Authetic)	Argon matrix 3MF (1600 K)	Argon matrix DMF (1600 K)
a'	ν_1	C-H str	3079	3080	3079
			3058	3058	
	ν_2	CH_3 s-str "out of plane"	2916	2916	
	ν_3	CH_3 s-str "in plane"	2878		
	ν_4	C=C=O str	2129	2129	2129
	ν_5		1471		1471
	ν_6	CH_3 umbrella	1385	1385	1385
	ν_7		1377		1377 (shoulder)
	ν_8	CCH bend	1155		
	ν_9		1076	1075	1075
	ν_{10}	CH_3 wag	892	891	891
	ν_{11}	CCO bend	634		
	ν_{12}	CCC bend			
a"	ν_{13}	CH_3 a-str	2954		
	ν_{14}		1447		
	ν_{15}	CH_3 rock	1043		
	ν_{16}	O-C-C-H bend	532	533	
	ν_{17}	CH bend	521	521	521
	ν_{18}	CH_3 torsion			

Reference for Chapter III

(1) Roman-Leshkov, Y.; Barrett, C. J.; Liu, Z. Y.; Dumesic, J. A. *Nature* **2007**, *447*, 982.

(2) Wang, C.; Xu, H.; Daniel, R.; Ghafourian, A.; Herreros, J. M.; Shuai, S.; Ma, X. *Fuel* **2013**, *103*, 200.

(3) Binder, J. B.; Raines, R. T. *Journal of the American Chemical Society* **2009**, *131*, 1979.

(4) Grela, M. A.; Amorebieta, V. T.; Colussi, A. J. *The Journal of Physical Chemistry* **1985**, *89*, 38.

(5) Lifshitz, A.; Tamburu, C.; Shashua, R. *Journal of Physical Chemistry A* **1997**, *101*, 1018.

(6) Simmie, J. M.; Curran, H. J. *The Journal of Physical Chemistry A* **2009**, *113*, 5128.

(7) Vogelhuber, K. M.; Wren, S. W.; Sheps, L.; Lineberger, W. C. *Journal of Chemical Physics* **2011**, *134*.

(8) Thewes, M.; Muether, M.; Pischinger, S.; Budde, M.; Brunn, A.; Sehr, A.; Adomeit, P.; Klankermayer, J. *Energy & Fuels* **2011**, *25*, 5549.

(9) Wu, X. S.; Daniel, R.; Tian, G. H.; Xu, H. M.; Huang, Z. H.; Richardson, D. *Applied Energy* **2011**, *88*, 2305.

(10) Vasiliou, A.; Nimlos, M. R.; Daily, J. W.; Ellison, G. B. *The Journal of Physical Chemistry A* **2009**, *113*, 8540.

(11) Urness, K. N.; Golan, A.; Daily, J. W.; Nimlos, M. R.; Stanton, J. F.; Ahmed, M.; Ellison, G. B. *J. Chem. Phys.* **2013**, *in press*.

(12) Veszpremi, T.; Nyulaszi, L.; Nagy, J. *Journal of Organometallic Chemistry* **1987**, *331*, 175.

(13) Gilbert, T.; Pfab, R.; Fischer, I.; Chen, P. *Journal of Chemical Physics* **2000**, *112*, 2575.

(14) Xing, X.; Bahng, M.-K.; Reed, B.; Lam, C. S.; Lau, K.-C.; Ng, C. Y. *The Journal of Chemical Physics* **2008**, *128*, 094311.

(15) Bieri, G.; Burger, F.; Heilbronner, E.; Maier, J. P. *Helvetica Chimica Acta* **1977**, *60*, 2213.

(16) Blush, J. A.; Chen, P.; Wiedmann, R. T.; White, M. G. *Journal of Chemical Physics* **1993**, *98*, 3557.

(17) Niu, B. H.; Bai, Y.; Shirley, D. A. *Journal of Chemical Physics* **1993**, *99*, 2520.

(18) Vasiliou, A.; Piech, K. M.; Zhang, X.; Nimlos, M. R.; Ahmed, M.; Kostko, O.; Golan, A.; Osborn, D. L.; Daily, J. W.; Stanton, J. F.; Ellison, G. B. *Journal of Chemical Physics* **2011**, *135*, 14306.

(19) Pratt, S. T.; Dehmer, P. M.; Dehmer, J. L. *Journal of Chemical Physics* **1993**, *99*, 6233.

(20) Bock, H.; Hirabayashi, T.; Mohmand, S.; Solouki, B. *Angewandte Chemie* **1977**, *89*, 106.

(21) Scheer, A. M., University of Colorado, 2011.

(22) Scheer, A. M.; Mukarakate, C.; Robichaud, D. J.; Nimlos, M. R.; Carstensen, H.-H.; Ellison, G. B. *The Journal of Chemical Physics* **2012**, *136*, 044309.

(23) Saussey, J.; Lamotte, J.; Lavalley, J. C. *Spectrochimica Acta Part A: Molecular Spectroscopy* **1976**, *32*, 763.

(24) Crowder, G. A.; Fick, H. *Journal of Molecular Structure* **1986**, *147*, 17.

(25) Jochnowitz, E. B.; Zhang, X.; Nimlos, M. R.; Varner, M. E.; Stanton, J. F.; Ellison, G. B. *The Journal of Physical Chemistry A* **2005**, *109*, 3812.

(26) Yang, Z. Z.; Wang, L. S.; Lee, Y. T.; Shirley, D. A.; Huang, S. Y.; Lester, W. A. *Chemical Physics Letters* **1990**, *171*, 9.

(27) Spilker, R.; Grutzmacher, H. F. *Organic Mass Spectrometry* **1986**, *21*, 459.

(28) Gao, H.; Xu, Y. T.; Yang, L.; Lam, C. S.; Wang, H. L.; Zhou, J. A.; Ng, C. Y. *Journal of Chemical Physics* **2011**, *135*.

(29) Parker, J. K.; Davis, S. R. *The Journal of Physical Chemistry A* **1999**, *103*, 7280.

(30) Lau, K. C.; Ng, C.-Y. *Accounts of Chemical Research* **2006**, *39*, 823.

(31) Evans, M.; Ng, C. Y. *Journal of Chemical Physics* **1999**, *111*, 8879.

(32) Ormond, T. K. *Unpublished data* **2012**.

(33) Brandsma, L.; Verkruijsse, H. D. *Synthesis of Acetylens, Allens, and Cumulens*; Elsevier: Amsterdam, 1981.

(34) Wrobel, R.; Sander, W.; Cremer, D.; Kraka, E. *The Journal of Physical Chemistry A* **2000**, *104*, 3819.

(35) Nakata, M.; Frei, H. *J. Am. Chem. Soc.* **1992**, *114*, 1363.

(36) Shimanouchi, T. *Tables of Vibrational Frequencies, Consolidated Vol. I*; NSRDS-NBS 39, 1972.

(37) Kwiatkowski, J. S.; Leszczynski, J. *Theochem-Journal of Molecular Structure* **1995**, *342*, 43.

(38) Tørneng, E.; Nielsen, C. J.; Klaeboe, P.; Hopf, H.; Priebe, H. *Spectrochimica Acta Part a-Molecular and Biomolecular Spectroscopy* **1980**, *36*, 975.

(39) Miller, F. A.; Matsubara, I. *Spectrochimica Acta* **1966**, *22*, 173.

(40) Saussey, J.; Lamotte, J.; Lavalley, J. C. *Spectrochimica Acta Part a-Molecular and Biomolecular Spectroscopy* **1976**, *32*, 763.

(41) Crowder, G. A.; Fick, H. *Journal of Molecular Structure* **1986**, *147*, 17.

Chapter IV Pyrolysis of 2,5-dimethylfuran

4.1 Introduction

As discussed earlier in this thesis, substituted furans are being considered as 2nd generation biofuels. The decomposition mechanism for the parent species, furan, is shown in Fig. 3.2. Elaborating this mechanism for 2MF and 3MF is done in Fig. 3.3 and 3.15. In this Chapter, we will further extend the carbene mechanism of Fig. 3.2 for furan decomposition to 2, 5-dimethylfuran, DMF.

First, the previous literature for DMF pyrolysis is reviewed. There have been previous studies of the thermal decomposition of DMF. In 1985, Grela *et al.*[1] pyrolyzed DMF at low pressures (1 mTorr) in a heatable molecular flow reactor over the temperature range 1050 – 1270 K and analyzed products with on-line EI-mass spectrometer. They concluded that 2,5-dimethylfuran isomerizes easily to 2,4-dimethylfuran. Decomposition of DMF led to a mixture of products with ions of m/z 18 (H_2O), 78 (C_6H_6), 66 (C_5H_6), 68 (C_5H_8) and 28 (CO). Analysis of the kinetics of decomposition yielded a rate constant, log ($k_{2,DMF}$, s^{-1}) = 15.6 – 74.1/θ, (θ = 4.575 × 10^{-3}T kcal mol^{-1}). As the furan ring is further alkylated, the decomposition rate constant increases. In subsequent years, Lifshitz *et al.*[2,3] carried out single pulse shock tube experiments of the mixture gas (700 Torr) of 0.5% DMF with argon gas at temperatures of 1070 – 1370 K. The products were identified *via* gas chromatographic/FID analysis on packed column. The initial step in DMF pyrolysis was interpreted as formation of a carbene. Subsequent decomposition of the carbene is shown in Fig. 4.1 and is believed to produce a number of secondary fragmentation products.

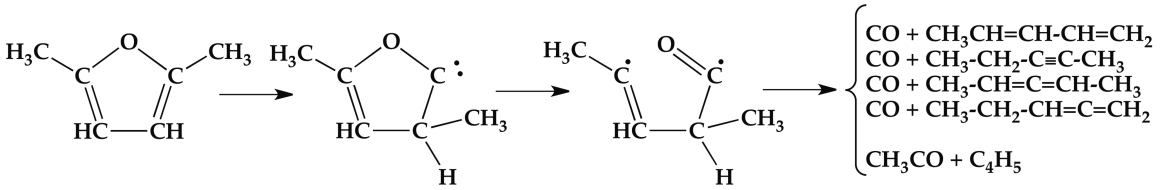

Figure 4.1 Pathway proposed[3] for the unimolecular decomposition of DMF.

In 2009, Simmie and Curran performed *ab initio* electronic structure calculations of formation enthalpy and bond dissociation energies of alkylfurans.[4,5] It was revealed that the dissociation energies of the ring carbon-H bonds on DMF are very high; roughly 115 kcal mol^{-1}. This agrees with the measured bond dissociation energy of furan,[6] DH_{298}(furan, C-H) = 120 ± 2 kcal mol^{-1}. In contrast, C-H bond in the methyl group is relatively weak (86 kcal mol^{-1}) because of the formation[7] of a benzylic radical, the 5-methyl-2-furanylmethyl radical.

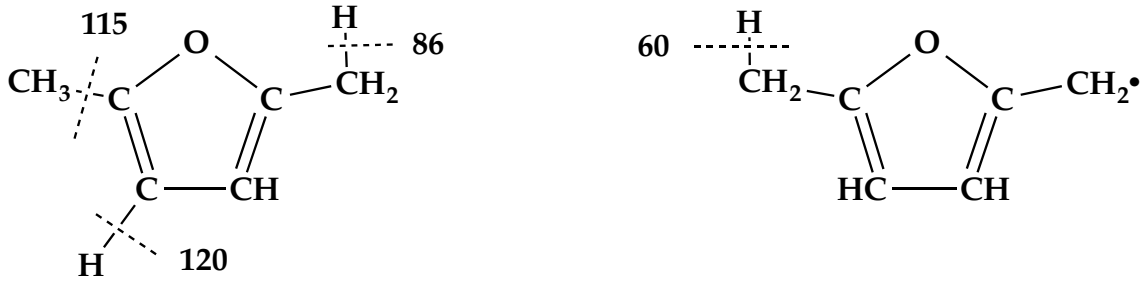

2, 5-dimethylfuran
Calculated (CBS-QB3) Bond Enthalpies, DH_{298}/kcal mol^{-1}

Figure 4.2 Bond Enthalpies[4,5,7] for DMF.

Experimental studies to characterize the performance of DMF in combustion have been reported by Wu *et al*.[8] DMF was studied in a low-pressure, premixed laminar DMF/oxygen/argon flames; product detection was by tunable synchrotron VUV PIMS.

Products were identified by ionization energies and PIE curves. Comparison of ionization energies with literature values or calculated values permitted the identification of over 70 different species.

In a computational study[5] of the unimolecular decomposition of DMF, it was predicted that the initial steps would be carbene formation or H atom release from the –CH_3 group. These conclusions were supported by an additional theoretical study by Sirjean and Fournet.[9] In 2013, Friese *et al.*[10] studied DMF in a shock tube study over a temperature range of 970 —1240 K and at pressures of 1.6 — 4.8 bar. Analysis of kinetics of decomposition yielded a decomposition rate constant $k_1(DMF) = 4.4 \times 10^{-11}\exp(-1180\ K/T)\ cm^{-3}s^{-1}$ with an estimated uncertainty of 30 %. No significant pressure dependence was observed. Addition of H atoms to the ring was observed to be the major channel (>75 %) leading to the formation of 2MF and CH_3 radicals.

Finally Djokic *et al.*[11] reported DMF pyrolysis using an on-line GC × GC-FID/(TOF-MS) for product analysis. The reactor temperature was 873 — 1098 K at a constant pressure of 1.7 bar, while the residence time was 300 – 400 ms. Low conversion was observed and the main products were H_2, CO, CH_4, phenol, 2MF, 1,3-cyclopentadiene, and $C_7H_{10}O$ isomers. At higher conversion rates of DMF, mono- and poly-aromatics such as benzene, toluene, indene and naphthalene were produced. These species seemed to be secondary reaction products of 1,3-cyclopentadiene. At the highest temperatures more than 10 mol% of 2,5-dimethylfuran is converted into mono-, di-, tri- and tetra-aromatic products, which are known soot precursors. This high tendency to form molecular weight growths species even under dilute conditions might pose a threat for the use of 2,5-dimethylfuran as a fuel.

The thermodynamics of DMF has been measured[12] using combustion calorimetry. These experiments found $\Delta_f H_{298}$(2, 5-dimethylfuran) equal to -30.6 ± 0.2 kcal

mol^{-1} (-128.13 ± 0.98 kJ mol^{-1}). The thermochemistry of methylated furans has been examined by *ab initio* electronic structure calculations.[13,14] A high-level *ab initio* thermochemical technique, known as the Feller-Petersen-Dixon method, was used[14] to calculate the total atomization energies and hence the enthalpies of formation of 2,5-dimethylfuran, 2-methylfuran, and furan itself as a means of rationalizing significant discrepancies in the literature. The results of these calculations find $\Delta_f H_{298}$(2, 5-dimethylfuran) to be -29.8 ± 1.4 kcal mol^{-1} (-124.6 ± 1.4 kJ mol^{-1}).

In analogy with the furan pyrolysis mechanism in Fig. 3.2, a mechanism for DMF can be predicted (Fig. 4.3).

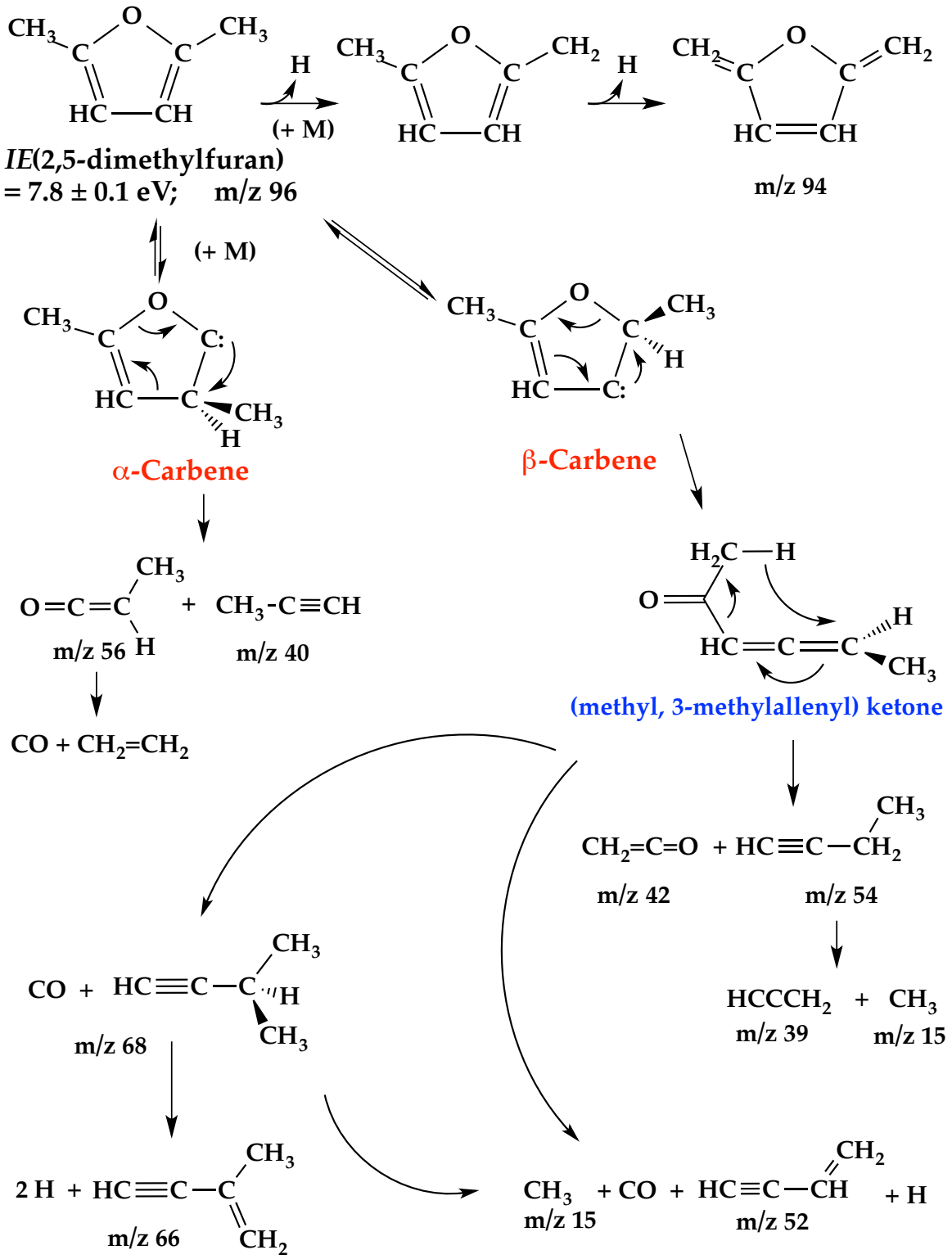

Figure 4.3 Predicted mechanism of thermally decomposed DMF.

The bond energies calculated in Fig. 4.2 suggest possible formation of the 5-methyl-2-furanylmethyl radical. Under the conditions of the heated microtubular reactor, one would expect this radical to decompose to yield H atom and 2, 5-dimethylene-2, 5-dihydrofuran. Ionization of this species would generate an ion at m/z 94. Alternatively, DMF could rearrange to a pair of carbenes in Fig. 4.3. The α-carbene is expected to dissociate to $CH_3C{\equiv}CH$ (with a corresponding ion at m/z 40) and $CH_3CH{=}C{=}O$ (the ion would be m/z 56). Methylketene is not a very stable molecule and could be expected to fragment to carbon monoxide and methylcarbene. The carbene would rapidly rearrange to ethylene: $CH_3CH{=}C{=}O$ (+ M) → CO + $[CH_3CH]^*$ → CO + $CH_2{=}CH_2$. The β-carbene in Fig. 4.3 is predicted to isomerize to the (methyl, 3-methylallenyl) ketone that can fragment in several ways. As shown in Fig. 4.3, the ketone, $CH_3CO\text{-}CH{=}C{=}CHCH_3$, can rearrange to form ketene and 1-butyne. While $CH_2{=}C{=}O$ (m/z 42) is stable, $HC{\equiv}C\text{-}CH_2CH_3$ (m/z 54) is known to fragment to $HCCCH_2$ (m/z 39) and CH_3 (m/z 15) radicals; see Fig. 3.5. Alternatively the ketone could transfer a CH_3- group to yield $HC{\equiv}C\text{-}CH(CH_3)_2$ (m/z 68) and CO.

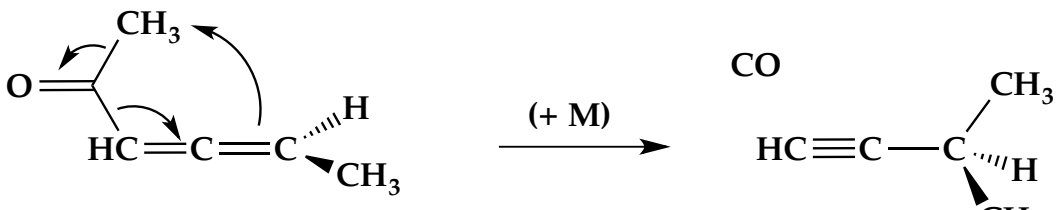

(methyl, 3-methylallenyl) ketone

The resulting 3-methyl-1-butyne could further fragment to H atom and the dimethylpropargyl radical, $HC{\equiv}C\text{-}C(CH_3)_2$ (m/z 67). This propargyl radical could shed

a final H atom to generate HC≡C-C(CH_3)=CH_2 (m/z 66). Finally the (methyl, 3-methylallenyl) ketone in Fig. 4.3 could fragment to a pair of radicals: CH_3CO-CH=C=$CHCH_3$ (+ M) → CH_3 + CO + $HCCCHCH_3$. The methyl-propargy radical would not survive and would fragment to vinylacetylene and H atoms: $HCCCHCH_3$ → H + HC≡C-CH=CH_2 (m/z 52).

In order to validate mechanism in Fig. 4.3, DMF samples were thermally decomposed in a heated SiC flow reactor.

4.2 Results and Discussion

The PIMS spectra of the pyrolysis products of DMF at various temperatures are shown in Fig. 4.4. At 300 K, m/z 96 arises from DMF parent ion and is the ^{13}C isotope peak is m/z 97; the measured isotope ratio (97/96) is 6.3 %. The ionization energy of DMF has been reported[15] to be 7.8 eV. Though DMF is ionized by 10.487 eV VUV light, no fragments from dissociative ionization are detected. Upon heating the SiC reactor up to 1400 K, product ions are detected at m/z 15, 39, 40, 42, 52, 53, 65, 66, 67 and 68. Ion signals at m/z 15, 39, 40, and 42 arise from methyl radical[16] (CH_3), propargyl radical[17] ($HCCCH_2$), methylacetylene[18] (HC≡CCH_3) and ketene[19] (CH_2=C=O). Vinylacetylene[20] (HC≡C-CH=CH_2) is assigned at m/z 52 and m/z 53 is likely the isotope peak of HC≡C-CH=CH_2; the ratio of m/z (53/52) is 5.7 %. The ions of m/z 66 and 68 result from 2-methyl-1-buten-3-yne[20] and 3-methyl-1-butyne:[20] HC≡CC(CH_3)=CH_2 and HC≡CCH(CH_3)CH_3. Presumably the ion of m/z 67 derives from 3-methyl-1-butyne in a heated SiC flow tube: HC≡CCH(CH_3)CH_3 (m/z 68) → [HC≡CC(CH_3)CH_3 (m/z 67) + H] → HC≡CC(CH_3)=CH_2 (m/z 66) + 2H. Likewise, the ion of m/z 65 can be identified:

$HC{\equiv}CC(CH_3){=}CH_2$ (m/z 66) → $CH_2C(C{\equiv}CH)CH_2$ (m/z 65) + H. The species, $CH_2C(C{\equiv}CH)CH_2$, is an allylic radical and may be stabilized enough to survive the hot reactor. The *IE*[$CH_2C(C{\equiv}CH)CH_2$] has not been reported but it is surely lower that that of the allyl radical, *IE*(CH_2CHCH_2), which is known[21] to be 65 584.6 ± 2.0 cm^{-1} (8.13146 ± 0.00025 eV).

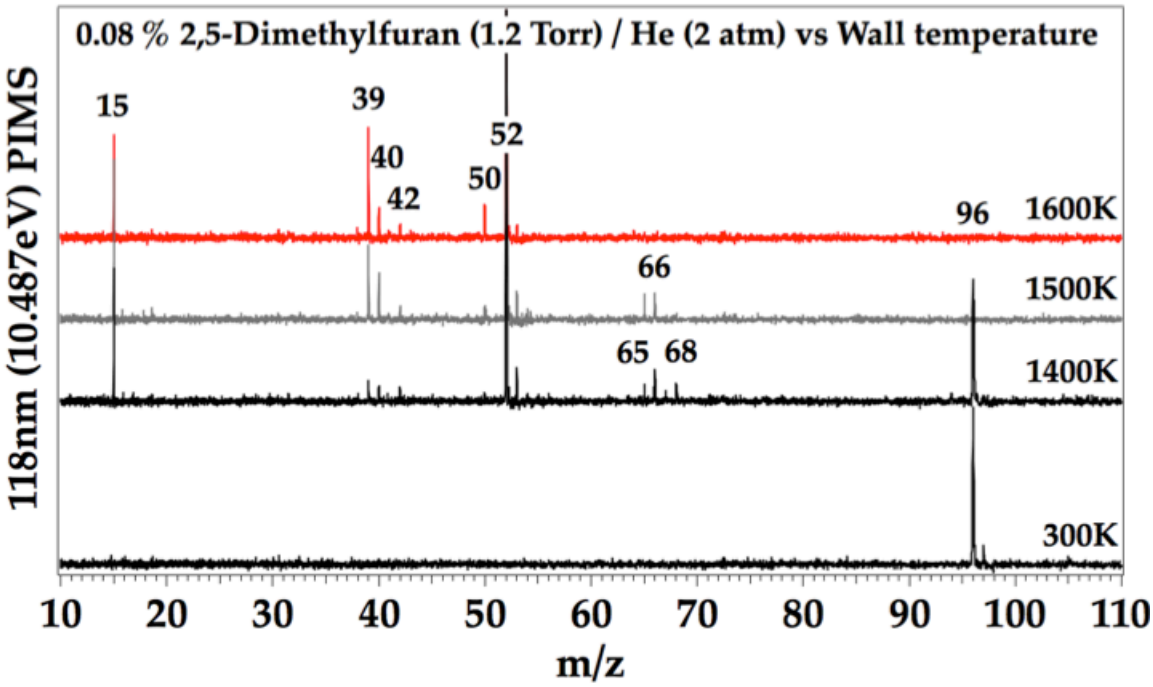

Figure 4.4 PIMS spectra of pyrolysis of 2, 5-dimethylfuran diluted to 0.08 % in He buffer gas at various temperatures in a pulsed SiC flowtube.

Heating the SiC flow reactor to 1600 K produces an intense feature at m/z 50 which is assigned to diacetylene[20] ($HC{\equiv}C\text{-}C{\equiv}CH$). At this high temperature, the ions of m/z 65, 66, 67, and 68 disappear. It is likely that (methyl, 3-methylallenyl) ketone cascades to m/z 68 → m/z 67 → m/z 66. The species responsible for m/z 66, $HC{\equiv}C\text{-}C(CH_3){=}CH_2$, can release a CH_3 fragment and produce $HC{\equiv}C\text{-}C{\equiv}CH$, m/z 50. The parent DMF, m/z 96, is completely destroyed.

All detectable products in Fig. 4.3 are identified by 10.487 eV VUV PIMS in Fig. 4.4 except 1-butyne[20] and methylketene:[22] $HC{\equiv}CCH_2CH_3$ and $CH_3CH{=}C{=}O$, respectively. The ionization energies of both species are known to be *IE*($HC{\equiv}CCH_2CH_3$) at 10.20 ± 0.02 eV and *IE*($CH_3CH{=}C{=}O$) at 8.95 eV. The lack of signals at m/z 54 and m/z 56 suggests that both do not survive in the heated reactor. The mechanism in Fig. 4.3 predicts the α-carbene produces both $CH_3C{\equiv}CH$ (m/z 40) and $CH_3CH{=}C{=}O$ while one of the decomposition channels for the (methyl, 3-methylallenyl) ketone is $CH_2{=}C{=}O$ (m/z 42) and $HC{\equiv}C\text{-}CH_2CH_3$. Fig. 4.4 reveals signals from both m/z 40 and m/z 42.

In Chapter III, it was demonstrated by 118.2 VUV PIMS that both 1-butyne (m/z 54) and methylketene (m/z 56) are unstable above 1500 K (see Figs. 3.5 and 3.17). However both species were identified by their characteristic IR spectra (see Figs. 3.8 and 3.18).

Infrared spectroscopy confirms the presence of both 1-butyne and methylketene as decomposition products of DMF, see Fig. 4.5.

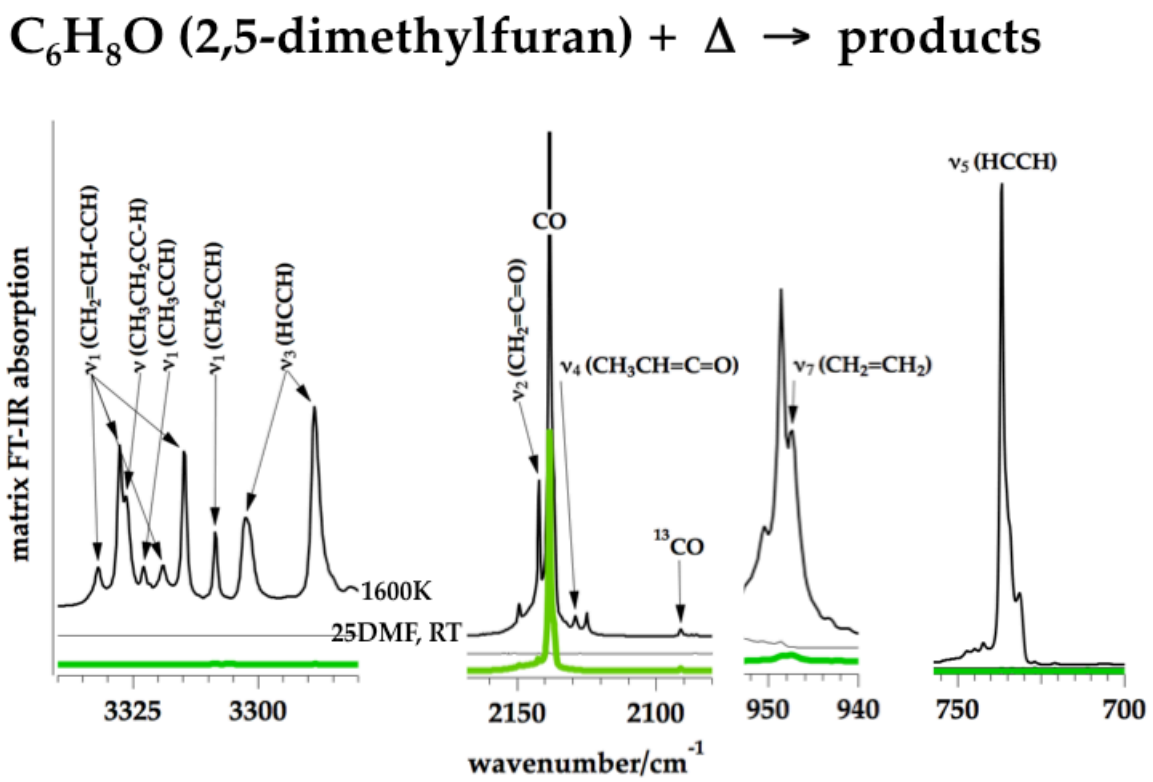

Figure 4.5 Argon matrix FT-IR spectrum of thermally decomposed DMF at 1600 K. The green trace indicates background absorption of the buffer gas, Ar, heated to 1600 K; the narrow black spectrum is DMF at room temperature; and the thick black spectrum results from heating DMF to 1600K. (All IR bands are tabulated in Table 3.1 – 3.11.)

In Fig. 4.5 one can identify vinylacetylene,[23,24] ethylacetylene,[25,26] methylacetylene,[27] propargyl radical,[28] and acetylene[27] over 3000 cm^{-1} region: ν_1(HC≡C-CH=CH_2), ν_1(HC≡CCH_2CH_3), ν_1(CH_3C≡CH), ν_1(CH_2CCH), and ν_3(HC≡CH), respectively. Consequently, while HC≡CCH_2CH_3 could not be detected in the 118.2 nm VUV PIMS in Fig. 4.4, it is clearly present in the IR spectrum in Fig. 4.5. In the mid-IR range in Fig. 4.5, carbon monoxide (both CO and ^{13}CO) and ν_2(CH_2=C=O) are identified.[27] Likewise methylketene, ν_4(CH_3CH=C=O), is detected at 2129 cm^{-1}. The identity of methylketene was confirmed by reference to an authentic sample.[29] Fig. 4.5 also contains bands for

ethylene, $\nu_7(CH_2{=}CH_2)$, and acetylene, $\nu_5(HC{\equiv}CH)$. The IR spectrum in Fig. 4.5 provides evidence for the missing 1-butyne and methylketene, $\nu_1(HC{\equiv}CCH_2CH_3)$ and $\nu_4(CH_3CH{=}C{=}O)$. The PIMS (Fig. 4.4) and IR spectrum (Fig. 4.5) appear to confirmed all products predicted by the mechanism (Fig. 4.3) for the thermal cracking DMF. The presence of acetylene in Fig. 4.5, both $\nu_3(HC{\equiv}CH)$ and $\nu_5(HC{\equiv}CH)$, also suggests some bimolecular chemistry in the pyrolysis of DMF in pulsed reactor.

In addition to all of the species predicted in Fig. 4.3, the IR spectrum also shows evidence for the presence of allene; see Fig. 4.6.

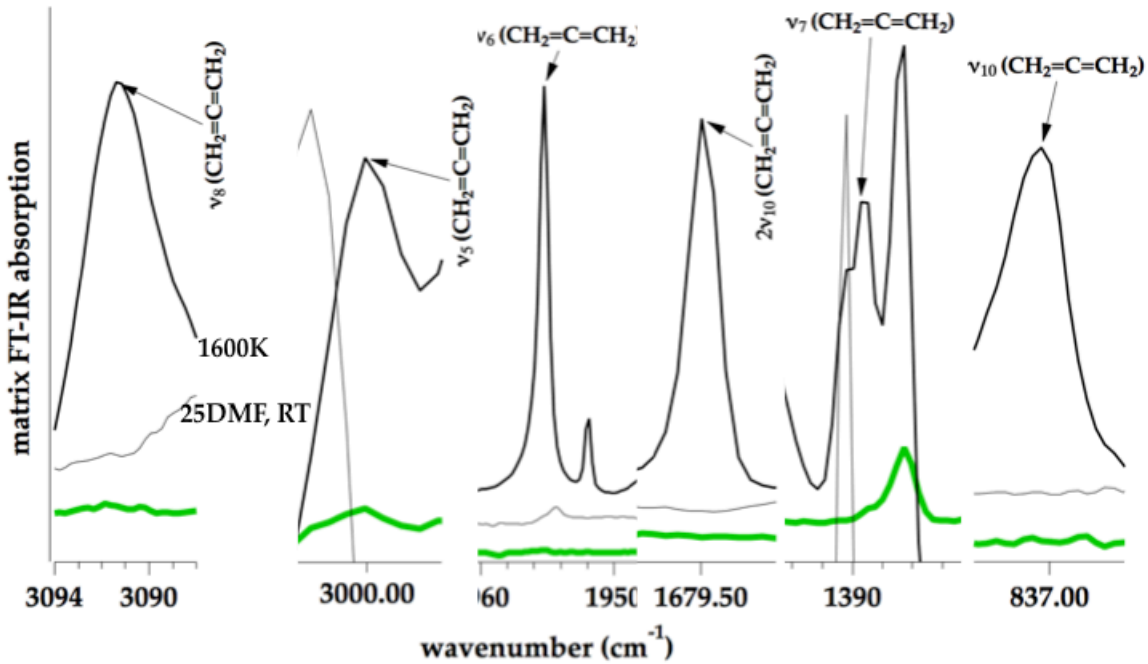

Figure 4.6 Argon matrix FT-IR spectrum of $CH_2{=}C{=}CH_2$ from pyrolysis of DMF at 1600 K. The green trace indicates background absorption of the buffer gas, Ar, heated to 1600 K; the narrow black spectrum is DMF at room temperature; and the thick black spectrum results from heating DMF to 1600K. (All IR bands are tabulated in Table 3.1 – 3.11.)

Fig. 4.6 shows that CH_2=C=CH_2 results from bimolecular reactions in the SiC flow reactor heated to 1600 K. Comparison of IR spectrum in Fig. 4.6 to that to the authentic sample in Fig. 3.11 demonstrates that most of the fundamentals of CH_2=C=CH_2 are present. In particular, the intense ν_6 is clearly present. As described in Chapter III (Fig. 3.10), addition/elimination reactions of H atoms with $CH_3C{\equiv}CH$ will produce both (CH_3, HCCH) and (H, CH_2=C=CH_2). It appears that bimolecular reactions of $CH_3C{\equiv}CH$ and H cannot be avoided even at 0.1 % concentration of DMF in Ar carrier gas.

Because of calculated CH_2-H bond energies for DMF in Fig. 4.2, it has been suggested[5] a low energy pyrolysis route would be formation of the 5-methyl-2-furanylmethyl radical (86 kcal mol^{-1}) which fragments to 2,5-dimethylene-2, 5-dihydrofuran plus H atoms (60 kcal mol^{-1}). The 118.2 nm VUV PIMS in Fig. 4.4 shows no sign of ions at m/z 94 which would be the signature for 2,5-dimethylene-2, 5-dihydrofuran (see top of Fig. 4.3). It appears that the thresholds for isomerization of DMF to either the α-carbene or the β-carbene are below that for fragmentation to H atoms and the 5-methyl-2-furanylmethyl radical.

To further investigate the decomposition mechanisms of DMF, pyrolysis experiments were carried out[30] on Beamline 9.0.2 of LBNL's Advanced Light Source in Nov. 2012. All of the experiments carried out in Colorado use a pulsed SiC reactor with either He (PIMS) or Ar (IR) as the carrier gas. In contrast, the experiments were performed at Lawrence Berkeley National Laboratory's Advanced Light Source (ALS) use a continuous flow (CW) μtubular reactor and time-of-flight photoionization mass spectrometry (PIMS) to identify the mass to charge ratio (m/z) of the molecular species at the reactor exit. A similar version of the reactor was described in detail in a recent publication.[31] For the experiments presented in this work, the reactor is a silicon carbide

(SiC) tube (0.6 mm i.d, 2 mm o.d., 2.5 cm long), mounted to a standard stainless steel Swagelok fitting (1/8″ to 3/8″ reducing union) and secured with a graphite ferrule (Restek, 1/8″ tube, inner diameter drilled out to fit reactor). For all experiments, the mass flow rate was held constant at 280 sccm He with a commercial mass flow controller (MKS P4B 0-200 sccm N_2). The pressure upstream of the reactor was measured with a capacitance monometer pressure gauge. Since the mass flow rate was held constant, the upstream pressure increases with the temperature of the SiC wall due to the larger frictional effects in the flow. With the reactor at room temperature, the upstream pressure was about 100 Torr. Increasing the measured SiC wall temperature to 1600 K increased the upstream pressure to about 300 Torr. The reactor exhausts into a chamber at a pressure of 10 μTorr. The pressure profile inside the reactor monotonically decreases along the 2.5 cm length of the reactor. With a measured wall temperature of 1600 K the pressure profile along the centerline has been estimated by computational fluid dynamics to decrease from about 300 Torr at the entrance to 50 Torr at the exit.[32] Approximately 2 cm of the SiC is resistively heated, with the temperature of the outer wall measured with a Type C thermocouple[33] and also monitored with an infrared thermometer (Omega iR2P temperature controller, range 600˚C to 1600˚C). Reactant mixtures were made in stainless steel cylinders with concentrations between 0.0075% and 0.15% DMF (Sigma Aldrich, 99%) in helium (final tank pressure between 3 to 6.5 atm).

Fig. 4.7 is PIMS of the products of pyrolysis of DMF with the synchrotron set to 10.5 eV. These results from a CW reactor largely confirm the pulsed PIMS in Fig. 4.4. The assignments for the 1400 K features in the CW spectrum in Fig. 4.7 are CH_3^+ (m/z 15), $HCCCH_2^+$ (m/z 39), $CH_3C{\equiv}CH^+$ (m/z 40), $CH_2{=}C{=}O^+$ (m/z 42), $HC{\equiv}C\text{-}C{\equiv}CH^+$ (m/z

50), HC≡C-CH=CH_2^+ (m/z 52), $CH_2C(C{\equiv}CH)CH_2^+$ (m/z 65), and HC≡C-C(CH_3)=CH_2^+ (m/z 66).

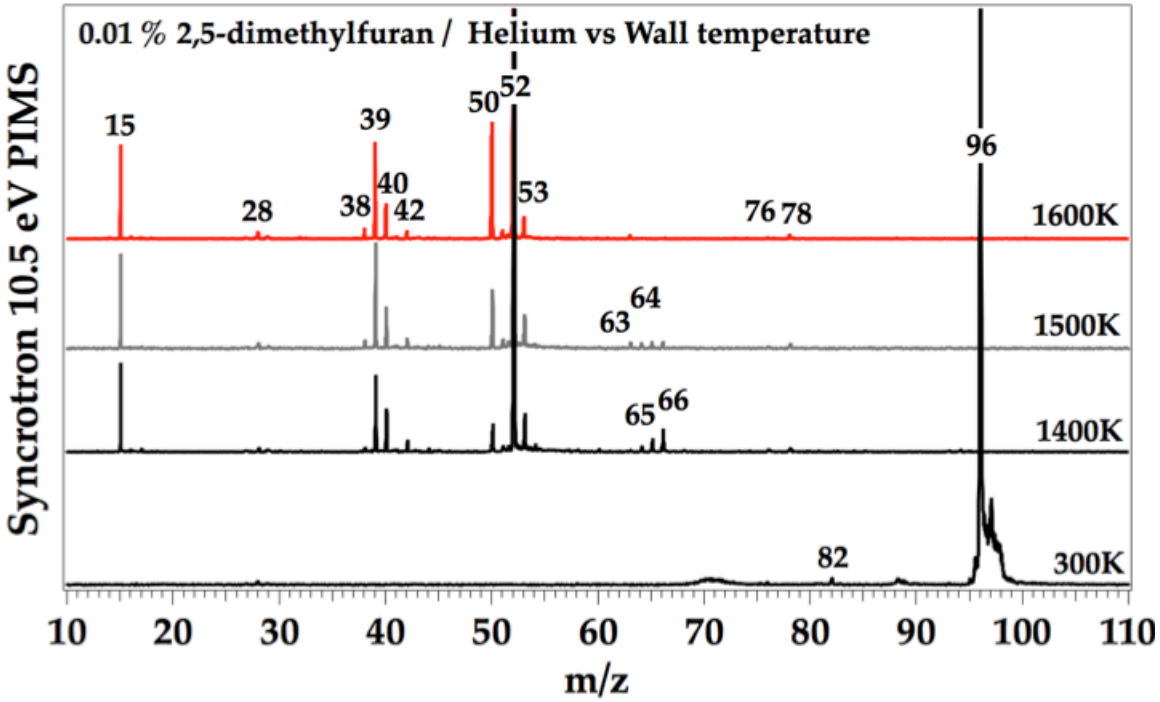

Figure 4.7 PIMS spectra of pyrolysis of DMF at various temperatures with 10.5 eV VUV in Advanced Light Source.

There are some discrepancies between the CW spectrum (Fig. 4.6) and the pulsed spectrum (Fig. 4.4) In the CW spectrum, the ions m/z 67, (HC≡CC$(CH_3)_2^+$, and m/z 68, (HC≡CCH$(CH_3)_2^+$, are missing. At the highest temperature (1600 K) in Fig. 4.7, two new species appear at m/z 38 and m/z 53. The ion at m/z 53 is probably the ^{13}C isotope of m/z 52; the ratio (53/52) is 5.0 %. The small signals at m/z 76 and m/z 78 are probably *o*-benzyne (*o*-C_6H_4) and benzene. There is a small signal at m/z 28 which is likely due to CO^+ resulting from higher VUV harmonics ionizing carbon monoxide.

Fig. 4.8 is the PIE(m/z 50) and this scan clearly identifies[20] this ion as diacetylene, HC≡C-C≡CH$^+$, *IE*(HC≡C-C≡CH) = 10.17 ± 0.02 eV.

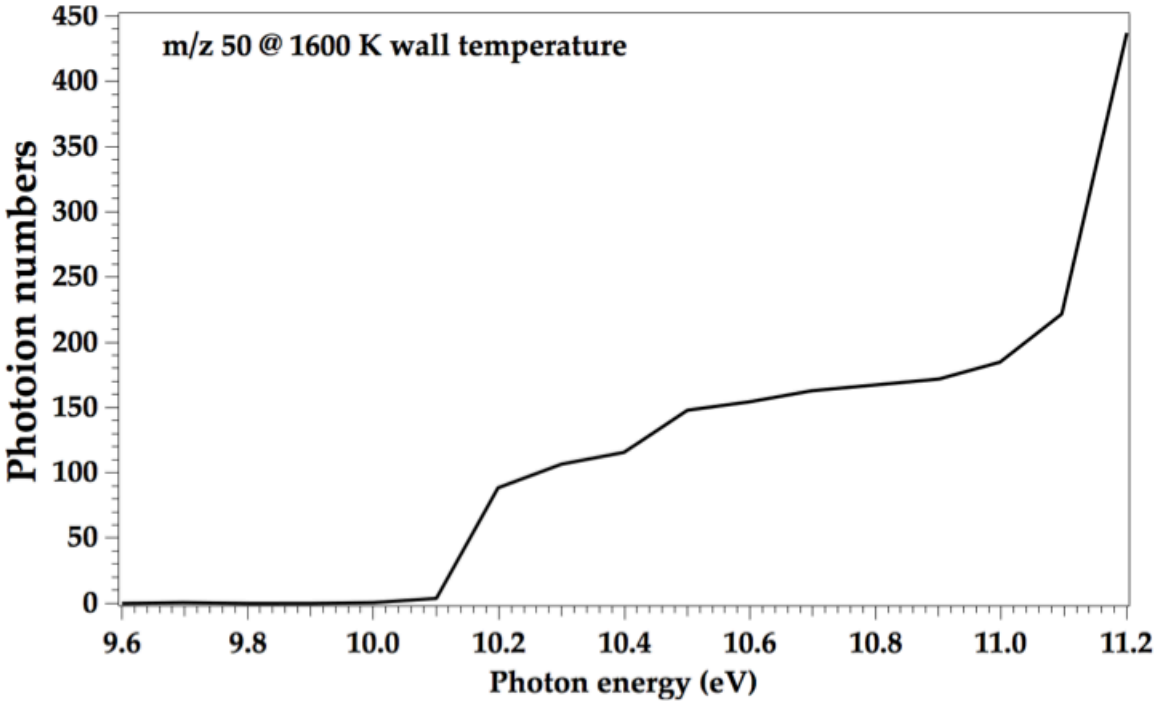

Figure 4.8 The photoionization energy curve of m/z 50 resulting from thermally decomposed DMF at 1600 K.

Fig. 4.9 is the 12.0 eV PIMS of the pyrolysis products of DMF at 1600 K. Surprisingly the m/z 26 ion, which is assigned as acetylene,[34] is very intense.

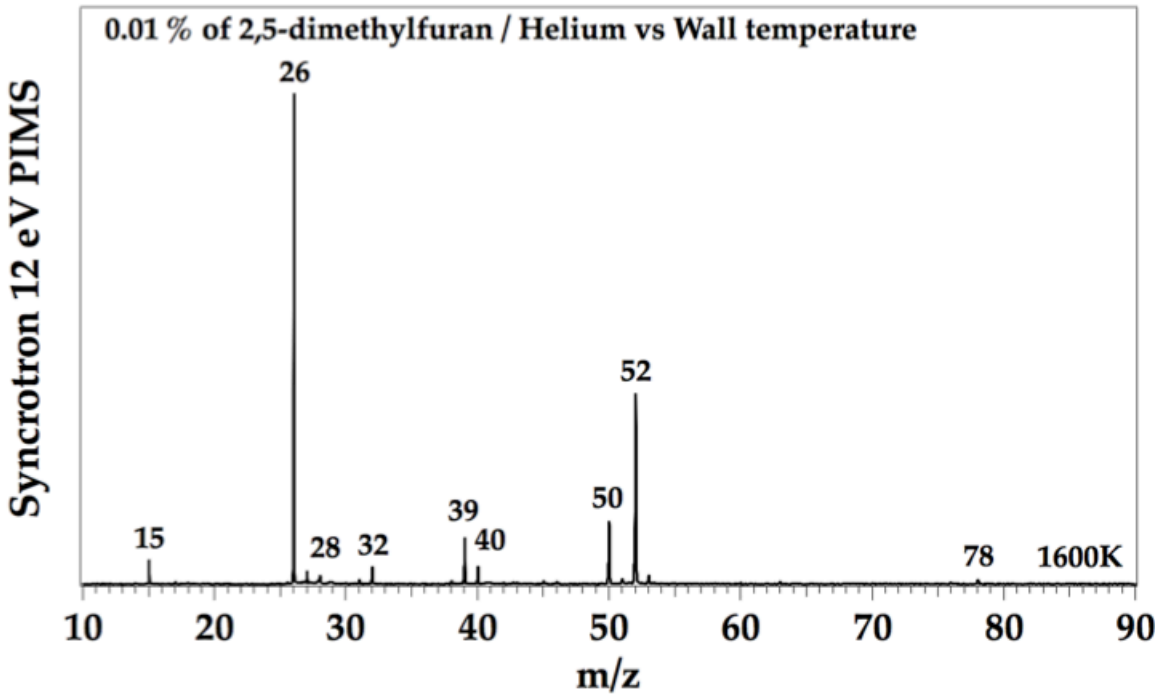

Figure 4.9 PIMS spectra of pyrolysis of DMF at 1600 K with 12 eV VUV in Advanced Light Source.

The feature at m/z 26 is positively identified as acetylene by the PIE(m/z 26) curve in Fig. 4.10. The HC≡CH in Fig. 4.10 results from pyrolysis of DMF at 1600 K; consequently the acetylene may be vibrationally excited with the apparent ionization threshold almost 0.1 eV below that[34] of *IE*(HC≡CH).

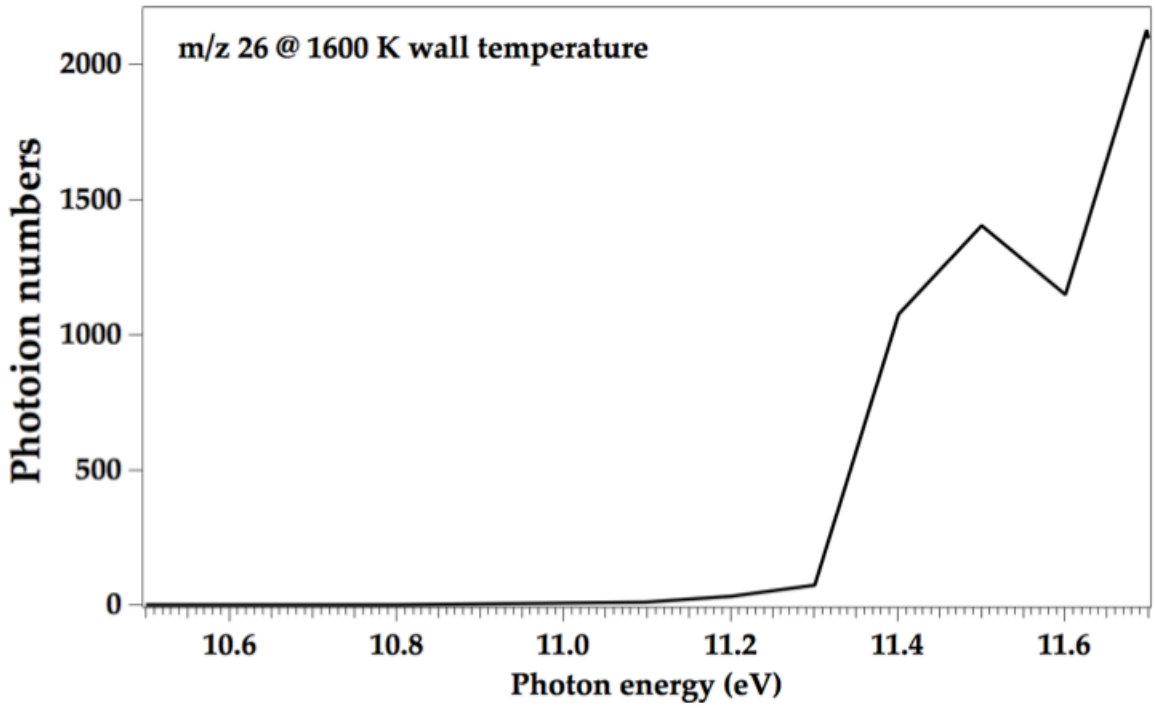

Figure 4.10 The photoionization energy curve of m/z 26 resulting from thermally decomposed DMF at 1600 K.

The proposed mechanism for DMF pyrolysis in Fig. 4.3 does not have HC≡CH as a decomposition product. Nevertheless, both the matrix IR spectra resulting from pyrolysis in a pulsed Ar reactor (Fig. 4.5) and the 12 eV PIMS of pyrolysis in a CW reactor (Fig. 4.9) clearly identify acetylene as a product resulting from the 1600 K pyrolysis of DMF. A possible route for the formation of HC≡CH was presented earlier in Chapter III (Fig. 3.10) and is the result of bimolecular chemistry of H atoms with $CH_3C{\equiv}CH$. The m/z 26 peak in Fig. 4.9 is very intense and indicates that secondary radical chemistry is important even in these very dilute DMF samples (0.01 % in He).

4.3 Conclusion

DMF has been thermally decomposed in a heated SiC flow reactor to verify the initial steps in the pyrolysis of DMF. Based on the established mechanism of the parent species, furan,[27,35] a mechanism for pyrolysis of DMF is proposed in Fig. 4.3. All of the decomposition products of DMF have been identified by three different techniques. All of the three detection schemes of a) 118.2 nm VUV PIMS of the pyrolysis products resulting from a pulsed He reactor, b) IR spectroscopy of the pyrolysis products resulting from a pulsed Ar reactor, and c) tunable VUV PIMS of the pyrolysis products resulting from a CW He reactor, all support the predicted mechanism of pyrolysis of DMF in Fig. 4.3. But it is clear that there are still interfering bimolecular reactions resulting from H atoms that obscure some of these fundamental processes.

Reference for Chapter IV

(1) Grela, M. A.; Amorebieta, V. T.; Colussi, A. J. *The Journal of Physical Chemistry* **1985**, *89*, 38.

(2) Lifshitz, A.; Tamburu, C.; Shashua, R. *Journal of Physical Chemistry A* **1997**, *101*, 1018.

(3) Lifshitz, A.; Tamburu, C.; Shashua, R. *Journal of Physical Chemistry A* **1998**, *102*, 10655.

(4) Simmie, J. M.; Curran, H. J. *The Journal of Physical Chemistry A* **2009**, *113*, 5128.

(5) Simmie, J. M.; Metcalfe, W. K. *The Journal of Physical Chemistry A* **2011**, *115*, 8877.

(6) Vogelhuber, K. M.; Wren, S. W.; Sheps, L.; Lineberger, W. C. *Journal of Chemical Physics* **2011**, *134*.

(7) Sirjean, B.; Fournet, R. *Journal of Physical Chemistry A* **2012**, *116*, 6675.

(8) Wu, X.; Huang, Z.; Yuan, T.; Zhang, K.; Wei, L. *Combustion and Flame* **2009**, *156*, 1365.

(9) Sirjean, B.; Fournet, R. *Physical Chemistry Chemical Physics* **2013**, *15*, 596.

(10) Friese, P.; Simmie, J. M.; Olzmann, M. *Proceedings of the Combustion Institute* **2013**, *34*, 233.

(11) Djokic, M.; Carstensen, H. H.; Van Geem, K. M.; Marin, G. B. *Proceedings of the Combustion Institute* **2013**, *34*, 251.

(12) Verevkin, S. P.; Welle, F. M. *Structural Chemistry* **1998**, *9*, 215.

(13) Vasiliu, M.; Guynn, K.; Dixon, D. A. *Journal of Physical Chemistry C* **2011**, *115*, 15686.

(14) Feller, D.; Simmie, J. M. *The Journal of Physical Chemistry A* **2012**, *116*, 11768.

(15) Veszpremi, T.; Nyulaszi, L.; Nagy, J. *Journal of Organometallic Chemistry* **1987**, *331*, 175.

(16) Lau, K. C.; Ng, C.-Y. *Accounts of Chemical Research* **2006**, *39*, 823.

(17) Gilbert, T.; Pfab, R.; Fischer, I.; Chen, P. *Journal of Chemical Physics* **2000**, *112*, 2575.

(18) Xing, X.; Bahng, M.-K.; Reed, B.; Lam, C. S.; Lau, K.-C.; Ng, C. Y. *The Journal of Chemical Physics* **2008**, *128*, 094311.

(19) Niu, B. H.; Bai, Y.; Shirley, D. A. *Journal of Chemical Physics* **1993**, *99*, 2520.

(20) Bieri, G.; Burger, F.; Heilbronner, E.; Maier, J. P. *Helvetica Chimica Acta* **1977**, *60*, 2213.

(21) Xing, X.; Reed, B.; Lau, K. C.; Ng, C. Y.; Zhang, X.; Ellison, G. B. *Journal of Chemical Physics* **2007**, *126*, 171170.

(22) Bock, H.; Hirabayashi, T.; Mohmand, S.; Solouki, B. *Angewandte Chemie* **1977**, *89*, 106.

(23) Scheer, A. M., University of Colorado, 2011.

(24) Scheer, A. M.; Mukarakate, C.; Robichaud, D. J.; Nimlos, M. R.; Carstensen, H.-H.; Ellison, G. B. *The Journal of Chemical Physics* **2012**, *136*, 044309.

(25) Saussey, J.; Lamotte, J.; Lavalley, J. C. *Spectrochimica Acta Part a-Molecular and Biomolecular Spectroscopy* **1976**, *32*, 763.

(26) Crowder, G. A.; Fick, H. *Journal of Molecular Structure* **1986**, *147*, 17.

(27) Vasiliou, A.; Nimlos, M. R.; Daily, J. W.; Ellison, G. B. *The Journal of Physical Chemistry A* **2009**, *113*, 8540.

(28) Jochnowitz, E. B.; Zhang, X.; Nimlos, M. R.; Varner, M. E.; Stanton, J. F.; Ellison, G. B. *The Journal of Physical Chemistry A* **2005**, *109*, 3812.

(29) Ormond, T. K. *Unpublished data* **2012**.

(30) The experimental studies on 2MF and DMF at LBNL's ALS were carried out by Kimberly Urness, Tom K. Ormond, Barney Ellison, and John Stanton in Fall, 2012.

(31) Vasiliou, A.; Piech, K. M.; Reed, B.; Zhang, X.; Nimlos, M. R.; Ahmed, M.; Golan, A.; Kostko, O.; Osborn, D. L.; Urness, K. N.; David , D. E.; Daily, J. W.; Stanton, J. F.; Ellison, G. B. *Journal of Chemical Physics* **2012**, *137*, 164308.

(32) Guan, Q.; Daily, J. W. **2013**, *to be published*.

(33) There are at least five potential sources of error for measuring the temperature of the SiC tube. (a) The inherent accuracy of the thermocouple is listed by Omega Engineering as the greater of 4.5 ºC or 1.0% from 0 — 2320 ºC. (b) Imperfect thermal contact between the thermocouple and the SiC tube. This is difficult to quantify but it is probably not the dominant factor since most of the heat transfer is expected to be by radiation, at least at higher temperatures. (c) Cooling along the thermocouple wire away from the thermocouple junction/SiC contact point. This is probably the most important loss factor and is likely on the order of 10s ºC. (d) Extra radiative losses from the surface area added by the thermocouple. (e) The thermocouple cold junction is at the vacuum feedthrough instead of at the meter (where it would be properly compensated). The latter consideration probably contributes less than a few ºC to the error. The best way to determine

the error is by experiment, either with a sample with known kinetics or by inserting a thermocouple inside the SiC tube during normal operation.

(34) Pratt, S. T.; Dehmer, P. M.; Dehmer, J. L. *Journal of Chemical Physics* **1993**, *99*, 6233.

(35) Urness, K. N.; Golan, A.; Daily, J. W.; Nimlos, M. R.; Stanton, J. F.; Ahmed, M.; Ellison, G. B. *J. Chem. Phys.* **2013**, *in press*.

Bibliography

Lifshitz, A.; Tamburu, C.; Shashua, R. *Journal of Physical Chemistry A* **1997**, *101*, 1018.

Lifshitz, A.; Tamburu, C.; Shashua, R. *Journal of Physical Chemistry A* **1998**, *102*, 10655.

Huber, G. W.; Iborra, S.; Corma, A. *Chemical Reviews* **2006**, *106*, 4044.

American energy: The renewable path to energy security, Worldwatch Institute Center for American Progress, 2006.

EPA, Major Crops Grown in the United States, http://www.epa.gov/agriculture/ag101/cropmajor.html.

McKendry, P. *Bioresource Technology* **2002**, *83*, 37.

Sannigrahi, P.; Ragauskas, A. J.; Tuskan, G. A. *Biofuels, Bioproducts and Biorefining* **2010**, *4*, 209.

Bose, S. K.; Francis, R. C.; Govender, M.; Bush, T.; Spark, A. *Bioresource Technology* **2009**, *100*, 1628.

Reale, S.; Di Tullio, A.; Spreti, N.; De Angelis, F. *Mass Spectrometry Reviews* **2004**, *23*, 87.

Vanholme, R.; Demedts, B.; Morreel, K.; Ralph, J.; Boerjan, W. *Plant Physiology* **2010**, *153*, 895.

Chen, P.; Colson, S. D.; Chupka, W. A.; Berson, J. A. *Journal of Physical Chemistry* **1986**, *90*, 2319.

Chen, P.; Pallix, J. B.; Chupka, W. A.; Colson, S. D. *Journal of Chemical Physics* **1987**, *86*, 516.

Kohn, D. W.; Clauberg, H.; Chen, P. *Review of Scientific Instruments* **1992**, *63*, 4003.

Blush, J. A.; Clauberg, H.; Kohn, D. W.; Minsek, D. W.; Zhang, X.; Chen, P. *Accounts Chem. Res.* **1992**, *25*, 385.

Chen, P. In *Unimolecular and Bimolecular Ion-Molecule Reaction Dynamics*; Ng, C. Y., Baer, T., Powis, I., Eds.; John Wiley: Cambridge, UK, 1994, p 371.

Rohrs, H. W.; Wickham-Jones, C. T.; Berry, D.; Ellison, G. B.; Argrow, B. M. *Rev. Sci. Instrum.* **1995**, *66*, 2430.

Zhang, X.; Friderichsen, A. V.; Nandi, S.; Ellison, G. B.; David, D. E.; McKinnon, J. T.; Lindeman, T. G.; Dayton, D. C.; Nimlos, M. R. *Review of Scientific Instruments* **2003**, *74*, 3077.

Guan, Q.; Daily, J. W. **2013**, *to be published*.

Vasiliou, A.; Piech, K. M.; Reed, B.; Zhang, X.; Nimlos, M. R.; Ahmed, M.; Golan, A.; Kostko, O.; Osborn, D. L.; Urness, K. N.; David , D. E.; Daily, J. W.; Stanton, J. F.; Ellison, G. B. *Journal of Chemical Physics* **2012**, *137*, 164308.

Urness, K. N.; Golan, A.; Daily, J. W.; Nimlos, M. R.; Stanton, J. F.; Ahmed, M.; Ellison, G. B. *J. Chem. Phys.* **2013**, *in press*.

There are at least five potential sources of error for measuring the temperature of the SiC tube. (a) The inherent accuracy of the thermocouple is listed by Omega Engineering as the greater of 4.5 ºC or 1.0% from 0 — 2320 ºC. (b) Imperfect thermal contact between the thermocouple and the SiC tube. This is difficult to quantify but it is probably not the dominant factor since most of the heat transfer is expected to be by radiation, at least at higher temperatures. (c) Cooling along the thermocouple wire away from the thermocouple junction/SiC contact point. This is probably the most important loss factor and is likely on the order of 10s ºC. (d) Extra radiative losses from the surface area added by the thermocouple. (e) The thermocouple cold junction is at the vacuum feedthrough instead of at the meter (where it would be properly compensated). The latter consideration probably contributes less than a few ºC to the error. The best way to determine the error is by experiment, either with a sample with known kinetics or by inserting a thermocouple inside the SiC tube during normal operation.

The leak rate of Ar is measured through a pulsed reactor to be 1 Torr min^{-1} as it passes through a SiC reactor at 300 K that is pulsed at 20 Hz and opens for 1 msec. The Ar gas is leaking from a reservior of 1.2 L at 1 atm pressure. Since PV = nRT, we can use: dn/dt = (dP/dt)(V/RT) = (1 Torr min^{-1}) (1.2 L) (62.4 Torr L mol^{-1} K^{-1} * 300 K)$^{-1}$ which yields dn/dt = 6.4 x 10^{-5} mol min^{-1} or 1 x 10^{-7} mol sec^{-1}. The pulsed valve fires at 20 Hz and delivers 3 x 10^{16} Ar atoms $pulse^{-1}$. Typical gas mixtures are 1 Torr CH_3CHO in 1 atm Ar or 0.1 %; consequently the reactor delivers about 4 x 10^{13} organics $pulse^{-1}$.

Wiley, W. C.; McLaren, I. H. *Review of Scientific Instruments* **1955**, *26*, 1150.

Wiza, J. L. *Nuclear Instruments & Methods* **1979**, *162*, 587.

Jacox, M. E. *Chemical Society Reviews* **2002**, *31*, 108.

Jacox, M. E. *Journal of Molecular Spectroscopy* **1985**, *113*, 286.

Roman-Leshkov, Y.; Barrett, C. J.; Liu, Z. Y.; Dumesic, J. A. *Nature* **2007**, *447*, 982.

Wang, C.; Xu, H.; Daniel, R.; Ghafourian, A.; Herreros, J. M.; Shuai, S.; Ma, X. *Fuel* **2013**, *103*, 200.

Binder, J. B.; Raines, R. T. *Journal of the American Chemical Society* **2009**, *131*, 1979.

Grela, M. A.; Amorebieta, V. T.; Colussi, A. J. *The Journal of Physical Chemistry* **1985**, *89*, 38.

Simmie, J. M.; Curran, H. J. *The Journal of Physical Chemistry A* **2009**, *113*, 5128.

Vogelhuber, K. M.; Wren, S. W.; Sheps, L.; Lineberger, W. C. *Journal of Chemical Physics* **2011**, *134*.

Thewes, M.; Muether, M.; Pischinger, S.; Budde, M.; Brunn, A.; Sehr, A.; Adomeit, P.; Klankermayer, J. *Energy & Fuels* **2011**, *25*, 5549.

Wu, X. S.; Daniel, R.; Tian, G. H.; Xu, H. M.; Huang, Z. H.; Richardson, D. *Applied Energy* **2011**, *88*, 2305.

Vasiliou, A.; Nimlos, M. R.; Daily, J. W.; Ellison, G. B. *The Journal of Physical Chemistry A* **2009**, *113*, 8540.

Veszpremi, T.; Nyulaszi, L.; Nagy, J. *Journal of Organometallic Chemistry* **1987**, *331*, 175.

Gilbert, T.; Pfab, R.; Fischer, I.; Chen, P. *Journal of Chemical Physics* **2000**, *112*, 2575.

Xing, X.; Bahng, M.-K.; Reed, B.; Lam, C. S.; Lau, K.-C.; Ng, C. Y. *The Journal of Chemical Physics* **2008**, *128*, 094311.

Bieri, G.; Burger, F.; Heilbronner, E.; Maier, J. P. *Helvetica Chimica Acta* **1977**, *60*, 2213.

Blush, J. A.; Chen, P.; Wiedmann, R. T.; White, M. G. *Journal of Chemical Physics* **1993**, *98*, 3557.

Niu, B. H.; Bai, Y.; Shirley, D. A. *Journal of Chemical Physics* **1993**, *99*, 2520.

Vasiliou, A.; Piech, K. M.; Zhang, X.; Nimlos, M. R.; Ahmed, M.; Kostko, O.; Golan, A.; Osborn, D. L.; Daily, J. W.; Stanton, J. F.; Ellison, G. B. *Journal of Chemical Physics* **2011**, *135*, 14306.

Pratt, S. T.; Dehmer, P. M.; Dehmer, J. L. *Journal of Chemical Physics* **1993**, *99*, 6233.

Bock, H.; Hirabayashi, T.; Mohmand, S.; Solouki, B. *Angewandte Chemie* **1977**, *89*, 106.

Scheer, A. M., University of Colorado, 2011.

Scheer, A. M.; Mukarakate, C.; Robichaud, D. J.; Nimlos, M. R.; Carstensen, H.-H.; Ellison, G. B. *The Journal of Chemical Physics* **2012**, *136*, 044309.

Saussey, J.; Lamotte, J.; Lavalley, J. C. *Spectrochimica Acta Part A: Molecular Spectroscopy* **1976**, *32*, 763.

Crowder, G. A.; Fick, H. *Journal of Molecular Structure* **1986**, *147*, 17.

Jochnowitz, E. B.; Zhang, X.; Nimlos, M. R.; Varner, M. E.; Stanton, J. F.; Ellison, G. B. *The Journal of Physical Chemistry A* **2005**, *109*, 3812.

Yang, Z. Z.; Wang, L. S.; Lee, Y. T.; Shirley, D. A.; Huang, S. Y.; Lester, W. A. *Chemical Physics Letters* **1990**, *171*, 9.

Spilker, R.; Grutzmacher, H. F. *Organic Mass Spectrometry* **1986**, *21*, 459.

Gao, H.; Xu, Y. T.; Yang, L.; Lam, C. S.; Wang, H. L.; Zhou, J. A.; Ng, C. Y. *Journal of Chemical Physics* **2011**, *135*.

Parker, J. K.; Davis, S. R. *The Journal of Physical Chemistry A* **1999**, *103*, 7280.

Lau, K. C.; Ng, C.-Y. *Accounts of Chemical Research* **2006**, *39*, 823.

Evans, M.; Ng, C. Y. *Journal of Chemical Physics* **1999**, *111*, 8879.

Ormond, T. K. *Unpublished data* **2012**.

Brandsma, L.; Verkruijsse, H. D. *Synthesis of Acetylens, Allens, and Cumulens*; Elsevier: Amsterdam, 1981.

Wrobel, R.; Sander, W.; Cremer, D.; Kraka, E. *The Journal of Physical Chemistry A* **2000**, *104*, 3819.

Nakata, M.; Frei, H. *J. Am. Chem. Soc.* **1992**, *114*, 1363.

Shimanouchi, T. *Tables of Vibrational Frequencies, Consolidated Vol. I*; NSRDS-NBS 39, 1972.

Kwiatkowski, J. S.; Leszczynski, J. *Theochem-Journal of Molecular Structure* **1995**, *342*, 43.

Tørneng, E.; Nielsen, C. J.; Klaeboe, P.; Hopf, H.; Priebe, H. *Spectrochimica Acta Part a-Molecular and Biomolecular Spectroscopy* **1980**, *36*, 975.

Miller, F. A.; Matsubara, I. *Spectrochimica Acta* **1966**, *22*, 173.

Saussey, J.; Lamotte, J.; Lavalley, J. C. *Spectrochimica Acta Part a-Molecular and Biomolecular Spectroscopy* **1976**, *32*, 763.

Crowder, G. A.; Fick, H. *Journal of Molecular Structure* **1986**, *147*, 17.

Simmie, J. M.; Metcalfe, W. K. *The Journal of Physical Chemistry A* **2011**, *115*, 8877.

Sirjean, B.; Fournet, R. *Journal of Physical Chemistry A* **2012**, *116*, 6675.

Wu, X.; Huang, Z.; Yuan, T.; Zhang, K.; Wei, L. *Combustion and Flame* **2009**, *156*, 1365.

Sirjean, B.; Fournet, R. *Physical Chemistry Chemical Physics* **2013**, *15*, 596.

Friese, P.; Simmie, J. M.; Olzmann, M. *Proceedings of the Combustion Institute* **2013**, *34*, 233.

Djokic, M.; Carstensen, H. H.; Van Geem, K. M.; Marin, G. B. *Proceedings of the Combustion Institute* **2013**, *34*, 251.

Verevkin, S. P.; Welle, F. M. *Structural Chemistry* **1998**, *9*, 215.

Vasiliu, M.; Guynn, K.; Dixon, D. A. *Journal of Physical Chemistry C* **2011**, *115*, 15686.

Feller, D.; Simmie, J. M. *The Journal of Physical Chemistry A* **2012**, *116*, 11768.

Xing, X.; Reed, B.; Lau, K. C.; Ng, C. Y.; Zhang, X.; Ellison, G. B. *Journal of Chemical Physics* **2007**, *126*, 171170.

The experimental studies on 2MF and DMF at LBNL's ALS were carried out by Kimberly Urness, Tom K. Ormond, Barney Ellison, and John Stanton in Fall, 2012.